MODELING HYDROLOGICAL PROCESSES AND KEY FACTORS INFLUENCING NONPOINT SOURCE POLLUTION IN AGRICULTURAL AND URBAN SETTINGS

By

MUGAL SAMRAT DAHAL

A dissertation submitted in partial fulfillment of
the requirements for the degree of

DOCTOR OF PHILOSOPHY

WASHINGTON STATE UNIVERSITY
Department of Biological Systems Engineering

DECEMBER 2023

To the Faculty of Washington State University:

The members of the Committee appointed to examine the dissertation of MUGAL SAMRAT DAHAL find it satisfactory and recommend that it be accepted.

Joan Q. Wu, Ph.D., Chair

Anand Jayakaran, Ph.D.

Jan Boll, Ph.D.

Kirti Rajagopalan, Ph.D.

ACKNOWLEDGMENT

I extend my profound gratitude to everyone who has contributed, in both major and minor capacities, to the fruition of my PhD Dissertation. Foremost, I am indebted to Dr. Joan Wu, my advisor. Her candid feedback, meticulous attention to detail, and deep scientific understanding were paramount in elevating the quality and rigor of my research. I cherish the time we have spent together in these years and will forever be grateful to her for her kindness, flexibility, and insights. I have learned so much from her through her guidance, encouragement, and criticisms. I will carry the lessons I have learned from her through my professional career for years to come.

I am grateful to Dr. Anand Jayakaran. His expertise and guidance are utmost important for the completion of my PhD Study. I appreciate his knowledge of Green Stormwater Infrastructure and urban stormwater management, and his guidance throughout my graduate study. He has always encouraged me to look at the “big picture”, and his unwavering support has been invaluable. His counsel has consistently illuminated the path forward in completing this thesis. I will cherish the time I have spent with him during both professional work and after work. Gratitude is also due to Dr. Jan Boll, for sharing his expertise in hydrologic modeling and water erosion research. I thank him for raising critical questions that have expanded the scope of my doctoral research and refined the rigor of my dissertation. I am greatly thankful to Dr. Kirti Rajagopalan for her steadfast support and adept guidance. Her expertise, especially in climate modeling was crucially helpful in assimilating future climate data and analyzing future erosion results, which in turn enriches my work. Our discussions have been enlightening and instrumental in shaping my research trajectory.

My interactions with Dr. Robert Ewing were pivotal. The discussions I have had with him were thought provoking, prompting me to examine my study from new perspectives. I deeply appreciate his editorial inputs and consistent guidance that has helped to improve my communication skills. I thank him for always finding the time to listen to my draft presentation and read my draft manuscripts. I thank Dr. Mariana Dobre for her support and responsiveness. Her guidance with setting up WEPP runs and her expertise of WEPP simulation were valuable.

I am deeply grateful to my colleagues: Anish Mahat, Supriya Savalkar, Daniel Ullom, Chelsea Mitchell, Dr. Yingxue Yu, and Prabesh Khanal. I cherish the myriad discussions about my study and perspectives they have offered. I would always remember the fun times we have spent together. I also express my gratitude to friends from the Graduate House and Puyallup Research and Extension Center for their camaraderie and resolute support. I thank Ms. Joanna Dreger for her extensive administrative support, especially her patience with missed deadlines was indispensable.

On a personal note, I am extremely thankful to my parents, Mr. Keshab Dahal and Mrs. Kalika Khanal, for their undying love and invaluable encouragement. I am thankful to my sister Manashi, for looking up to me and keeping me in check. Lastly, my profound gratitude goes to my wife, Namika, for hearing my frustrations and always believing in me. She has been a pillar of strength, offering constant support, friendship, and love throughout this journey.

MODELING HYDROLOGICAL PROCESSES AND KEY FACTORS INFLUENCING NONPOINT SOURCE POLLUTION IN AGRICULTURAL AND URBAN SETTINGS

Abstract

by Mugal Samrat Dahal, Ph.D.
Washington State University
December 2023

Chair: Joan Q. Wu

Nonpoint-source pollution from agricultural and urban landscape is a major threat to water quality worldwide. This doctoral research aims to assess the spatiotemporal variations of nonpoint-source pollution and elucidate key factors at play in representative agricultural and urban settings in the US Pacific Northwest (PNW). The main objectives were to:

1) elucidate the long-term historical soil erosion trend, as affected by climatic and management conditions;
2) assess changes in water erosion as impacted by the projected future climate and the effect of conservation practices using WEPP; and
3) optimize placement of rain gardens in an urbanizing watershed, south Puget Sound, using the Hydrologic Sensitivity Index (HSI) method.

For the first study, I delineated a watershed within the low-, intermediate-, and high-precipitation zones of eastern Washington, and simulated water erosion over two time periods: past and present, under different tillage practices and crop rotations. The average annual erosion rates decreased from the past by 32%, 57%, and 70%, respectively, for the three watersheds. The decrease was due to the combined effects of changing climate and implementation of conservation practices.

For the second study, I modeled water erosion for the same three watersheds for two time periods: historical and future using downscaled climates. Future average annual precipitation and daily temperature increase by 4–6% and 7–10%, respectively. Projected annual water erosion generally decreased by 0–4% for the three watersheds, owing to improvement in winter conditions. Future annual water erosion exceeds 50 Mg ha^{-1} in areas with steeper slopes and years with wheat, especially in intermediate-, and high-precipitation zones. I recommend targeted land management practices for erosion reduction.

In the third study, I used the HSI approach to identify areas prone to runoff generation and suitable areas for rain gardens, a small-scale Green Stormwater Infrastructure (GSI). I conducted hydrologic modeling to assess the adequacy of the HSI method. The simulated runoff was positively correlated with HSI. The locations most suitable for rain gardens were concentrated in the northeastern-central parts of the study watershed. This study demonstrated the adequacy of HSI method and provided a strategy for practitioners and regulatory personnel in optimizing the placement of rain gardens.

Findings from this dissertation advance the understanding of nonpoint-source pollution and contribute to conservation planning in both agricultural and urban areas.

TABLE OF CONTENTS

Page

LIST OF FIGURES

Page

LIST OF TABLES

Page

Dedication

For the mountains, hills, valleys,

and rivers of the Pacific Northwest

which always remind me of home.

1. INTRODUCTION

1.1. Nonpoint-source pollution

Nonpoint-source pollution refers broadly to pollution from multiple sources without having a single point source of origin (Xepapadeas, 2011). Non-point source pollution is responsible for major degradation of surface waters around the world (Baker, 1992; Shen et al., 2012), and is the major water quality threat in the US (Horan and Ribaudo, 1999) accounting for nearly all suspended solids and most phosphorus, nitrogen, and toxins discharged into the downstream water bodies (Harrington et al., 1985). Hydrological processes, such as precipitation, runoff, and snowmelt, drive nonpoint-source pollution (Shen et al., 2012). However, runoff is the most significant carrier of pollutants from agricultural fields and urban settings (Parikh et al., 2005; Xia et al., 2020). Land use, topographic features, and soil properties and conditions within a watershed all affect the hydrological processes and nonpoint-source pollution (Panagopoulos et al., 2011; Wu et al., 2019).

1.2. Nonpoint-source pollution from agricultural lands

In an agricultural field, runoff detaches and washes away the top fertile soil, carrying with it various agrichemicals such as fertilizers and pesticides. Globally, from the mid-20th to early 21st century, conventionally tilled croplands have caused soil erosion one to two orders of magnitude greater than soil production (Montgomery, 2007). Annual soil erosion was estimated at 6.7 t ha^{-1} on average for 2017 within the cultivated croplands of the United States. A remote sensing study in the corn belt of the midwestern US estimates the loss of one-third of the A-horizon soil through erosion (Thaler et al., 2021). In the Palouse region of the inland Pacific Northwest, historical water erosion rates went above 20.0 t ha^{-1} on average, far exceeding the tolerance level of 11 t ha^{-1} (USDA, 1978). Erosion degrades soil by removing its organic matter

and nutrients, reduces biomass production and surface protection, which in turn leads to more erosive conditions (Cruz et al., 2023). This negative feedback causes excessive erosion from cropland, decreasing crop yield and instigating economic losses (Trimble and Crosson, 2000; Wei et al., 2010).

1.3. Nonpoint-source pollution in urban areas

In urban areas, an increase in construction increases impervious areas, disrupting the hydrological cycle and augmenting runoff regimes (Yoo et al., 2021). Stormwater runoff mixes and transports pollutants that accumulate on non-permeable surfaces. Among the common pollutants in stormwater runoff are nitrogen, phosphorus, heavy metals (e.g., lead, zinc, copper, and cadmium), polycyclic aromatic hydrocarbons (PAH), mineral oil hydrocarbons (MOH), and easily soluble salts (Gobel et al., 2007). Various studies have reported an increasing trend in phosphorus, nitrogen, and metals in streams across the US (Lin et al., 1997; Yang & Toor, 2018; Joyce et al., 2020), which poses a threat to the ecosystem (McCarthy et al., 2008; WSDE, 2021). For example, an overabundance of phosphorus and nitrogen in streams and lakes can cause eutrophication due to overgrowth of aquatic plants, depleting dissolved oxygen and adversely impacting aquatic life (Vitousek et al., 1997). In western Washington, Puget Sound and its adjacent waters receive nearly 11,000 tons of inorganic nitrogen and 2,100 tons of total phosphorus, most of which are from nearby agricultural lands (Inkpen et al., 1998).

1.4. Conservation practices in agricultural and urban areas

Conservation practices are recommended for agricultural production and urban development to reduce nonpoint-source pollution. Federal and state regulations have prompted increasing adoption of conservation practices by farmers, ranchers, and urban planners. The Clean Water Act of 1972 prohibited the discharge of any pollutant into navigable water, and the

Farm Bill of 1985 and 1990 encouraged farmers to use conservation practices to prevent soil erosion from highly erodible lands (Franzetti, 2005; Kok et al., 2009). The USDA Soil Conservation Service (now Natural Resources Conservation Service), established in 1933, and US Environmental Protection Agency, established in 1970, have worked extensively with land owners and producers to implement conservation practices (Franzetti, 2005; Kok et al., 2009).

Agricultural conservation practices focus on decreasing runoff and preventing soil detachment to curtail nonpoint-source pollution. Conservation tillage practices promote increase in crop residue and reduce impacts on the soil surface, which can be evaluated with the Soil Tillage Intensity Rating (STIR), a measure that reflects soil disturbance by field operation (Claassen et al., 2018). A STIR value < 80 is generally recommended (Claassen et al., 2018). Reduced tillage practices involve a decrease in the number of tillage passes and depth of tillage to decrease the pulverization of soil (Moldenhauer et al., 1983; Coolman and Hoyt, 1993). No-till practices, with a STIR value <30, refer to seedbed preparation without disturbance to, and increasing the amount of residue on, the soil surface (McGregor et al., 1975; NRCS, 2005; Triplett et al., 2008).

Other major conservation practices include crop rotation, cover crop, buffer, and Conservation Reserve Program (CRP). Crop rotation is used to increase soil water and decrease soil disturbance by planting a high residue crop (e.g., wheat or corn) and a low residue crop (e.g., legume) in the same cropland during successive growth periods (Zhou et al., 2019). Cover crops are planted during the off-season to reduce runoff and soil erosion (Malik et al., 2000; De Baets et al., 2011; Kaspar et al., 2011). Conservation buffers are placed at the bottom of the hillslopes and along the streams to filter pollutants and trap sediments (Gilley et al., 2000; Lovell and

Sullivan, 2006). The CRP is a voluntary land retirement program subsidized by the US government to cease cultivation on vulnerable areas (Dunn et al., 1993; Stubbs, 2014).

In urban settings, managing pollution close to the source has gained traction (Wanielista et al., 1992; Sage et al., 2015). Conservation practices, such as Green Stormwater Infrastructures (GSI) practices, are installed in targeted areas for stormwater runoff reduction and water reuse (Davis et al., 2009; Hunt et al., 2012). Rain barrels and rain gardens are small-scale GSI practices that promote infiltration, whereas bioretention systems are more complex, larger-scale GSI that not only increase the residence time of, but also treat and remove nutrients from runoff (Martin-Mikle et al., 2015).

1.5. Targeted placement of conservation practices

Proper placement of conservation practices is critical to ensure maximum effectiveness in agricultural and urban settings (Kurkalova et al., 2015; Dagenais et al., 2017; Christman et al., 2018). Due to a lack of understanding of the factors involved, optimizing the siting of these conservation practices remains a challenge (Brooks et al., 2015; Martin-Mikle et al., 2015; Young et al., 1989).

Runoff generation and pollutant transport are not uniform across a watershed; instead, some areas exhibit greater potential for runoff and pollutant transport (Walter et al., 2000). These areas are called “hydrologically sensitive”, and are often the sources of runoff and water quality problems. Using WEPP (Water Erosion Prediction Project), a continuous process-based erosion model (Flanagan, 1995), Brooks et al. (2015) conducted a simulation study and showed that about 1% of the area in a model watershed contributed to more than 30% of erosion. As such, it is crucial to identify and target these hydrologically-sensitive areas in the watershed for

implementing conservation practices and maximizing their efficiency (Young et al., 1989; Brooks et al., 2015).

1.6. Hydrological modeling

Owing to the advancement in computing capabilities, modeling approaches, ranging from simplistic with a few parameters to more sophisticated, physically-based can be adapted to solve eco-hydrological problems (Diodata et al., 2014). Compared to field investigations, models are time- and cost-effective to use (Osei-Twumasi et al., 2015). Hydrological models can be used for general decision support (Berberoglu et al., 2020) and for detailed assessment of hydrological and pollutant transport processes and the effects of conservation practices (Borah et al., 2006; Srivastava et al., 2007). Computer models have been widely used for prioritizing conservation practices and aiding decisions in both agricultural and urban settings (Perez-Pedini et al., 2005; Himansu et al., 2019). Further, hydrological models can quantify changes in hydrological outcomes in response to future climate, and provide information for adaptive management (Rittenburg et al., 2015; Gould et al., 2016; Anache et al., 2018).

Hydrological processes vary temporally. Their temporal assessment allows detailed analysis of the timing, duration, and magnitude of hydrological processes as well as temporal-spatial-anthropogenic interactions (Yair et al., 2004; Sajikumar and Remya, 2017). Findings from such analyses are valuable and important in developing water resources management strategies (Chen et al., 2007; Nikolic et al., 2013).

1.7. WEPP

The Water Erosion Prediction Project (WEPP) model is a widely used, physically-based computer program designed to simulate hydrological processes, soil detachment and transport, and vegetation growth on a hillslope or watershed scale. WEPP is a continuous-simulation,

distributed-parameter model capable of simulating key hydrological processes in response to various land management conditions (Flanagan et al., 1995).

The water balance components of WEPP are computed daily for each Overland Flow Element (OFE) of a hillslope. An OFE is the smallest homogenous hydrological unit in the model. Infiltration from precipitation or irrigation is calculated with the Green-Ampt-Mein-Larson model (Mein and Larson, 1973). The excess of the water input is routed as surface runoff after adjusting for depression storage (Flanagan et al., 1995). For each OFE, the infiltrated water is distributed to other mass balance components on a daily time step, in the order of downward percolation, soil evaporation, subsurface lateral flow, saturation excess, and plant transpiration (Dun et al., 2009). The soil profile in each OFE is divided into 100-mm increments for the first two layers to better simulate surface effects, and 200-mm layers for the remainder of the soil depth (Flanagan et al., 1995; Dun et al., 2009). Downword movement is computed when the water content exceeds field capacity in a layer and the percolation through the last layer of the soil profile is considered lost and termed deep percolation.

Potential evapotranspiration (ET) in WEPP is computed with the Penman-Monteith equation when wind and solar radiation data are available, which is then used to compute potential soil evaporation and plant transpiration (Flanagan et al., 1995). Soil water is withdrawn from the soil profile when rainfall interception by plants and residue cannot fulfill the potential ET.

Subsurface lateral flow is computed using the kinematic storage model when the soil water content exceeds the soil field capacity after adjustment for entrapped air (Flanagan et al., 1995). Soil water content in the soil profile is adjusted after each process, and saturation excess

is computed from bottom to top by comparing the soil water content with the soil porosity. The excess water is added to the layer above, and when the soil water in the first layer exceeds the porosity, the excess water is exfiltrated as a saturation-excess runoff (Dun et al., 2009). Multiple OFEs are used to better characterize the water balance in different parts of the hillslope (Boll et al., 2015). In the case of multiple OFEs, the subsurface lateral flow from the upland OFE is modeled as an input to the downstream OFE (Dun et al., 2009).

Soil erosion is computed for interrill and rill separately in WEPP (Flanagan et al., 1995). Interrill erosion is the sediment detachment and delivery to a rill as affected by the rainfall intensity and runoff rate. Interrill erodibility dictates soil susceptibility to rainfall impact and directly affects interrill erosion. Rill erosion is the sediment detachment by concentrated flows. Rill erodibility dictates the susceptibility of the soil to detachment by concentrated flows. Soil loss occurs when the transport capacity of the concentrated flow in a rill exceeds the sediment load, and the shear stress of the flow is larger than the critical shear stress of the soil. Soil deposition occurs when the sediment load in the flow is greater than the transport capacity. Erodibility and critical shear stress parameters are adjusted throughout the simulation period based on varying management and climatic conditions, such as the amount of residue, tillage, and freeze-thaw conditions.

WEPP has been extensively applied to simulate hydrological processes and water erosion on crop-, range-, and forestlands as well as in urban settings (e.g., Singh et al., 2011; Guo et al., 2021; Dobre et al., 2022). For inland Pacific Northwest, WEPP has been tested and used to estimate water erosion under different land use and management conditions (Greer et al., 2006; Pieri et al., 2007; Singh et al., 2009; Dun et al., 2009; Williams et al., 2010; Srivastava et al., 2011; Srivastava et al., 2013; Boll et al., 2015; Dahal et al., 2022). Recently, a new online web

interface called WEPPcloud has been developed, simplifying the WEPP modeling process and model parameters setup (Lew et al., 2022).

1.8. Goal and Objectives

Understanding how topographic, geological, and climatic factors interact with anthropogenic activities to influence hydrological and erosion processes is crucial to implementing targeted mitigation. The primary goal of this doctoral research is to assess critical factors and their interactions affecting nonpoint-source pollution in representative agricultural and urban settings in the US Pacific Northwest (PNW). The main objectives were to:

- elucidate the long-term historical soil erosion trend, as affected by climatic and management conditions;
- assess changes in water erosion as impacted by the projected future climate and the effect of conservation practices; and
- optimize placement of rain gardens in an urbanizing watershed, south Puget Sound, using the Hydrologic Sensitivity Index (HSI) method.

1.9 Dissertation Outline

This dissertation consists of three technical chapters following the introduction chapter. Chapter 2 assesses the long-term changes in water erosion in the rainfed wheat-based croplands of eastern Washington as impacted by climate and management practices via WEPP modeling, with a focus on three watersheds in the three distinct precipitation zones (low, intermediate, and high). This chapter was accepted for publication in the *Journal of ASABE*. Chapter 3 determines changes in water erosion in these three model watersheds of eastern Washington as impacted by projected future climate and select conservation practices. Chapter 4 identifies suitable locations for siting rain gardens in an urbanizing watershed in western Washington using an index

approach. In this study, I examine the interactive effect of land use and cover as well as soil and topographic factors on stormwater runoff in the Lower Puyallup River watershed of south Puget Sound. Chapter 5 summarizes the major results and findings of this dissertation and provides recommendation for future work.

REFERENCES

Anache, J.A., Flanagan, D.C., Srivastava, A., & Wendland, E.C. (2018). Land use and climate change impacts on runoff and soil erosion at the hillslope scale in the Brazilian Cerrado. *Science of the Total Environment, 622*, 140–151.

Baker, L.A. (1992). Introduction to nonpoint source pollution in the United States and prospects for wetland use. *Ecological Engineering, 1*(1–2), 1–26.

Boll, J., Brooks, E.S., Crabtree, B., Dun, S., & Steenhuis, T.S. (2015). Variable source area hydrology modeling with the water erosion prediction project model. *Journal of the American Water Resources Association, 51*(2), 330–342.

Borah, D.K., Yagow, G., Saleh, A., Barnes, P.L., Rosenthal, W., Krug, E.C., & Hauck, L.M. (2006). Sediment and nutrient modeling for TMDL development and implementation. *Transactions of ASABE, 49*, 967–986.

Boyabatlı, O., Nasiry, J., & Zhou, Y. (2019). Crop planning in sustainable agriculture: Dynamic farmland allocation in the presence of crop rotation benefits. *Management Science, 65*(5), 2060–2076.

Brooks, E.S., Saia, S.M., Boll, J., Wetzel, L., Easton, Z.M., & Steenhuis, T.S. (2015). Assessing BMP effectiveness and guiding BMP planning using process-based modeling. *Journal of American Water Resources Association, 51*, 343–358.

Chen, H., Guo, S., Xu, C.Y., & Singh, V.P. (2007). Historical temporal trends of hydro-climatic variables and runoff response to climate variability and their relevance in water resource management in the Hanjiang basin. *Journal of Hydrology, 344*(3–4), 171–184.

Christman, Z., Meenar, M., Mandarano, L., & Hearing, K. (2018). Prioritizing suitable locations for green stormwater infrastructure based on social factors in Philadelphia. *Land, 7*(4), 145.

Claassen, R., Bowman, M., McFadden, J., Smith, D., & Wallander, S. (2018). Tillage intensity and conservation cropping in the United States (No. 1476-2018-5723).

Coolman, R.M., & Hoyt, G.D. (1993). The effects of reduced tillage on the soil environment. *HortTechnology, 3*(2), 143–145.

Cruse, R. M., Herzmann, D.E., Gelder, B.K., James, D.E., & Flanagan, D.C. (2023). Impacts of Changing Precipitation Events on Landscape Soil Erosion Estimates. In *Soil Erosion Research Under a Changing Climate*, January 8–13, 2023, Aguadilla, Puerto Rico, USA (p. 1). American Society of Agricultural and Biological Engineers.

Dagenais, D., Thomas, I., & Paquette, S. (2017). Siting green stormwater infrastructure in a neighbourhood to maximise secondary benefits: Lessons learned from a pilot project. *Landscape Research, 42*(2), 195–210.

Dahal, M. S., Wu, J.Q., Boll, J., Ewing, R.P., & Fowler, A. (2022). Spatial and agronomic assessment of water erosion on inland Pacific Northwest cereal grain cropland. *Journal of Soil and Water Conservation, 77*(4), 347–364.

Davis, A.P., Hunt, W.F., Traver, R.G., & Clar, M. (2009). Bioretention technology: Overview of current practice and future needs. *Journal of Environmental Engineering*, 135(3), 109–117.

De Baets, S., Poesen, J., Meersmans, J., & Serlet, L. (2011). Cover crops and their erosion-reducing effects during concentrated flow erosion. *Catena*, 85(3), 237–244.

Devia, G.K., Ganasri, B.P., & Dwarakish, G.S. (2015). A review on hydrological models. *Aquatic Procedia*, 4, 1001–1007.

Diodato, N., Guerriero, L., Fiorillo, F., Esposito, L., Revellino, P., Grelle, G., & Guadagno, F.M. (2014). Predicting monthly spring discharges using a simple statistical model. *Water Resources Management*, 28(4), 969–978.

Dobre, M., Srivastava, A., Lew, R., Deval, C., Brooks, E.S., Elliot, W.J., & Robichaud, P. R. (2022). WEPPcloud: An online watershed-scale hydrologic modeling tool. Part II. Model performance assessment and applications to forest management and wildfires. *Journal of Hydrology*, 610, 127776.

Dun, S., Wu, J.Q., Elliot, W.J., Robichaud, P.R., Flanagan, D.C., Frankenberger, J. R., Brown, R. E., & Xu, A. C. (2009). Adapting the Water Erosion Prediction Project (WEPP) model for forest applications. *Journal of Hydrology*, 366(1–4), 46–54. https://doi.org/10.1016/j.jhydrol.2008.12.019

Dunn, C.P., Stearns, F., Guntenspergen, G.R., & Sharpe, D.M. (1993). Ecological benefits of the conservation reserve program. *Conservation Biology*, 7(1), 132–139.

Flanagan, D.C., & Nearing, M.A. ed. (1995). USDA-Water Erosion Prediction Project hillslope profile and watershed model documentation. National Soil Erosion Research Laboratory Report No. 10. West Lafayette, IN: USDA ARS National Soil Erosion Research Laboratory.

Franzetti, S.M. (2005). Background and history of stormwater regulations. Sponsored by Lorman Education Services: Oak Brook, IL.

Gilley, J.E., Eghball, B., Kramer, L.A., & Moorman, T.B. (2000). Narrow grass hedge effects on runoff and soil loss. *Journal of Soil and Water Conservation*, 55(2), 190–196.

Göbel, P., Dierkes, C., & Coldewey, W.G. (2007). Storm water runoff concentration matrix for urban areas. *Journal of Contaminant Hydrology*, 91(1–2), 26–42.

Gould, G.K., Liu, M., Barber, M.E., Cherkauer, K.A., Robichaud, P.R., & Adam, J.C. (2016). The effects of climate change and extreme wildfire events on runoff erosion over a mountain watershed. *Journal of Hydrology*, 536, 74–91.

Greer, R.C., Wu, J.Q., Singh, P., & McCool, D.K. (2006). WEPP simulation of observed winter runoff and erosion in the US Pacific Northwest. *Vadose Zone Journal*, 5(1), 261–272.

Harrington, W., Krupnick, A.J., & Peskin, H.M. (1985). Policies for nonpoint-source water pollution control. *Journal of Soil and Water Conservation*, 40(1), 27–32.

Himanshu, S.K., Pandey, A., Yadav, B., & Gupta, A. (2019). Evaluation of best management practices for sediment and nutrient loss control using SWAT model. *Soil and Tillage Research*, 192, 42–58.

Horan, R.D., & Ribaudo, M.O. (1999). Policy objectives and economic incentives for controlling agricultural sources of nonpoint pollution 1. *Journal of the American Water Resources Association*, 35(5), 1023–1035.

Hunt, W.F., Davis, A.P., & Traver, R.G. (2012). Meeting hydrologic and water quality goals through targeted bioretention design. *Journal of Environmental Engineering*, 138(6), 698–707.

Inkpen, E.L., & Embrey, S.S. (1998). Nutrient transport in the major rivers and streams of the Puget Sound Basin, Washington. US Department of the Interior, US Geological Survey.

Jarihani, B., Sidle, R.C., Bartley, R., Roth, C.H., & Wilkinson, S.N. (2017). Characterisation of hydrological response to rainfall at multi spatio-temporal scales in savannas of semi-arid Australia. *Water*, 9(7), 540.

Junhua, Y., Guoyi, Z., Deqiang, Z., & Xu, W. (2003). Spatial and temporal variations of some hydrological factors in a climax forest ecosystem in the Dinghushan region. *Acta Ecologica Sinica*, 23(11), 2359–2366.

Kaspar, T.C., & Singer, J.W. (2011). The use of cover crops to manage soil. Soil management: Building a stable base for agriculture, p. 321–337.

Kurkalova, L.A. (2015). Cost-effective placement of best management practices in a watershed: Lessons learned from conservation effects assessment project. *Journal of the American Water Resources Association*, 51(2), 359–372.

Lew, R., Dobre, M., Srivastava, A., Brooks, E.S., Elliot, W.J., Robichaud, P.R., & Flanagan, D.C. (2022). WEPPcloud: An online watershed-scale hydrologic modeling tool. Part I. Model description. *Journal of Hydrology.*, 608, 127603. https://doi.org/10.1016/j.jhydrol.2022.127603

Lovell, S.T., & Sullivan, W.C. (2006). Environmental benefits of conservation buffers in the United States: Evidence, promise, and open questions. *Agriculture, Ecosystems & Environment*, 112(4), 249–260.

Malik, R.K., Green, T.H., Brown, G.F., & Mays, D. (2000). Use of cover crops in short rotation hardwood plantations to control erosion. *Biomass and Bioenergy*, 18(6), 479–487.

Martin-Mikle, C.J., de Beurs, K.M., Julian, J.P., & Mayer, P.M. (2015). Identifying priority sites for

low impact development (LID) in a mixed-use watershed. *Landscape and Urban Planning*, 140, 29–41. https://doi.org/10.1016/j.landurbplan.2015.04.002

McGregor, K.C., Greer, J.D., & Gurley, G.E. (1975). Erosion control with no-till cropping practices. *Transactions of the ASAE*, 18(5), 918–920.

McCarthy, S.G., Incardona, J.P., & Scholz, N.L. (2008). Coastal storms, toxic runoff, and the sustainable conservation of fish and fisheries. In *American Fisheries Society Symposium* (Vol. 64, No. 12, pp. 7–27).

Mein, R.G., & Larson, C.L. (1973). Modeling infiltration during a steady rain. *Water Resources Research*, 9(2), 384–394.

Montgomery, D. R. (2007). Soil erosion and agricultural sustainability. *Proceedings of the National Academy of Sciences of the United States of America*, 104, 13268–13272.

Moldenhauer, W.C., Langdale, G.W., Frye, W., McCool, D.K., Papendick, R.I., Smika, D.E., & Fryrear, D.W. (1983). Conservation tillage for erosion control. *Journal of Soil and Water Conservation*, 38(3), 144–151.

Nikolic, V.V., Simonovic, S.P., & Milicevic, D.B. (2013). Analytical support for integrated water resources management: a new method for addressing spatial and temporal variability. *Water Resources Management*, 27, 401–417.

NRCS, U. (2005). Residue and tillage management no till/strip till/direct seed. Conservation National Conservation Practice Standard, 329.

Osei-Twumasi, A., Falconer, R.A., & Bockelmann-Evans, B.N. (2015). Experimental studies on water and solute transport processes in a hydraulic model of the Severn estuary, UK. *Water Resources Management*, 29(6), 1731–1748.

Panagopoulos, Y., Makropoulos, C., & Mimikou, M. (2011). Diffuse surface water pollution: driving factors for different geoclimatic regions. *Water Resources Management*, 25, 3635–3660.

Parikh, P., Taylor, M.A., Hoagland, T., Thurston, H., & Shuster, W. (2005). Application of market mechanisms and incentives to reduce stormwater runoff: An integrated hydrologic, economic and legal approach. *Environmental Science & Policy*, 8(2), 133–144.

Perez-Pedini, C., Limbrunner, J.F., & Vogel, R.M. (2005). Optimal location of infiltration-based best management practices for storm water management. *Journal of Water Resources Planning and Management*, 131(6), 441–448.

Pieri, L., Bittelli, M., Wu, J.Q., Dun, S., Flanagan, D.C., Pisa, P.R., ... & Salvatorelli, F. (2007). Using the Water Erosion Prediction Project (WEPP) model to simulate field-observed runoff and erosion in the Apennines mountain range, Italy. *Journal of hydrology*, 336(1–2), 84–97.

Rittenburg, R.A., Squires, A.L., Boll, J., Brooks, E.S., Easton, Z.M., & Steenhuis, T.S. (2015).

Agricultural BMP effectiveness and dominant hydrological flow paths: concepts and a review. *Journal of the American Water Resources Association*, 51(2), 305–329.

Sage, J., Berthier, E., & Gromaire, M.C. (2015). Stormwater management criteria for on-site pollution control: A comparative assessment of international practices. *Environmental Management*, 56, 66–80.

Sajikumar, N., & Remya, R.S. (2015). Impact of land cover and land use change on runoff characteristics. *Journal of Environmental Management*, 161, 460–468.

Singh, P., Wu, J.Q., McCool, D.K., Dun, S., Lin, C.H., & Morse, J.R. (2009). Winter hydrologic and erosion processes in the US Palouse region: Field experimentation and WEPP simulation. *Vadose Zone Journal*, 8(2), 426–436.

Singh, R.K., Panda, R.K., Satapathy, K.K., & Ngachan, S.V. (2011). Simulation of runoff and sediment yield from a hilly watershed in the eastern Himalaya, India using the WEPP model. *Journal of Hydrology*, 405(3-4), 261–276.

Snyder, K.A., & Tartowski, S.L. (2006). Multi-scale temporal variation in water availability: implications for vegetation dynamics in arid and semi-arid ecosystems. *Journal of Arid Environments*, 65(2), 219–234.

Srivastava, A., Dobre, M., Bruner, E., Elliot, W.J., Miller, I.S., & Wu, J.Q. (2011). Application of the Water Erosion Prediction Project (WEPP) model to simulate streamflow in a PNW forest watershed. In *International Symposium on Erosion and Landscape Evolution (ISELE)*, 18-21 September 2011, Anchorage, Alaska (p. 40). American Society of Agricultural and Biological Engineers.

Srivastava, A., Dobre, M., Wu, J.Q., Elliot, W.J., Bruner, E.A., Dun, S., ... & Miller, I.S. (2013). Modifying WEPP to improve streamflow simulation in a Pacific Northwest watershed. *Transactions of the ASABE*, 56(2), 603-611.

Srivastava, P., Migliaccio, K.W., and Simune, J. (2007), Landscape models for simulating water quality at point, field, and watershed scales. *Transaction of ASABE*, 50, 1683–1693.

Stubbs, M. (2014). *Conservation Reserve Program (CRP): Status and Issues*. Washington, DC, USA: Library of Congress, Congressional Research Service.

Shen, Z., Liao, Q., Hong, Q., & Gong, Y. (2012). An overview of research on agricultural nonpoint source pollution modelling in China. *Separation and Purification Technology*, 84, 104–111.

Thaler, E.A., Larsen, I.J., & Yu, Q. (2021). The extent of soil loss across the US Corn Belt. *Proceedings of the National Academy of Sciences*, 118(8), e1922375118.

Trimble, S.W., & Crosson, P. (2000). US soil erosion rates--myth and reality. *Science*, 289(5477), 248–250.

Triplett Jr, G.B., & Dick, W.A. (2008). No-tillage crop production: A revolution in agriculture!. *Agronomy Journal*, 100, S-153.

United States Department of Agriculture (USDA). (1978). *Palouse Cooperative River Basin Study*. USDA Soil Conservation Service, Forest Service, and Economics, Statistics, and Cooperative Service.

Vitousek, P.M., Aber, J.D., Howarth, R.W., Likens, G.E., Matson, P.A., Schindler, D.W., … & Tilman, D.G. (1997). Human alteration of the global nitrogen cycle: Sources and consequences. *Ecological Applications, 7*(3), 737–750.

Walter, M.T., Walter, M.F., Brooks, E.S., Steenhuis, T.S., Boll, J., & Weiler, K. (2000). Hydrologically sensitive areas: Variable source area hydrology implications for water quality risk assessment. *Journal of Soil and Water Conservation, 55*(3), 277–284.

Wanielista, M.P., & Yousef, Y.A. (1992). *Stormwater management*. John Wiley & Sons.

Washington State Department of Ecology (WSDE). (2021). Water Quality. https://ecology.wa.gov/About-us/Who-we-are/Our-Programs/Water-Quality Accessed on September 2021

Wei, W., Chen, L., Fu, B., & Chen, J. (2010). Water erosion response to rainfall and land use in different drought-level years in a loess hilly area of China. *Catena, 81*(1), 24–31.

Williams, J.D., Dun, S., Robertson, D.S., Wu, J.Q., Brooks, E.S., Flanagan, D.C., & McCool, D.K. (2010). WEPP simulations of dryland cropping systems in small drainages of northeastern Oregon. *Journal of Soil and Water Conservation, 65*(1), 22–33.

Wu, J., & Lu, J. (2019). Landscape patterns regulate nonpoint source nutrient pollution in an agricultural watershed. *Science of the Total Environment, 669*, 377–388.

Xepapadeas, A. (2011). The economics of non-point-source pollution. *Annual Review of Resources Economic, 3*(1), 355–373.

Xia, Y., Zhang, M., Tsang, D.C., Geng, N., Lu, D., Zhu, L., ... & Ok, Y.S. (2020). Recent advances in control technologies for nonpoint source pollution with nitrogen and phosphorous from agricultural runoff: current practices and future prospects. *Applied Biological Chemistry, 63*(1), 1–13.

Yair, A. (2004). Raz**-** Yassif N. Hydrological Processes in a Small Arid Catchment: Scale Effects of Rainfall and Slope Length, 6(1/2), 155–169.

Yang, Y.Y., & Toor, G.S. (2018). Stormwater runoff driven phosphorus transport in an urban residential catchment: Implications for protecting water quality in urban watersheds. *Scientific reports, 8*(1), 11681.

Young, R.A., Onstad, C.A., Bosch, D.D., & Anderson, W.P. (1989). AGNPS: A nonpoint-source

pollution model for evaluating agricultural watersheds. *Journal of Soil and Water Conservation, 44*(2), 168–173.

2. SIMULATION OF LONG-TERM WATER EROSION IN RAINFED CROPLANDS OF EASTERN WASHINGTON

2.1. Introduction

In the inland Pacific Northwest (PNW), water erosion has been a significant threat to agricultural production and the environment since the area's large-scale wheat production began in the early 1880s (USDA, 1978). Major factors of erosion in this area include hilly topography, wet winters with numerous freeze-thaw cycles, rain on thawing soil, silt loam soil prone to erosion, and conventional tillage that pulverizes the soil and leaves it bare (Papendick et al., 1995; Greer et al., 2006). Annual precipitation varies across the region, with distinct annual precipitation zones from west to east: low (<380 mm), intermediate (380–460 mm), and high (>460 mm). Highly variable erosion rates across the area have been reported (Kok et al., 2009; Dahal et al., 2022).

Multiple studies have been carried out to assess water erosion in the area. USDA (1978) applied the USLE technique (Wischmeier and Smith, 1978) to estimate erosion for major soils and crop rotations of that time for all three precipitation zones of the Palouse River Basin, located in the southern part of the inland PNW. Average annual erosion rates were estimated as 29, 45, and 27 Mg ha^{-1} for the low-, intermediate-, and high-precipitation zones, far exceeding the NRCS's soil loss tolerance level of 11 Mg ha^{-1} yr^{-1} (Soil Science Division Staff, 2017).

Extensive field assessment of soil erosion in Whitman County, WA, was conducted across 400,000 ha of cropland by USDA Soil Conservation Service agronomist Verle Kaiser during 1940–1982. The survey involved visually assessing soil loss due to different types of erosion (rill, gully, and soil-slip) for various "land capability classes" (USDA, 1978), which represent land types classified by their suitability for agricultural use (Klingebiel and

Montgomery, 1961). The same fields were surveyed and sampled each spring, mainly within the intermediate- and high-precipitation zones (Figure 1). The Alutin method, which measures multiple cross-sectional areas of a rill, each along a transect, was used to quantify rill erosion. This investigation revealed a high annual erosion rate averaging 53.8 Mg ha^{-1} (McCool and Roe, 2005). Erosion rate decreased from 1983 to 2004, possibly due to less severe weather conditions and an increase in conservation farming practices (McCool and Roe, 2005).

A long-term experimental study was carried out by McCool et al. (2006) at the Palouse Conservation Field Station near Pullman, WA, in the high-precipitation zone. Water erosion from natural precipitation events was measured in multiple runoff plots from 1978 to 1991. Various crop rotations, including (i) continuous bare fallow and (ii) winter wheat followed by one of winter wheat, summer fallow, spring peas, or another small grain, were implemented under either tilled or no-till conditions. The authors report annual erosion rates as high as 120.6 Mg ha^{-1} for continuous bare fallow, 18.2 Mg ha^{-1} for winter-wheat summer fallow for the tilled condition, and 0.12 Mg ha^{-1} for continuous winter wheat under no-till.

Kok et al. (2009) applied RUSLE2 (Renard et al., 1996; Foster et al., 2003) to simulate soil erosion for all three precipitation zones in the study area. The study was part of Solutions To Environmental and Economic Problems (STEEP), a USDA-funded project. For the years 1975, 1990, and 2005, corresponding to the beginning, middle, and end of STEEP, crop rotations and tillage practices typical of those periods were used in the simulation. The simulated average erosion rates were 20, 27, and 45 Mg ha^{-1} in 1975, 14, 16, and 24 Mg ha^{-1} in 1990, and 10, 13, and 11 Mg ha^{-1} in 2005 for the low-, intermediate-, and high-precipitation zones, respectively, showing a consistent decrease in erosion over the course of the STEEP project.

Dahal et al. (2022) simulated 30-year (1989–2018) water erosion for 12 counties of eastern Washington using the WEPP (Water Erosion Prediction Project; Flanagan and Nearing, 1995; Flanagan et al., 2007) model. Their purpose was to understand the interacting effects of soil, climate, topography, crop rotation, and tillage on erosion, and to assess the spatial distribution of erosion in the area. The authors classified slopes (5 classes) and soil (3 classes), and overlaid the combination with the three precipitation zones and their unique crop rotations. Using three levels of tillage (intense, reduced, and no-till), they simulated 135 (5×3×3×3) scenarios and obtained countywide erosion results by area-weighting for each county. They showed that steep slopes and shallow soils generally led to the highest erosion rates, and reported the long-term average annual erosion in the low-, intermediate-, and high-precipitation zones as 3.8, 15.8, and 14.4 Mg ha^{-1}. For Whitman County, simulated average annual erosion rates were 13.0, 19.0, and 15.4 Mg ha^{-1} in the aforementioned precipitation zones, with 59, 57, and 54% of the areas having erosion rates exceeding the current NRCS soil loss tolerance level of 11 Mg ha^{-1} yr^{-1}. The erosion rates reported by Dahal et al. (2022) were slightly higher than those of Kok et al. (2009). In addition, the intermediate-precipitation zone generated the highest erosion rate in Dahal et al. (2022), while results were mixed in Kok et al. (2009).

Climate and management practices crucially influence soil erosion, causing considerable variation year-to-year (Li and Fang, 2016). Lin et al. (2020) assessed the temporal erosion trend during the period 1982–2015 in the semi-arid Hexi corridor of China using the integrated RUSLE-TLSD (Transport Limited Sediment Delivery; Renard et al., 1996) model. Their results showed remarkable variation in annual erosion rate due to variations in precipitation patterns and changes in crop management and conservation practice. For instance, erosion rates in 2012 were 1.3–5.0 times higher than in other years, even though the total annual precipitation was not

significantly higher than in other years. The high erosion rate was attributed to multiple heavy precipitation events with elevated erosive power, which was not experienced in other years. Similar temporal variation in erosion rates has been reported for eastern Washington (USDA, 1978; Ebbert and Roe, 1998; McCool and Roe, 2005; Dahal et al., 2022), with management practices (crop rotation, tillage) and variations in precipitation and temperature patterns being contributing factors (USDA, 1978; McCool and Roe, 2005; Dahal et al., 2022). A disproportionately large amount of erosion can occur in the wheat-planting portion of the crop rotation (Papendick, 1984; Dahal et al., 2022). The number of freeze-thaw cycles, the number of rain on thawing soil events, and the length of the frost period all vary year to year, and can also cause fluctuations in annual erosion (McCool and Roe, 2005; McCool et al., 2011).

Erosion simulation models have proven a more cost-effective tool than field experimentation for assessing management scenarios over large study areas (Panagopoulos et al., 2015). WEPP, a continuous, process-based, distributed-parameter simulation model for hydrology and water erosion (Flanagan and Nearing, 1995), has been previously applied to evaluate erosion effects of critical physical and management conditions, such as soil, topography, and various tillage practices (Williams et al., 2014; Brooks et al., 2015; Dahal et al., 2022).

Conservation practices have been adopted in the inland PNW since the mid-1980s (Kok, 2007; Dahal et al., 2022). Reduced tillage and annual cropping, instead of intensive tillage and fallow rotation, have been increasingly implemented by farmers in this region (Kok, 2007; Van Wie et al., 2013; Dahal et al., 2022). Assessing long-term erosion from the past to the present can help us understand the effects of changing management practices and climate processes that drive erosion. Therefore, the objectives of this study were to (i) apply the WEPP model to

simulate soil erosion in eastern Washington and evaluate the interactive effects of climate and management, in addition to topography and soil, on water erosion in the study area, and (ii) compare the simulation results with Kaiser's historical field dataset and elucidate the long-term soil erosion trend.

2.2. Materials and Methods

2.2.1. Study Area

Whitman County was chosen as the study area because it has more area in cereal-grain production (3.0×10^5 ha; USDA NASS 2018) than any other county in the region. Numerous studies on water erosion have been conducted in the area, including the collection of long-term field erosion data by Verle Kaiser (McCool and Roe, 2005). The county, located in southeastern Washington, has elevation ranging from 160–1250 m a.m.s.l. (USGS, 2019; Figure 1). The climate in the area is Mediterranean, with dry summers and wet winters. The low-, intermediate-, and high-precipitation zones respectively have 355, 450, and 533 mm of long-term average annual precipitation (NCDC, 2022), and are classified as Dsb per the Köppen-Geiger system (Kottek et al., 2006).

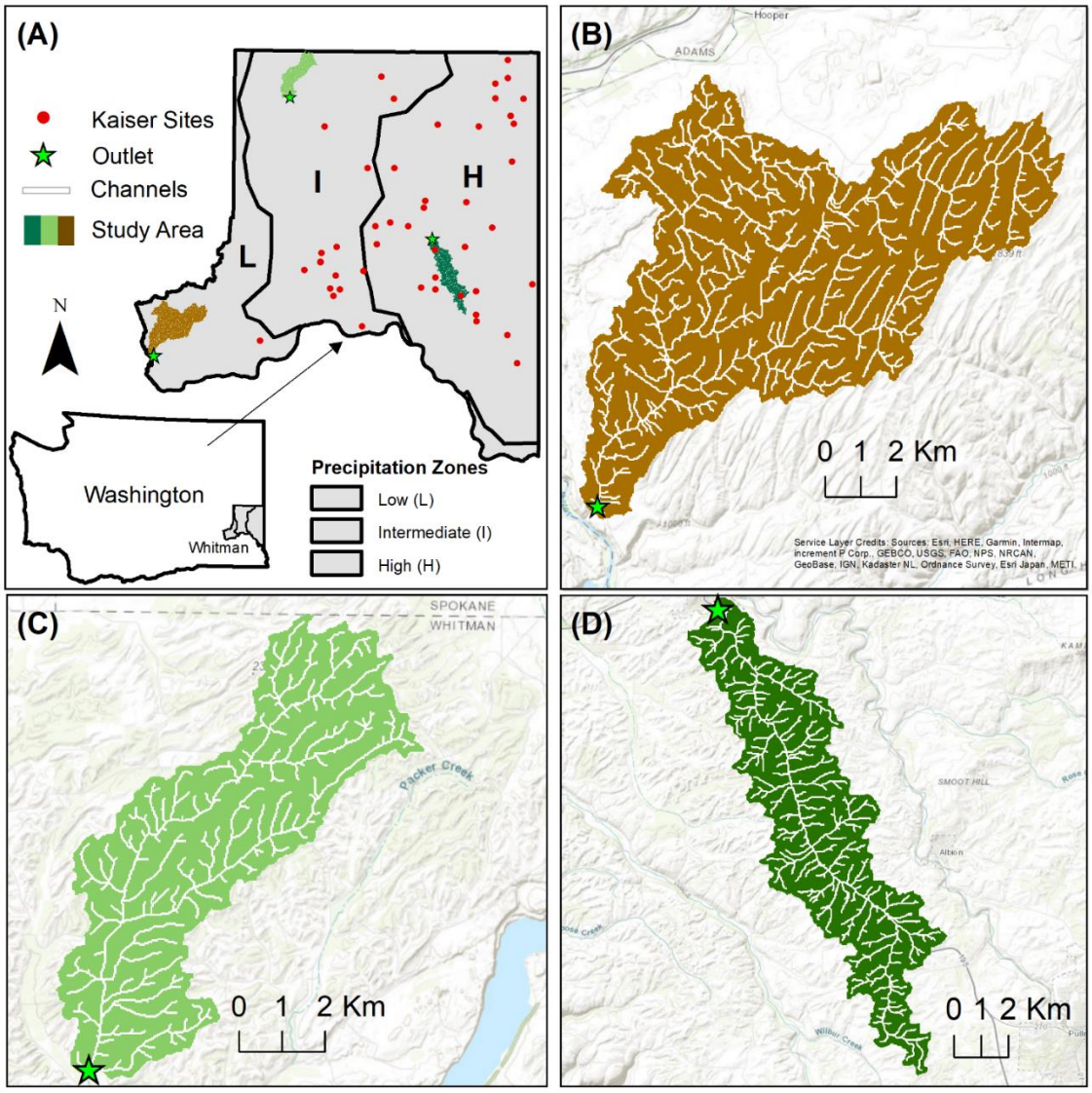

Figure 2.1. Model watersheds in Whitman County, Washington, delineated through the WEPPcloud interface (a), and close-ups of this study's (b) low-, (c) intermediate-, and (d) high-precipitation watersheds. Kaiser Sites are the field sites denoted "Sites with long history of observation" in the Kaiser study (Kaiser, 2021).

Topography varies from flat to having slope gradient greater than 45%, with steep slopes primarily present near the Snake River Canyon and in the high-precipitation zone, and gentle slopes predominating in the low-precipitation zone. Soil texture is mainly silt loam, with most soils being either Mollisols formed from aeolian deposits, or Andisols formed from volcanic ash (Papendick et al., 1995; Shepherd, 1985). Intense tillage with multiple operations and a winter wheat-summer fallow rotation were commonly used in the past. Since the mid-1980s, reduced-

and no-till, together with crop rotations, have been increasingly adopted (McCool and Roe, 2005; Kok, 2007). Limited by available soil water, dominant crop rotations in the low-, intermediate-, and high-precipitation zones are respectively winter wheat (*Triticum aestivum L.*)-fallow, winter wheat-spring barley (*Hordeum vulgare L.*)-fallow, and winter wheat-spring barley-pea (*Pisum sativum L.*) (Kok et al., 2007). One HUC-12 watershed within each precipitation zone was selected for WEPP simulation: Winn Lake Canyon Watershed (WLCW, HUC170601080805, henceforth WLCW-Low), Upper Imbler Creek Watershed (UICW, HUC170601090403, UICW-Intermediate), and Spring Flat Creek Watershed (SFCW, HUC170601080209, SFCW-High) for the low-, intermediate-, and high-precipitation zone (Figure 2.1).

2.2.2. Climate Analyses

Daily inputs of precipitation and temperature were obtained from weather stations (NCDC, 2022) within each of the precipitation zones: Pullman 2 NW WA 456789 (9 km from SFCW-High), Rosalia WA 457180 (30 km from UICW-Intermediate), and La Crosse 3 ESE WA 454338 (27 km from WLCW-Low). Inverse-distance-weighting was used to fill any missing data, using values from other stations within 100 km of the aforementioned three stations. Daily precipitation and minimum (T_{min}) and maximum temperatures (T_{max}) were aggregated to monthly, seasonally, and yearly values, and descriptive statistics were obtained. Climate data were divided into the "past" (1940–1982) during which the Kaiser data were collected, and the "present" (1983–2020) during which conservation farming has increasingly been adopted. The climate data within these two time periods were analyzed for:

- the number of precipitation events exceeding specified thresholds in each season,
- the number of freeze-thaw cycles and rain-on-thawing-soil events for each winter, with a thawing (frozen) soil defined as having frozen water in the soil profile less (more) than

the previous day, and a complete freeze-thaw cycle defined as the soil surface changing from unfrozen to frozen and back again, and

- (a) normality (Shapiro-Wilkes test), (b) change in means (annual average precipitation and average daily T_{max} and T_{min} with two-sample Student's *t*-test or Wilcoxon rank-sum test), and (c) linear trends (climate data in the past and present combined with linear regression or Mann Kendall test) in R (R Core Team, 2022), with parametric tests applied for normally-distributed data and non-parametric tests for non-normal distributions.

2.2.3. WEPP Simulations

The three model watersheds were initially selected using StreamStats (USGS, 2019), and their outlet information was used for watershed delineation in the WEPPcloud interface (Lew et al., 2022). Soil inputs were built for each hillslope, and WEPP was run to create a WEPPcloud project with detailed slope configuration and soil profile. This process was repeated to discretize the three model watersheds (Table 2.1). The three WEPPcloud projects were downloaded. Python scripts were developed to refine inputs, including dividing the default single Overland Flow Element (OFE) into two to better simulate saturation-excess runoff at the lower part of the hillslope (Boll et al., 2015; Brooks et al., 2015), which tends to occur near the bottom of a hillslope. WEPP simulation was again conducted with revised inputs using the utility program *wepppy* (Lew et al. 2021; https://github.com/rogerlew/wepppy), with Python scripts that execute command-prompt WEPP for each model watershed.

Table 2.1. Watershed discretization

	Area (ha)	Number of Hillslopes	Number of Channel Segments
WLCW-Low	8094	1632	721
UICW-Intermediate	3602	801	341
SFCW-High	5261	1163	507

2.2.3.1. WEPP Model Inputs

Climate

Six climate input files were created for the combination of two periods and three precipitation zones. The daily observed precipitation and temperature data for the three weather stations (near Pullman, Rosalia, and La Crosse) were used along with additional WEPP climate inputs. Event characteristics (duration, time to peak, peak intensity), dew-point temperature, and wind speed and direction were generated using CLIGEN 5.3 (Nicks et al., 1995, Srivastava et al., 2019) due to lack of observed data, breakpoint or in other forms of fine temporal resolution (e.g. 5-min), which often do not match the actual weather patterns and could be a potential source of error.

Slope

SFCW-High and UICW-Intermediate are dominated by rolling hills, with 53% and 57% of area falling in the 10–15% slope steepness, respectively (Figure 2.2). In contrast, WLCW-Low is flatter, with slopes <10% and 10–15% covering 61% and 26% of the area, respectively. Delineated hillslopes shorter than 50 m or longer than 300 m account for less than 14% in each of the three watersheds. Hillslopes 100–200 m long are the most common, covering 39% of WLCW-Low, 56% of UICW-Intermediate, and 52% of SFCW-High. Each hillslope was divided into two OFEs of equal length. Slope length was limited to 200 m, the maximum value in Meyer (1982) reporting soil losses measured on experimental plots of varying slope lengths across the United States.

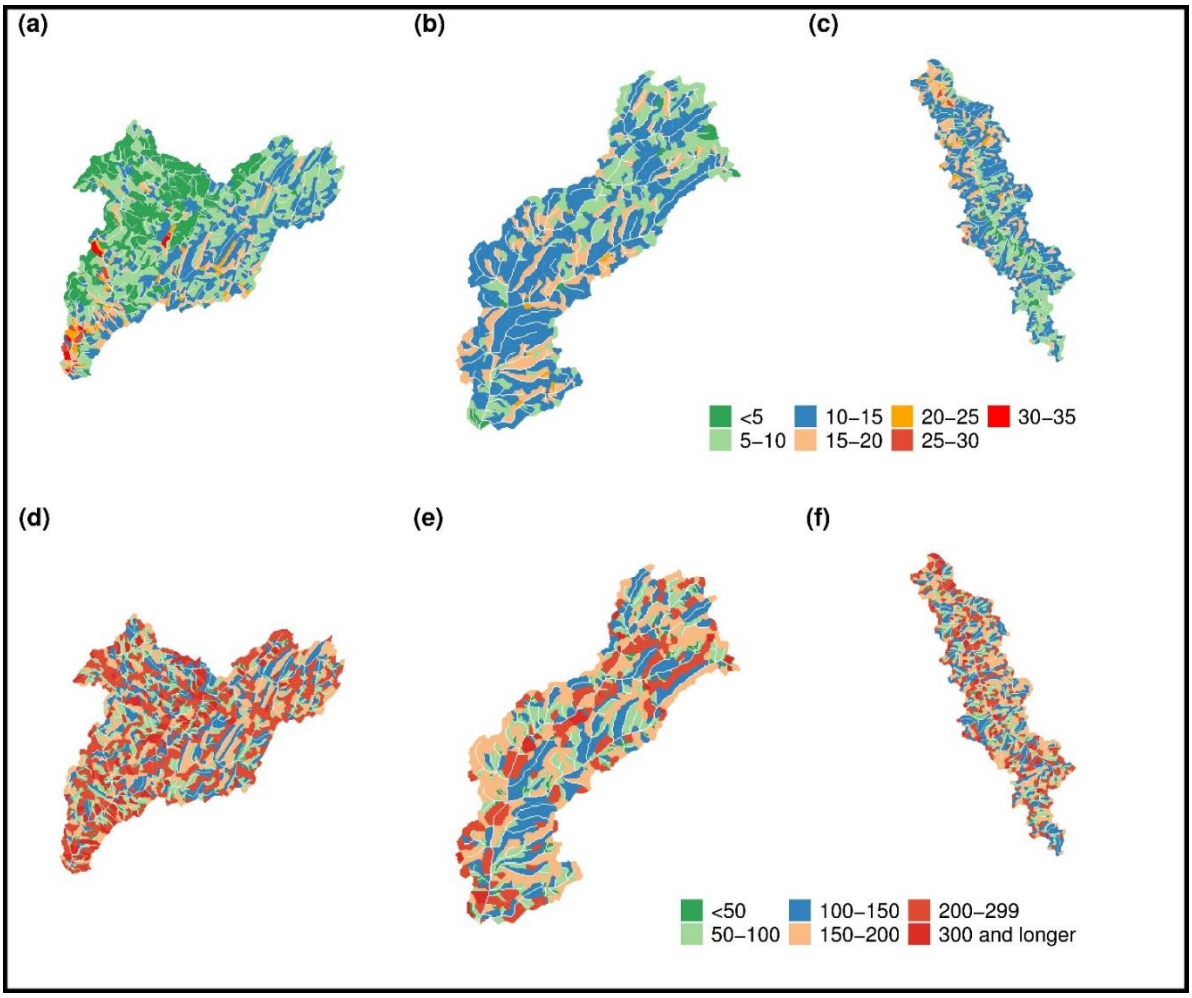

Figure 2.2. Variation of percent slope gradient (a: WLCW-Low, b: UICW-Intermediate, c: SFCW-High) and slope length in m (d, e, f) across the selected watersheds.

Soil

The soils in both UICW-Intermediate and SFCW-High tend to be deep, with 100% and 92% >1200 mm, whereas only 41% of the soils in WLCW-Low are >1200 mm, and 55% are 800–1200 mm deep. Hillslope soil inputs were extracted from SSURGO and further synthesized and computed based on literature (e.g. WEPP Technical Documentation, Flanagan and Nearing, 1995) within WEPPcloud. Key hydraulic and erosion properties of the soil, namely the baseline hydraulic conductivity (K_b, mm hr^{-1}), interrill erodibility (K_i, kg s m^{-4}), rill erodibility (K_r, s m^{-1}), and critical shear (τ_c, N m^{-2}), were adjusted following the WEPP User Summary (Flanagan and Livingston, 1995) and applied following Dahal et al. (2022) (Table 2.2).

Management

A single crop rotation of winter wheat-fallow with 100% intense tillage was used for the past (1940–1982) following McCool and Roe (2005). For the present (1983–2020), crop rotations vary by precipitation zone, and tillage practices were comprised of intense-, reduced-, and no-till with their annual percentages interpolated or extrapolated from county-level data reported by USDA NASS (2012, 2017) following Dahal et al. (2022). Because there was no tillage information by precipitation zone, the county-level tillage areal percentages were assumed for each watershed. Management input parameters for various tillage operations and specific crops for each rotation-tillage combination were based on Dahal et al. (2022); an example is presented in Table 2.3.

Table 2.2. Major soil inputs for a predominantly deep soil (Palouse silt loam)

Soil inputs	Value
Texture	Silt loam
Soil name	Palouse Silt Loam
Mukey	68563
Albedo	0.16
Initial saturation of soil, $m^3\ m^{-3}$	0.4
Baseline interrill erodibility K_i, kg s m^{-4}	9.8×10^6
Baseline rill erodibility K_r, s m^{-1}	0.0178
Baseline critical shear τ_c, N m^{-2}	0.35
Depth to the restrictive layer, m	1.5
Restrictive layer hydraulic conductivity, mm hr^{-1}	0.00072

Table 2.3. Major management inputs for wheat under intense tillage in a wheat-barley-pea rotation

Management inputs	Value
Ridge height value after tillage, m	0.075
Ridge interval, m	0.30
Fraction of residue buried by chisel plow*	0.65
Fraction of residue buried by moldboard plow*	0.80
Depth of tillage for chisel and moldboard plow, m	0.20
Depth of tillage for spike tooth harrow, m	0.076
Random roughness value after spike tooth harrowing, m	0.025
Fraction of surface area disturbed	1.0
Row width, m	0.18
Maximum canopy height for winter wheat, m	1.0
Canopy cover coefficient for winter wheat	5.2
Initial ridge height after last tillage, m	0.08
Initial ridge roughness after last tillage, m	0.05
Initial snow depth, m	0.0
Initial frost depth, m	0.0
Initial dead root mass, kg m−2	0.4

*From Table 9.5.1 of WEPP documentation (Stott et al., 1995)

2.2.3.2. Simulations Scenarios

WEPP watershed (*v.* 2020.5) simulations were performed for the two time periods and three watersheds, with crop rotations and tillage intensities appropriate to the simulation periods and precipitation zones (Table 2.4). To account for the interactions between climatic and crop management conditions, we ran WEPP for each crop rotation with all possible starting phases. For example, for the first year of simulation for the present (1983), each of the three phases in the wheat-barley-pea (WBP) rotation could have been present in the field. Accordingly, this rotation was simulated three times by starting the crop rotation differently resulting in WBP, BPW, and PWB (Table 4, scenarios 24, 27, and 30). Likewise, WEPP runs with the past cropping system (wheat-fallow rotation and intense tillage) and the present climate were conducted starting with each phase for SFCW-High and UICW-Intermediate watersheds (Table 4, scenarios 20, 21, 33, and 34) to elucidate the erosion effect of climate.

Table 2.4. WEPP simulation scenarios

Winn Lake Canyon Watershed (WLCW-Low)				Upper Imbler Creek Watershed (UICW-Intermediate)				Spring Flat Creek Watershed (SFCW-High)			
Sce.	Period	Rotation*	Tillage	Sce.	Period	Rotation*	Tillage	Sce.	Period	Rotation*	Tillage
1	Past	WF	Intense	9	Past	WF	Intense	22	Past	WF	Intense
2		FW	Intense	10		FW	Intense	23		FW	Intense
3	Present	WF	Intense	11	Present	WBF	Intense	24	Present	WBP	Intense
4			Reduced	12			Reduced	25			Reduced
5			No-till	13			No-till	26			No-till
6		FW	Intense	14		BFW	Intense	27		BPW	Intense
7			Reduced	15			Reduced	28			Reduced
8			No-till	16			No-till	29			No-till
				17		FWB	Intense	30		PWB	Intense
				18			Reduced	31			Reduced
				19			No-till	32			No-till
				20		WF	Intense	33		WF	Intense
				21		FW	Intense	34		FW	Intense

*W: wheat; B: barley; P: pea; F: fallow; Sce. = Scenario

2.2.4. Analysis of WEPP Simulation Results

2.2.4.1. Aggregation

Annual (water years from October 1–September 30 of the following year) and monthly water balance and erosion results were aggregated for all hillslopes within each watershed for each scenario. Channel erosion was not examined in this study. The results from the scenarios testing different starting phases of the same crop rotation (e.g., scenarios 24, 27, and 30, Table 2.4) were averaged (assuming equal areal fraction) for each combination of tillage type, watershed, and simulation period. Subsequently, the averages for the three tillage types for each model watershed and period were area-weighted based on Whitman County tillage type proportions projected from data reported in USDA NASS (2017) as described by Dahal et al. (2022).

Statistical comparison ($\alpha = 0.05$) of the mean annual erosion rates was made for the two periods using either two-sample *t*-tests or the Wilcoxon rank-sum test, depending on the normality of the data. Correlation analysis ($\alpha = 0.05$) of event and annual erosion rate (Mg ha^{-1}),

water input (rain + melt) and runoff (mm), winter conditions, and hillslope properties was conducted for WLCW-Low, UICW-Intermediate, and SFCW-High for the "worst case" intense tillage scenarios.

2.2.4.2. Comparison with Kaiser Field Data

WEPP-simulated annual erosion results for the past were compared with the historical (Kaiser) annual field erosion data reported in McCool and Roe (2005). There is a lack of documentation in the literature of the specific fields examined in the Kaiser study, particularly their locations, even upon review of WSU library records of the survey archives (Kaiser, 2021). The fields denoted "sites with long history of observation" during the study had township and range information (Kaiser, 2021), which was digitized and mapped (Figure 1). Approximately 66% of these fields were in the high-precipitation zone, and 33% in the intermediate-precipitation zone. Based on this proportion, we area-weighted the WEPP-simulated annual erosion results for the high- and intermediate-precipitation zones, and compared the result with the Kaiser data.

2.3. Results and Discussion

2.3.1. Climate Characteristics

2.3.1.1. Mean comparison

Average annual precipitation increased from past to present by 24 mm in WLCW-Low and decreased by 41 mm in SFCW-High. In UICW-Intermediate, the 3 mm decrease is negligible (Table 2.5). The average daily temperatures (T_{max}, T_{min}) are greater in the present than in the past, except for average daily T_{min} in WLCW-Low. All increases in average daily temperatures except T_{min} in UICW-Intermediate were significant per the Wilcoxon rank-sum test (Table 5). The number of average annual rain-on-thawing-soil events increased significantly

from 19 to 23 in WLCW-Low and decreased significantly from 25 to 21 and 29 to 24 in UICW-Intermediate and SFCW-High, respectively.

Table 2.5. Comparison of means and long-term trends: average annual precipitation (P, mm), average daily maximum (Tmax) and minimum (Tmin) temperatures (°C), number of rain-on-thawing-soil events (RT), and freeze-thaw cycles (FT) of the past and present with p-values in parentheses. Non-parametric, Wilcoxon rank-sum and Mann Kendall tests were conducted for non-normal distributions. Significant tests (at $\alpha = 0.05$) are in bold face.

				Mean Comparison			Long-term Trend	
Watershed		Past	Present	Normality test $W^{*}(p)$	*t*-test $t(p)$	Wilcoxon rank-sum test $w^{**}(p)$	Linear Reg. slope $\beta^{\S}(p)$	Mann Kendall test $\tau^{\dagger}(p)$
WLCW-Low	P	353	377	0.99 (0.590)	−1.28 (0.205)		0.43 (0.280)	
	T_{max}	16.9	17.1	0.85 (<0.0001)		**638 (0.045)**		0.122 (0.103)
	T_{min}	2.9	2.7	0.94 (<0.0001)		941 (0.454)		−0.093 (0.214)
	FT	15	16	0.98 (0.25)	−0.92 (0.36)		0.02 (0.241)	
	RT	19	23	0.95 (0.010)		**535 (0.008)**		**0.247 (0.001)**
UICW-Intermediate	P	458	455	0.98 (0.410)	0.11 (0.911)		−0.15 (0.762)	
	T_{max}	14.4	14.9	0.91 (<0.0001)		**498 (0.001)**		**0.240 (0.001)**
	T_{min}	2.3	2.5	0.97 (0.050)		743 (0.298)		−0.043 (0.571)
	FT	16	15	0.97 (0.090)	0.92 (0.359)		0.01 (0.584)	
	RT	25	21	0.97 (0.040)		**1064 (0.020)**		**−0.138 (0.08)**
SFCW-High	P	552	511	0.98 (0.110)	1.75 (0.084)		−0.78 (0.117)	
	T_{max}	14.2	14.8	0.91 (<0.0001)		**474 (<0.0001)**		**0.228 (0.002)**
	T_{min}	2.6	2.9	0.96 (0.020)		**557 (0.006)**		**0.196 (0.009)**
	FT	17	16	0.98 (0.12)	0.064 (0.949)		0.01 (0.695)	
	RT	29	24	0.98 (0.40)	**2.99 (0.004)**		**−0.09 (0.021)**	

$^{*}W$, normality test statistic; $^{**}w$, Wilcoxon rank-sum test statistic; $^{\S}\beta$, linear regression slope; $^{\dagger}\tau$, Mann Kendall test statistic. WLCW, Winn Lake Canyon Watershed in the low-precipitation zone; UICW, Upper Imbler Creek Watershed in the intermediate-precipitation zone; SFCW, Spring Flat Creek Watershed in the high-precipitation zone

2.3.1.2. Long-term trend

Changes in annual precipitation were not significant (Table 5, Figure 2.3). T_{max} and T_{min} in SFCW-High and T_{max} in UICW-Intermediate have increased significantly, and long-term rain-on-thawing-soil events increased significantly in WLCW-Low and decreased significantly in UICW-Intermediate and SFCW-High (Table 5, Figure 3).

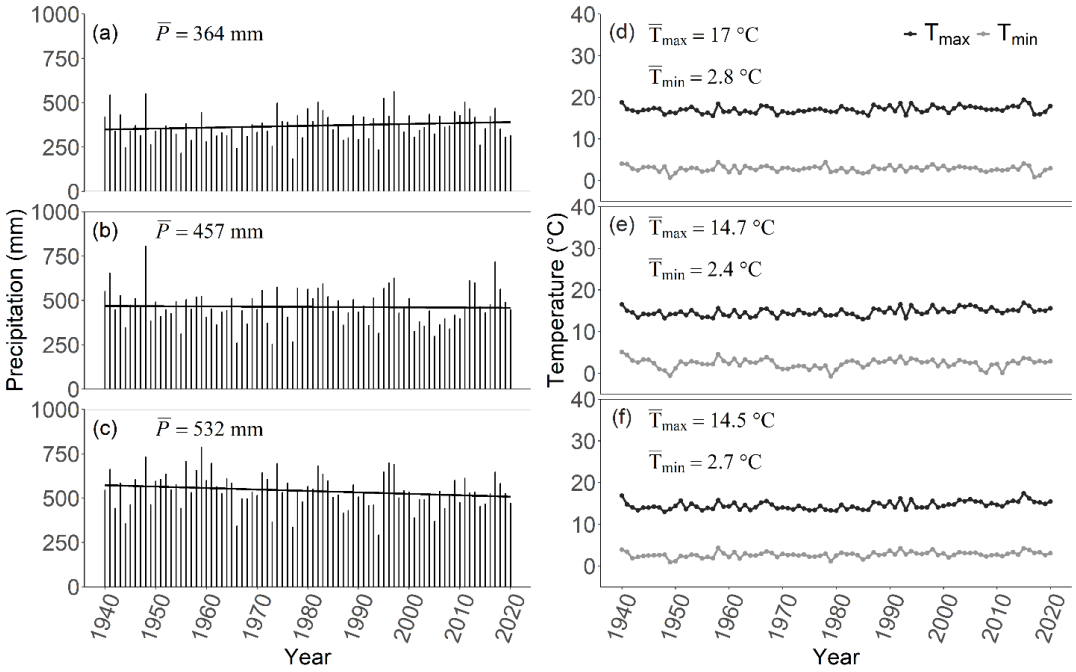

Figure 2.3. Temporal variation of annual precipitation (a, b, c) and mean daily temperatures (d, e, f) for the study watersheds WLCW-Low, UICW-Intermediate, and SFCW-High, respectively.

2.3.2. WEPP Simulation Results

2.3.2.1. Water balance

WEPP-simulated water balance for the three watersheds, WLCW-Low, UICW-Intermediate, and SFCW-High, changed from the past to the present, with change primarily due to changes in climatic conditions, or to changes in both climatic conditions and cropping systems (Table 2.6). In WLCW-Low, the cropping system (wheat-fallow rotation, intense tillage) has remained the same. However, the 7.3% increase in average annual precipitation increased the amount of every water balance component: soil water, runoff, ET, and lateral flow and deep percolation (together accounting for ~2%).

Table 2.6. Average annual water balance and erosion (with percentages of annual water balance outputs in parentheses) for the WLCW-Low, UICW-Intermediate, and SFCW-High study watersheds. Values are averages of results with different starting phases of crop rotation.

			Water Balance (mm)					
Watershed	Period	Tillage	Rain + snowmelt	Runoff	ET	LF + DP*	Soil water**	Erosion (Mg ha^{-1})
WLCW-Low	Past	Intense	357	32 (9)	315 (88)	6 (2)	180	13.5
	Present	Intense	383	41 (11)	333 (87)	7 (2)	190	13.3
		Reduced		31 (8)	343 (89)	8 (2)	198	5.8
		No-till		29 (7)	346 (90)	8 (2)	198	2.3
		Area-weighted¶						9.5
UICW-Intermediate	Past	Intense	464	87 (19)	368 (79)	5 (1)	309	34.5
	Present	Intense	462	77 (17)	383 (83)	3 (1)	270	22.9
		Reduced		59 (13)	400 (86)	3 (1)	288	8.0
		No-till		57 (12)	402 (87)	3 (1)	286	2.7
		Area-weighted						14.1
SFCW-High	Past	Intense	559	128 (23)	406 (73)	15 (3)	426	52.6
	Present	Intense	518	93 (18)	423 (82)	1 (0)	279	27.0
		Reduced		59 (11)	454 (87)	5 (1)	324	5.7
		No-till		55 (11)	457 (88)	5 (1)	324	2.2
		Area-weighted						15.5

*Lateral flow and deep percolation; **averaged daily, ¶Area-weighted average annual erosion based on percent areas of intense-, reduced-, and no-till in Whitman County

In UICW-Intermediate, changes in water balance are mainly due to changes in crop rotation, as average annual water input (rain + snowmelt) decreased by only 0.4%. For the intense tillage practice, the switch from the past wheat-fallow to a wheat-barley-fallow rotation increases annual crop consumptive use and total ET. The increase in ET in turn decreases soil water, which enhances infiltration and reduces runoff. These patterns also hold true under reduced- and no-till, which allowed even more ET and less runoff than intense tillage.

In SFCW-High, precipitation decreasing by 7.3% from past to present decreases the average annual runoff. For intense tillage, shifting from wheat-fallow to the three-year wheat-barley-pea rotation increases annual crop consumptive use and ET (Table 2.6), just as it did for

UICW-Intermediate. The increase in ET decreases soil water, enhances infiltration, and decreases runoff.

For all three watersheds within the present time period, a decrease in tillage intensity increases the amount of surface residue and resistance to surface water flow (Gilley and Weltz, 1995), thus decreasing runoff and increasing soil water and ET. The increase in ET removes more soil water, which allows more infiltration and in turn decreases runoff in a "virtuous" cycle.

3.3.2.2. Annual erosion

Area-weighted average annual simulated erosion decreased from the past by 32, 57, and 70% for the WLCW-Low, UICW-Intermediate, and SFCW-High watersheds, respectively. Area-weighting was based on the average erosion rates for intense-, reduced-, and no-till based on their present percent areas for Whitman County (Table 2.6). The decrease was not significant for WLCW-Low ($W = 998$, $p = 0.09$), but was significant for UICW-Intermediate ($W = 1280$, $p < 0.0001$) and SFCW-High ($W = 1484$, $p < 0.0001$) per the Wilcoxon rank-sum test. The non-parametric test was used because average annual erosion rates were non-normal for all three watersheds.

For WLCW-Low under a consistent wheat-fallow rotation and intense tillage, the erosion rate decreased by 1.5% (not significant; $W = 802$, $p = 0.891$) from past to present due to changes in climate (more detail in 3.2.2.1). Erosion rates under intense tillage decreased significantly from past to present by 34% for UICW-Intermediate ($W = 1065$, $p = 0.019$), and by 49% for SFCW-High ($W = 1294$, $p < 0.0001$). For the former, this is because runoff decreased due to the change in rotation from wheat-fallow to wheat-barley-fallow. For the latter, the even greater

decrease in erosion is due both to a similar change to a three-year crop rotation and to decreased average annual precipitation.

The simulated erosion rate also decreases with a decrease in tillage intensity, as the reduced- and no-till systems have more surface crop residues, which increase both infiltration and resistance to water flow and soil detachment. Overall, the WEPP-simulated erosion rates for all three watersheds decreased from past to present due to the combined effects of changes in climatic conditions and management practices, as elaborated in the next section.

Climate effect

Within any given crop rotation and tillage practice, WEPP-simulated erosion rate decreased from the past for all three watersheds. For WLCW-Low, the mean erosion rate for the past was 13.5 Mg ha^{-1} compared to the present 13.3 Mg ha^{-1} (Table 2.5). The simulation results differed according to the phase of the rotation. Starting the rotation with wheat yielded a decreased erosion rate at 12.6 Mg ha^{-1} compared to the past 14.3 Mg ha^{-1}, whereas starting with fallow led to an increased erosion rate at 14.0 Mg ha^{-1} compared to the past 12.7 Mg ha^{-1}. This discrepancy was due to a climate-rotation interaction: in the second scenario, the years with the highest annual precipitation, 1995 and 1997, coincide with wheat years, resulting in greater erosion in contrast to the first scenario in which these two years were fallow with lower erosion. For UICW-Intermediate and SFCW-High under intense tillage, annual erosion rates averaged over WF and FW were respectively 34.5 and 52.6 Mg ha^{-1} for the past, compared to 26.7 and 35.0 Mg ha^{-1} for the present.

For UICW-Intermediate, the decrease in annual precipitation by 0.7%, winter (Dec–Feb) precipitation by 5%, and the number of precipitation events greater than 15 mm (hereafter “large precipitation events”) by 25% led to a lower simulated average annual erosion. In SFCW-High,

the average annual precipitation, winter precipitation, and the number of large precipitation events all decreased from past to present (Table 2.5, Figure 2.4). This shift in precipitation patterns decreased the present simulated average annual runoff and erosion.

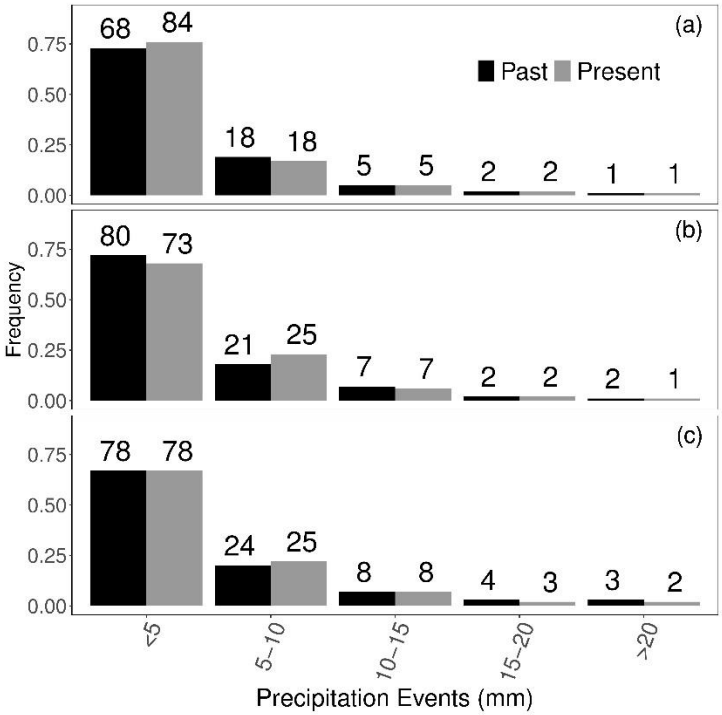

Figure 2.4. Distribution of size of precipitation events for the past and present. Bars represent event frequency, whereas values above the bars are averaged counts of annual precipitation events. (a) WLCW-Low, (b) UICW-Intermediate, and (c) SFCW-High study watersheds.

Management effect

Tillage effect

Decreasing tillage intensity (fewer tillage passes, shallower tillage, less residue buried) decreases simulated erosion rates for the same crop rotation and climate conditions. Incorporating conservation tillage practices in the present based on projected percent areas with conservation tillage in Whitman County led to the decrease in average annual erosion by 31%, 35%, and 40% in WLCW-Low, UICW-Intermediate, and SFCW-High, respectively, compared to the scenario where all the areas in the watershed remained under intense tillage (Table 2.5).

Crop rotation effect

The shift from wheat-fallow in the past to wheat-based three-year crop rotations in the present in UICW-Intermediate and SFCW-High contributes substantially to decreased erosion (Figure 2.5). WEPP-simulated average annual erosion rates under wheat-fallow for these two zones were 26.7 and 35.0 Mg ha^{-1}, both above those for wheat-barley-pea and wheat-barley-fallow regardless of the starting phase of the rotations.

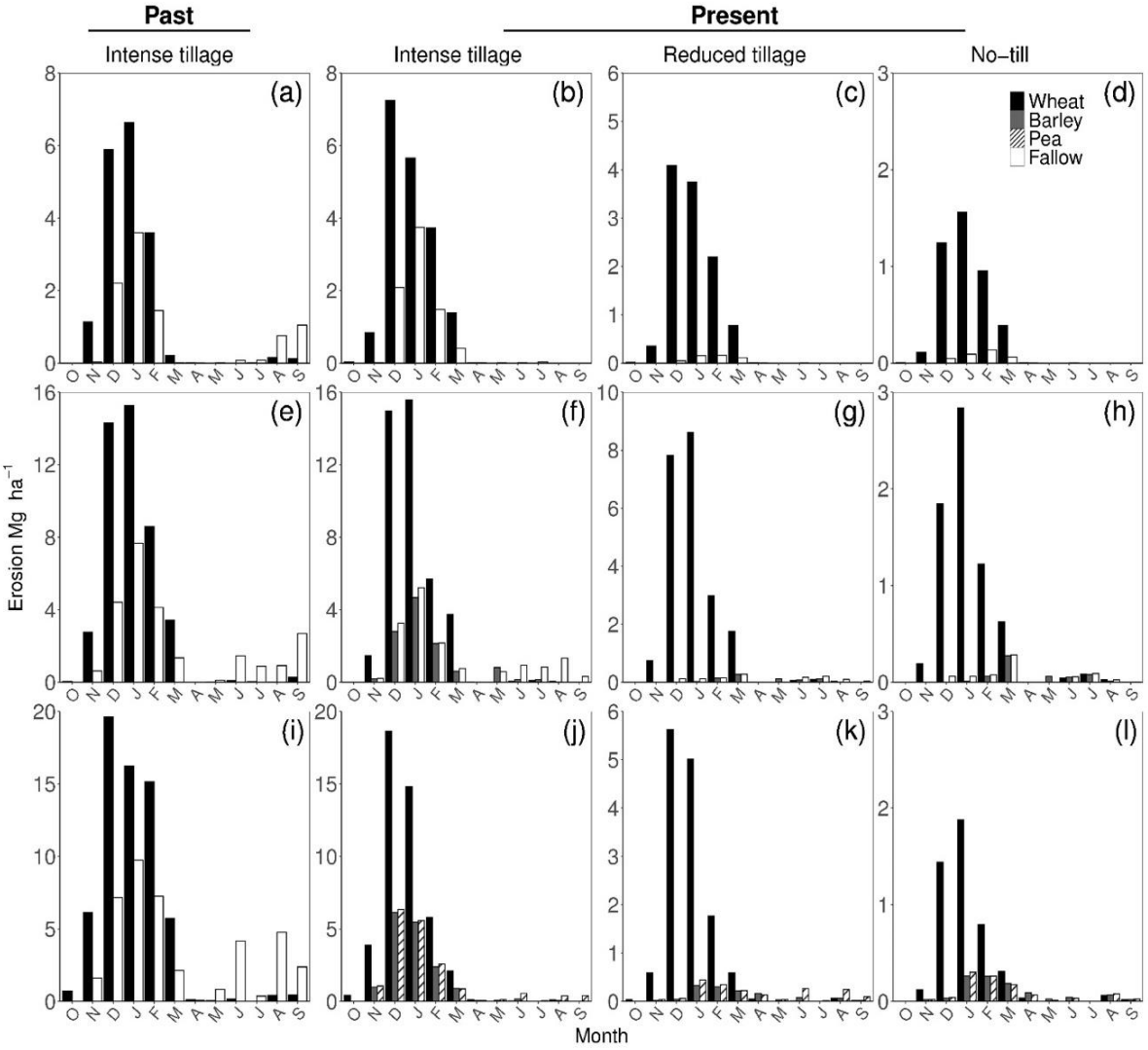

Figure 2.5. Average monthly erosion by crop year for the past and present. (a–d) WLCW-Low, (e–h) UICW-Intermediate, and (i–l) SFCW-High.

Wheat and fallow years tend to have high erosion rates. During wheat years, the winter rainy season coincides with low crop cover, as the late fall-planted crop may not have tillered yet. Additionally, in the intense tillage scenario, wheat requires multiple passes with intense pre-planting tillage in the fall, which increases soil erodibility. Fallow is practiced to accumulate soil water, but the greater soil water stored during the fallow year inhibits subsequent infiltration and in turn causes more runoff and erosion.

The "hypothetical" wheat-fallow rotation for the present (no longer practiced except in WLCW-Low) yielded an average daily soil water storage of 316 mm and 408 mm for UICW-Intermediate and SFCW-High, compared to 270 mm and 279 mm for the three-year (wheat-barley-fallow or wheat-barley-pea) rotations in their respective zones. In contrast, barley and pea, planted in mid-April after fewer tillage passes, provide crop cover, deplete soil water, allow more infiltration, and result in less runoff and erosion. In addition, barley and pea are harvested mid-August followed by only one secondary tillage pass in October, leaving more residue cover in these crop years, whereas the soil surface is left bare during the fallow years. Starting the rotation with different crop phases for the same precipitation zone and time period yielded different year-by-year erosion results, ranging from 0 to 140 Mg ha^{-1}. In most cases, large erosion events occur during the fallow or wheat year in combination with extreme precipitation events occurring shortly after tillage.

3.3.2.3 Comparison with Kaiser field data

WEPP-simulated average annual erosion for 1940–1982 was 45.3 Mg ha^{-1} for the area-weighted SFCW-High and UICW-Intermediate watersheds in Whitman County where Kaiser field data were collected, compared to the average of 53.8 Mg ha^{-1} of the Kaiser data reported in McCool and Roe (2005). WEPP simulation captured the long-term average annual erosion with

reasonable accuracy and 15% lower than that of Kaiser field data. WEPP-simulated annual erosion followed the trend of the observed for certain periods, including 1948–1979 (Figure 2.6a). However, disagreements exist in yearly comparisons (R^2 = 0.02, *RMSE* = 22.7 Mg ha^{-1}, Figure 2.6b). The discrepancies in both average annual and yearly erosion could be due to uncertainties in both our interpretation of the Kaiser data, and the WEPP simulations themselves. Specifically, erosion was surveyed at selected locations in the intermediate- and high-precipitation zones, while WEPP results represent area weighting of model watersheds. Further, crop rotations and their phases as well as tillage practices likely varied from farm to farm during the study period. Due to the lack of such historical details, these complexities could not be replicated in the WEPP simulation. Lastly, we used CLIGEN-generated precipitation events, which differ from the actual events in duration, time to peak, and peak intensity. This could also introduce errors into the simulated erosion.

Simulations with different starting crop phases (wheat or fallow) yielded similar annual averages (45.3 Mg ha^{-1} for fallow-wheat, 45.9 Mg ha^{-1} for wheat-fallow), but different periods of better agreement in terms of temporal trend: starting with wheat vs. fallow produced a simulated trend more similar to the observed for 1949–1970 vs. 1971–1982 (not shown). In both cases, erosion peaked prominently during the wheat years for reasons elaborated in section 3.2.2.

Yearly fluctuation in the observed erosion during 1940–1982 followed the annual precipitation trend, except for years 1941 and 1947. The observed annual erosion rates exceeded 100 Mg ha^{-1} for 1942, 1943, 1946, and 1963. WEPP-simulated values, however, were much lower, especially for 1942 and 1943. The observed erosion was greater than 150 Mg ha^{-1} for 1942 with an annual precipitation depth of 443 mm, which was lower by 90 mm than the average annual precipitation. During this year, a total of 114 precipitation events occurred (similar to the

average of 113), but the number of precipitation events greater than 10, 15, and 20 mm were all considerably fewer than the yearly averages. There were only three large precipitation events, at 17, 27, and 29 mm. These average- or below-average precipitation conditions resulted in a WEPP-simulated erosion rate of 35 Mg ha^{-1} for the year. On the other hand, the observed erosion for 1947 was exceptionally low despite above-average annual precipitation, such that the WEPP simulated results were high in comparison. This difference could have resulted from the use of stochastically generated precipitation events. The observed low erosion in 1977 was likely due to the below-average precipitation for that year, which was partially reproduced by WEPP model simulations.

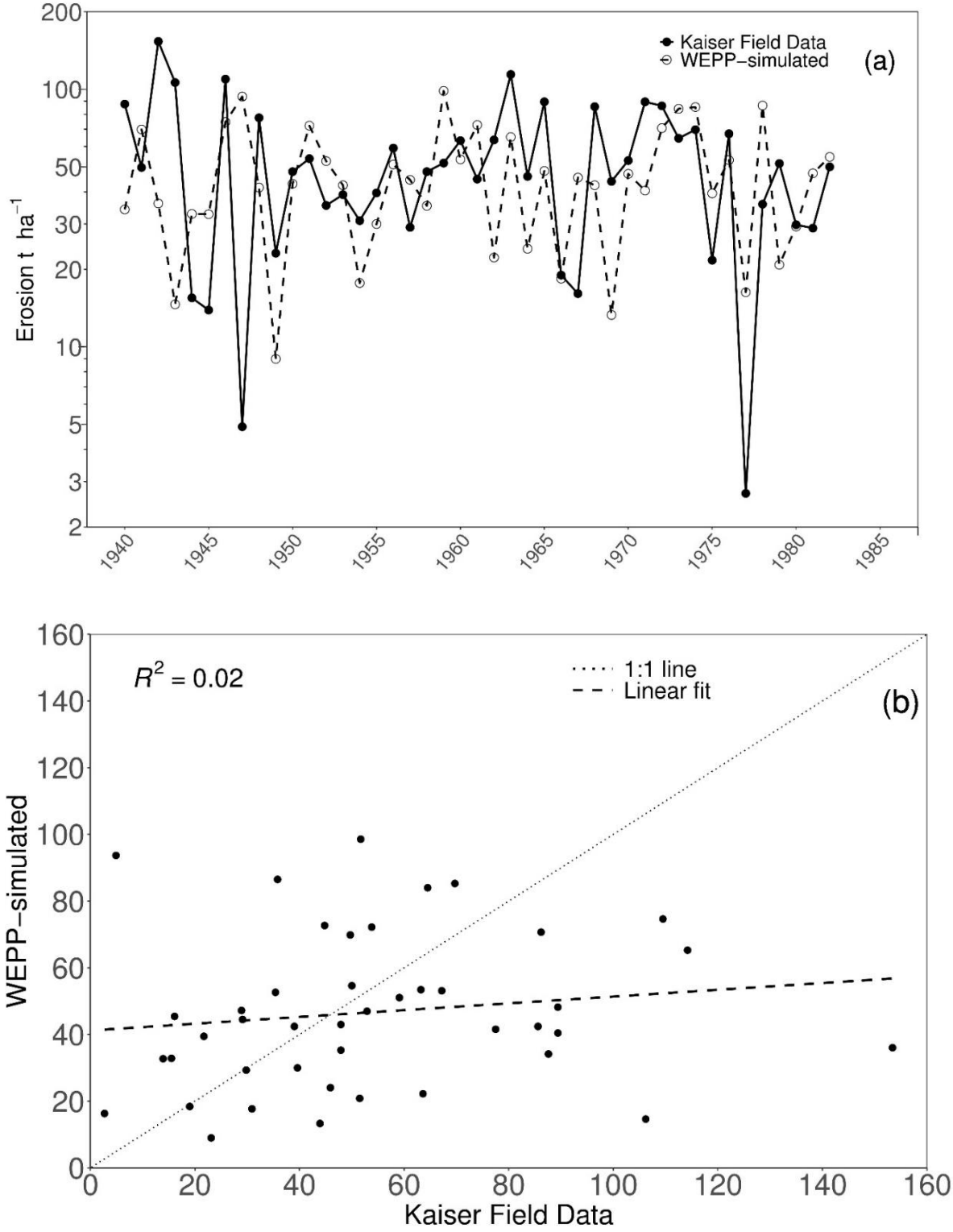

Figure 2.6. Observed and WEPP-simulated average annual erosion rates for the area-weighted UICW-Intermediate and SFCW-High watersheds where Kaiser field data were collected. (a) Yearly variation and (b) paired comparison.

3.3.2.4. Temporal trend

Erosion mostly occurs during the rainy season from November to March (Figure 2.5). WEPP-simulated erosion rates varied year by year, as both weather and cropping conditions also varied (Figure 2.7). A combination of above-average annual precipitation and a large number of rain-on-thawing-soil events led to high erosion rates in the years 1959, 1978, and 1995 for all three watersheds. The many precipitation events in 2016, especially rain-on-thawing-soil events, resulted in elevated erosion for both UICW-Intermediate and SFCW-High. That same year, lower-than-average winter precipitation and fewer rain-on-thawing-soil events in WLCW-Low resulted in low erosion. Further, low winter precipitation and fewer rain-on-thawing-soil events resulted in low erosion rates in the years 1993 and 2013 in all three watersheds.

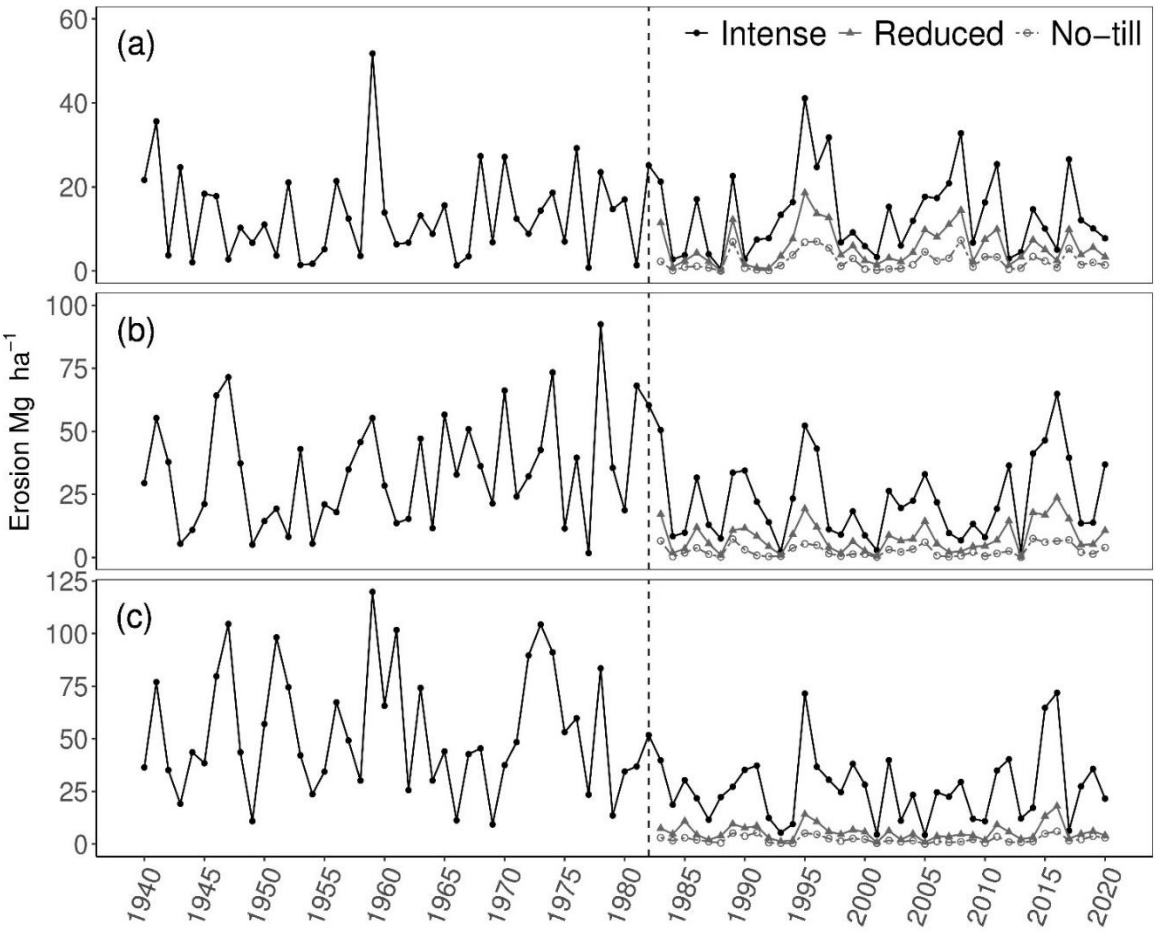

Figure 2.7. Temporal variations in WEPP-simulated annual erosion from the past to present. Study watersheds and their precipitation zones are (a) WLCW-Low, (b) UICW-Intermediate, and (c) SFCW-High. The vertical dashed line separates the past and present periods.

As expected, both event and annual erosion rates were significantly ($\alpha = 0.05$) correlated with runoff (Table 2.7). Likewise, runoff and erosion rates were significantly correlated with water input (rain + melt) for all three watersheds. Event erosion rate was positively correlated with T_{min}, as greater temperatures in winter tend to cause soils to thaw and to be more erodible. The effect of the number of cumulative freeze-thaw cycles prior to an erosion event was significant for SFCW-High but not for the other two watersheds. Annual erosion rate was correlated with the number of rain-on-thawing-soil events in WLCW-Low and SFCW-High, but not in UICW-Intermediate. For none of the three watersheds was there a significant correlation

between the annual erosion rate and the number of freeze-thaw cycles (Table 2.7), corroborating the findings of McCool et al., (2006).

Table 2.7. Pearson correlation analysis of event and annual erosion rate (Mg ha^{-1}), water input (rain + melt) and runoff (mm), and winter conditions for the study watersheds WLCW-Low, UICW-Intermediate, and SFCW-High. Non-significant (at $\alpha = 0.05$) tests are italicized, and *p*-values are shown in parentheses.

	Watershed		Erosion	Rain + Melt	Runoff	Cum. FT/FT[⁋]
Event	WLCW-Low	Rain + Melt	0.51 (<0.001)			
		Runoff	0.67 (<0.001)	0.69 (<0.001)		
		Cum. FT	*−0.03 (0.295)*	0.09 (<0.001)	−0.11 (<0.001)	
		T_{min}*	0.14 (<0.001)	0.26 (<0.001)	*−0.004 (0.865)*	0.22 (<0.001)
	UICW-Intermediate	Rain + Melt	0.52 (<0.001)			
		Runoff	0.58 (<0.001)	0.81 (<0.001)		
		Cum. FT	*−0.03 (0.258)*	0.17 (<0.001)	−0.07 (0.002)	
		T_{min}	0.27 (<0.001)	0.38 (<0.001)	0.12 (<0.001)	0.31 (<0.001)
	SFCW-High	Rain + Melt	0.44 (<0.001)			
		Runoff	0.51 (<0.001)	0.69 (<0.001)		
		Cum. FT	−0.04 (0.008)	0.09 (<0.001)	−0.10 (<0.001)	
		T_{min}	0.21 (<0.001)	0.32 (<0.001)	*0.02 (0.27)*	0.24 (<0.001)
Annual	WLCW-Low	Rain + Melt	0.41 (<0.001)			
		Runoff	0.69 (<0.001)	0.42 (<0.001)		
		FT	*−0.1 (0.227)*	−0.32 (<0.001)	0.05 (<0.001)	
		Rain-on-Thawing Soil	0.23 (0.004)	*0.10 (0.198)*	0.37 (<0.001)	0.25 (0.001)
	UICW-Intermediate	Rain + Melt	0.22 (<0.001)			
		Runoff	0.45 (<0.001)	0.55 (<0.001)		
		FT	*−0.11 (0.088)*	−0.14 (0.03)	*0.13 (0.053)*	
		Rain-on-Thawing Soil	*0.08 (0.218)*	0.22 (0.0005)	0.37 (<0.001)	0.27 (<0.001)
	SFCW-High	Rain + Melt	0.35 (<0.001)			
		Runoff	0.53 (<0.001)	0.57 (<0.001)		
		FT	*−0.03 (0.693)*	*−0.01 (0.88)*	0.18 (0.006)	
		Rain-on-Thawing Soil	0.20 (0.002)	0.33 (<0.001)	0.53 (<0.001)	0.36 (<0.001)

[⁋]Cum. FT, cumulative freeze-thaw cycles prior to an erosion event, for event analysis; FT, total number of freeze-thaw cycles in a water year, for annual analysis. *T_{min}, minimum air temperature

3.3.2.5 Spatial variation

WEPP-simulated average annual erosion rates vary spatially; the higher rates are associated with hillslopes with greater slope length and steepness (Table 2.8). In SFCW-High, the annual erosion rate was negatively correlated with soil depth, as deeper soils have larger storage and thus a lower potential for runoff and erosion, consistent with findings of previous studies (Brooks et al., 2015; Dahal et al., 2022). In contrast, for WLCW-Low, the annual erosion rate was positively correlated with soil depth, likely because of the combined effects of

confounding factors. Hillslopes with deeper soil in this watershed tend to be longer and steeper, with slightly lower saturated hydraulic conductivity and higher interrill and rill erodibilities. No analysis was made between erosion rate and soil depth for UICW-Intermediate because of the lack of variation of soil depth in this watershed.

Table 2.8. Pearson correlation between annual average erosion and hillslope properties for the WLCW-Low, UICW-Intermediate, and SFCW-High watersheds. Non-significant (at $\alpha = 0.05$) tests are italicized, and P-values are shown in parentheses.

		Erosion	Slope Length	Gradient
WLCW-Low	Slope Length	0.32 (<0.001)		
	Gradient	0.59 (<0.001)	−0.03 (−0.03)	
	Soil Depth	0.29 (<0.001)	*0.01 (−0.59)*	0.11 (<0.001)
UICW-Intermediate	Slope Length	0.42 (<0.001)		
	Gradient	0.41 (<0.001)	−0.22 (<0.001)	
	Soil Depth[¶]			
SFCW-High	Slope Length	0.35 (<0.001)		
	Gradient	0.41 (<0.001)	0.10 (<0.001)	
	Soil Depth	−0.19 (<0.001)	*0.02 (0.21)*	0.26 (<0.001)

[¶]No analysis for this watershed, which has only one soil depth

Areas with simulated erosion rates below the NRCS tolerable limit (<11 Mg ha^{-1} yr^{-1}) increased from past to present in all three watersheds, and areas with erosion rates far exceeding the tolerable limit (>30 Mg ha^{-1} yr^{-1}) decreased from the past (Table 2.9, Figure 2.8). Nonetheless, areas with simulated erosion rates above the tolerable limit still account for 34, 40, and 39% of the total areas in WLCW-Low, UICW-Intermediate-, and SFCW-High, respectively.

Table 2.9. Changes in percent areas of erosion from past to present in the WLCW-Low, UICW-Intermediate, and SFCW-High watersheds.

	Areas with erosion rate <11 Mg ha^{-1} (%)		Areas with erosion rate > 30 Mg ha^{-1} (%)	
	Past	Present	Past	Present
WLCW-Low	52	66	10	4
UICW-Intermediate	4	60	68	3
SFCW-High	4	60	82	3

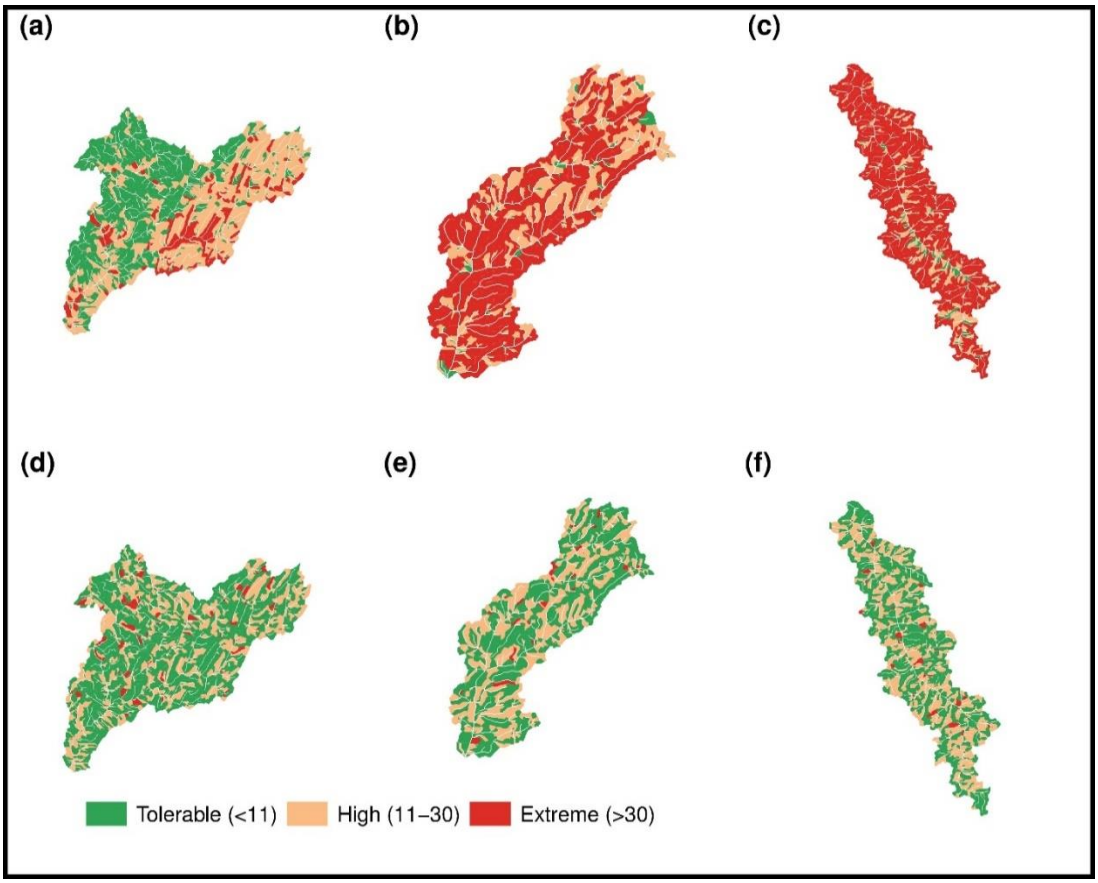

Figure 2.8. Average annual WEPP-simulated erosion rates (Mg ha^{-1}) for the past (a, b, c) and the present (d, e, f) in the WLCW-Low, UICW-Intermediate, and SFCW-High watersheds.

2.4. Conclusions

In this study, we applied WEPP (v. 2020.5) to assess the temporal trend of water erosion in the three precipitation zones of Whitman County, eastern Washington State. We separated the climate record into the past (1940–1982) and the present (1983–2020). We delineated a watershed within each precipitation zone and carried out WEPP model simulations over the two periods for the three watersheds under different tillage practices and crop rotations. Statistical

analyses were conducted to evaluate the long-term trends of climatic parameters, specifically annual precipitation and daily maximum and minimum temperatures, and to compare averaged and aggregated WEPP simulation results for the two time periods. Additionally, WEPP-simulated annual erosion rates for the past were compared with the Kaiser field data. Our major conclusions from this study are:

1. *Climate Trends* Daily maximum and minimum temperatures increased from the past in all three watersheds except T_{min} in the WLCW-Low. The increase in temperature was statistically significant except for T_{min} in UICW-Intermediate. The number of rain-on-thawing-soil events increased significantly in WLCW-Low and decreased significantly in UICW-Intermediate and SFCW-High.
2. *Erosion: Past vs. Present* WEPP-simulated average annual erosion rates decreased from the past to present by 32%, 57%, and 70% for the study watersheds in the low-, intermediate-, and high-precipitation zones, respectively. The decreases were due to the combined effects of changing climatic patterns and management practices.
3. *Climatic Effect* The decrease in annual, particularly winter, precipitation, and the number of large precipitation events were the key climatic factors (or parameters) that led to a decrease in erosion.
4. *Management Effect* The shifts from two-year to three-year rotation, and from intense tillage to conservation tillage, were the key management changes that caused a decrease in erosion. Incorporating reduced- and no-till decreased WEPP-simulated average annual erosion by 31%, 35%, and 40% in WLCW-Low, UICW-Intermediate, and SFCW-High, respectively.
5. *Comparison with Kaiser Field Data* WEPP-simulated average annual erosion rate

agreed with the Kaiser field data. WEPP reproduced year-by-year variations for certain periods, especially 1948–1979.

6. *Temporal and Spatial Assessment* Erosion varied year to year, driven by the annual precipitation events, number of precipitation events, and rain-on-thawing-soil events. Spatially, the areas with erosion rates below the NRCS tolerable limit increased from the past to the present in all three watersheds. Yet 34, 40, and 39% of the total areas in WLCW-Low, UICW-Intermediate, and SFCW-High watersheds, respectively, still generate erosion exceeding the NRCS tolerance limit of 11 Mg ha^{-1} yr^{-1}.
7. *Correlation with Climate Parameters* Erosion events were positively correlated with annual water input, runoff, and minimum temperature for all three watersheds. The number of annual freeze-thaw cycles was not correlated with annual erosion rates in the three watersheds. The number of annual rain-on-thawing-soil events was significantly correlated with annual erosion rates for the watersheds in the low- and high-precipitation zones.
8. *Correlation with Spatial Parameters* The average annual erosion rate was significantly correlated with hillslope length and steepness for all three watersheds. Average annual erosion rate in SFCW-High was negatively correlated with soil depth, as deep soils have lower potential for runoff and erosion. However, the erosion rate was positively correlated with soil depth in WLCW-Low, because hillslopes with deeper soils in this watershed tend to be longer and steeper, with lower hydraulic conductivity and higher erodibility.
9. *Limitations*: The study is limited by the lack of observed characteristics of precipitation events, which likely contributed to differences between WEPP-simulated and observed

erosion. The use of county-level tillage practice data for subareas within the county has likely also contributed to the simulation errors.

2.5. Acknowledgments

This study is in part supported by USDA AFRI NIFA (Grant No. 2018-68002-27920). We thank Dr. Markus Flury for suggesting the comparison between WEPP results and Kaiser field data. We thank Mr. Stephen Johnson, USDA NRCS, for providing information on common crop rotations and tillage practices in the study area. We are grateful to the two anonymous reviewers and the editor for their constructive comments, which improved the rigor and clarity of the paper.

REFERENCES

Boll, J., Brooks, E. S., Crabtree, B., Dun, S., & Steenhuis, T. S. (2015). Variable source area hydrology modeling with the water erosion prediction project model. *J. Am. Water Resour. Assoc.*, *51*(2), 330–342.

Brooks, E. S., Dobre, M., Elliot, W. J., Wu, J. Q., & Boll, J. (2016). Watershed-scale evaluation of the Water Erosion Prediction Project (WEPP) model in the Lake Tahoe basin. *J. Hydrol.*, *533*, 389–402.

Brooks, E. S., Saia, S. M., Boll, J., Wetzel, L., Easton, Z. M., & Steenhuis, T. S. (2015). Assessing BMP effectiveness and guiding BMP planning using process-based modeling. *J. Am. Water Resour. Assoc.*, *51*, 343–358. https://doi.org/10.1111/1752-1688.12296

Dahal, M. S., Wu, J. Q., Boll, J., Ewing, R. P., & Fowler, A. (2022). Spatial and agronomic assessment of water erosion on inland Pacific Northwest cereal grain cropland. *J. Soil Water Conserv.*, *77*(4), 347–364. https://doi.org/10.2489/jswc.2022.00091

Ebbert, J. C. & Roe, R. D. (1998). Soil erosion in the Palouse River basin: Indications of improvement. Washington, DC: US Department of the Interior, US Geological Survey.

Flanagan, D. C., Gilley, J. E., & Franti, T. G. (2007). Water Erosion Prediction Project (WEPP): Development history, model capabilities, and future enhancements. *Trans. ASABE*, *50*, 1603–1612.

Flanagan, D. C. & Nearing, M. A. (Eds.) (1995). Water Erosion Prediction Project Hillslope Profile and Watershed Model Documentation. NSERL Report 10. West Lafayette, IN: USDA ARS National Soil Erosion Research Laboratory.

Flanagan, D. C. & Livingston S. J. (Eds.) (1995). WEPP User Summary: USDA-water erosion prediction project. NSERL Report 11. West Lafayette, IN: USDA ARS National Soil Erosion Research Laboratory. Retrieved from https://www.ars.usda.gov/ARSUserFiles/50201000/WEPP/usersum.pdf

Foster, G. R., Toy, T. E., & Renard, K. G. (2003). Comparison of the USLE, RUSLE1.06c, and RUSLE2 for application to highly disturbed lands. In *First Interagency Conference on Research in Watersheds* (Vol. 27, No. 30, pp. 154–160). Washington, DC: USDA ARS.

Greer, R. C., Wu, J. Q., Singh, P., & McCool, D. K. (2006). WEPP simulation of observed winter runoff and erosion in the US Pacific Northwest. *Vadose Zone J.*, *5*(1), 261–272.

Gilley, J. E. & Weltz, M. A. (1995). Chapter 10. Hydraulics of overland flow. In Flanagan, D. C., & Nearing, M. A. (Eds.), *USDA-Water Erosion Prediction Project: Hillslope Profile and Watershed Model Documentation*, NSERL Report 10. West Lafayette, IN: USDA ARS National Soil Erosion Research Laboratory.

Kaiser, V. G. (2021). Verle G. Kaiser Papers, 1932–1982. Manuscripts, Archives, and Special

Collections. Pullman, WA: Washington State University Libraries.

Klingebiel, A. A. & Montgomery, P. H. (1961). Land-capability classification (No. 210). Soil Conservation Service, US Department of Agriculture.

Kok, H., Papendick, R., & Saxton, K. (2007). STEEP Impact Assessment. A report prepared by the STEEP Coordinating Committee. University of Idaho, Oregon State University, Washington State University, USDA ARS.

Kok, H., Papendick, R. I., & Saxton, K. E. (2009). STEEP: Impact of long-term conservation farming research and education in Pacific Northwest wheatlands. *J. Soil Water Conserv.*, *64*(4), 253–264. https://doi.org/10.2489/jswc.64.4.253

Kottek, M., Grieser, J., Beck, C., Rudolf, B., & Rubel, F. (2006). World map of the Köppen-Geiger climate classification updated. *Meteorol. Z.*, *15*, 259–263. https://doi.org/10.1127/0941-2948/2006/0130

Lew, R., Dobre, M., Deval, C., Srivastava, A., & Fowler, A. (2021). rogerlew/wepppy: 2021.05.18.01 (2021.05.18.01). Zenodo, European Organization for Nuclear Research, Digital Repositories Section, Geneva, Switzerland. https://doi.org/10.5281/zenodo.4771076

Lew, R., Dobre, M., Srivastava, A., Brooks, E. S., Elliot, W. J., Robichaud, P. R., & Flanagan, D. C. (2022). WEPPcloud: An online watershed-scale hydrologic modeling tool. Part I. Model description. *J. Hydrol., 608*, 127603. https://doi.org/10.1016/j.jhydrol.2022.127603

Li, Z. & Fang, H. (2016). Impacts of climate change on water erosion: A review. *Earth-Sci. Rev.*, *163*, 94–117.

Lin, J., Guan, Q., Tian, J., Wang, Q., Tan, Z., Li, Z., & Wang, N. (2020). Assessing temporal trends of soil erosion and sediment redistribution in the Hexi Corridor region using the integrated RUSLE-TLSD model. *Catena*, *195*, 104756.

McCool, D. K., Dun, S., Wu, J. Q., & Elliot, W. J. (2011). Seasonal change of WEPP erodibility parameters on a fallow plot. In D. C. Flanagan, J. C. II Ascough, & J. L. Neiber (Eds): *Proceedings International Symposium on Erosion and Landscape Evolution (ISELE)* Paper No. 11066. St. Joseph, MI: ASABE. https://elibrary.asabe.org/abstract.asp?JID=1&AID=39262&CID=isel2011&T=1

McCool, D. K., Saxton, K. E., & Kalita, P. K. (2006). Winter runoff and erosion on northwestern USA cropland. ASABE Paper No. 062190. St. Joseph, MI: ASABE.

McCool, D. K. & R. D. Roe. (2005). Long-term erosion trends on cropland in the Pacific Northwest. ASAE Section Meeting Paper No. PNW05-1002, St. Joseph, Mich.: ASAE.

McCool, D. K., Dun, S., Wu, J. Q., Elliot, W. J., & Brooks, E. S. (2013). Seasonal change of WEPP erodibility parameters for two fallow plots on a Palouse silt loam. *Trans. ASABE*, *56*, 711–718.

Meyer, L. D. (1982). Soil erosion research leading to development of the universal soil loss equation. In G. R. Foster (Ed.), *Proceedings of Workshop on Estimating Erosion and Sediment Yield on Rangelands* (pp. 1–16). Washington, DC: USDA ARS.

NCDC (National Climatic Data Center). (2022). NOAA satellite and information service. NCDC. Retrieved from https://www.ncdc.noaa.gov/cdo-web/

Nicks, A. D., Lane, L. J., & Gander, G. A. (1995). Chapter 2. Weather generator. In D. C. Flanagan & M. A. Nearing (Eds.), *USDA-Water Erosion Prediction Project: Hillslope profile and watershed model documentation* (pp. 2.1–2.22). NSERL Report 10. West Lafayette, IN: USDA ARS National Soil Erosion Research Laboratory.

O'Neal, M. R., Nearing, M. A., Vining, R. C., Southworth, J., & Pfeifer, R. A. (2005). Climate change impacts on soil erosion in Midwest United States with changes in crop management. *Catena*, *61*, 165–184.

Panagopoulos, T., Cakula, A., Ferreira, V., & Arvela, A. S. (2015). Simulation model for predicting soil erosion in a large reservoir of southern Portugal. *Int. J. Sustain. Agric. Manag. Inform.*, *1*(1), 3–25.

Papendick, R. I. (1986). Soil conservation and management in Palouse. In B. R. Bertramson (Ed.), *History of the Department of Agronomy and Soils*, WSU. Retrieved from https://css.wsu.edu/overview/history-of-the-department-of-agronomy-and-soils-wsu/

Papendick, R. I., Young, F. L., Pike, K. S., & Cook, R. J. (1984). Description of the region. In R. I. Papendick & W. C. Moldenhauer (Eds.), *Crop Residue Management to Reduce Erosion and Improve Soil Quality: Northwest* (CRR-40). Washington, DC: USDA ARS. https://s3.wp.wsu.edu/uploads/sites/3122/2022/09/V_Research-3.7_SoilConsMgmt.pdf

R Core Team. (2022). R: A Language and Environment for Statistical Computing. Vienna, Austria: R Foundation for Statistical Computing. Retrieved from https://www.R-project.org/

Renard, K. G., Foster, G. R., Weesies, G. A., McCool, D. K., & Yoder, D. C. (1996). Predicting Soil Erosion by Water: A Guide to Conservation Planning with the Revised Universal Soil Loss Equation RUSLE). US Department of Agriculture, Agriculture Handbook No. 703, Washington, D.C.: US Govt. Printing Office. 404 pp.

Shepherd, J. F. (1985). Soil conservation in the Pacific Northwest wheat-producing areas: Conservation in a hilly terrain. *Agric. Hist.*, *59*, 229–245.

Soil Science Division Staff. (2017). Soil Survey Manual. In C. Ditzler, K. Scheffe, & H. C. Monger (Eds.), *USDA Handbook 18*. Washington, DC: Government Printing Office. https://www.nrcs.usda.gov/wps/portal/nrcs/detail/soils/scientists/?cid=nrcs142p2_054262

Srivastava, A., Flanagan, D. C., Frankenberger, J. R., & Engel, B. A. (2019). Updated climate database and impacts on WEPP model predictions. *J. Soil Water Conserv.*, *74(4),* 334–349.

Stott, D. E., Alberts, E. E., & Weltz, M. A. (1995). Chapter 9. Residue decomposition and management. In D. C. Flanagan, & M. A. Nearing (Eds.): USDA-Water Erosion Prediction Project (WEPP) Hillslope Profile and Watershed Model Documentation. NSERL Report No. 10, National Soil Erosion Research Laboratory, USDA-Agricultural Research Service, West Lafayette, Indiana. pp. 9.1–9.16.

US Department of Agriculture. (1978). Palouse Cooperative River Basin Study. USDA Soil Conservation Service, Forest Service, and Economics, Statistics, and Cooperative Service.

US Department of Agriculture NASS. (2018). 2018 Washington Cropland Data Layer. USDA NASS. Retrieved from https://nassgeodata.gmu.edu/CropScape/

US Department of Agriculture NASS (National Agricultural Statistics Service). (2017). Census of Agriculture. Retrieved from www.nass.usda.gov/AgCensus.

US Geological Survey . (2019). USGS NED 1 arc-second ArcGrid 2019. USGS. Retrieved from https://apps.nationalmap.gov/downloader/

US Geological Survey. (2022). The StreamStats program. Retrieved from https://streamstats.usgs.gov/ss/

Van Wie, J. B., Adam, J. C., & Ullman, J. L. (2013). Conservation tillage in dryland agriculture impacts watershed hydrology. *J. Hydrol.*, *483*, 26–38.

Williams, J. D., Wuest, S. B., & Long, D. S. (2014). Soil and water conservation in the Pacific Northwest through no-tillage and intensified crop rotations. *J. Soil Water Conserv.*, *69*(6), 495–504.

Wischmeier, W. H. and D. D. Smith. (1978). Predicting Rainfall Erosion Losses: A Guide to Conservation Planning. USDA, Agriculture Handbook Number 537. Washington, DC: US Government Printing Office.

3. TEMPORAL CHANGE IN WATER EROSION IN RESPONSE TO FUTURE CLIMATE CHANGE

3.1. Introduction

Climate Change

Change in climate is evident as existing analyses show that the combined global average of land and ocean temperature has increased by 0.85ºC from 1880 to 2012 (Stocker et al., 2013). In the Pacific Northwest (PNW) the average annual temperature has increased by 0.7ºC in the past century, while the precipitation change has been insignificant (Abatzoglou et al., 2014). In the future, the annual temperature in PNW is predicted to increase by 1.1ºC, 1.8ºC, and 3.0ºC by 2020, 2040, and 2080, with autumn and winter increasingly wet and summer drier (Mote and Salathé, 2010) compared to the average annual temperature of 1970 to 1999. The future precipitation of the inland PNW is projected to increase by 8 to 12% and mean temperature in the growing season by 1.5 to 2.3ºC under RCP 4.5 and RCP 8.5 scenarios, respectively (Karimi et al., 2018).

Effects of Changing Climate on Agriculture

Climate change can increase CO_2 concentration, which will variably impact agriculture around the world (Aydilnap and Cresser, 2008). As agricultural systems are a major driver of soil erosion, change in climate will lead to a change in erosion. Changes in precipitation patterns, e.g., intensity and frequency of extreme events, will change the erosive power of rainfall and the amount of runoff, changing the erosion pattern (Adams et al., 1999; Nearing, 2001). Shifts in temperature will influence the frequency of freeze-thaw cycles of the soil (Henry et al., 2008), which affects the soil erodibility (Ferrick et al., 2005). An increase in temperature might indirectly affect soil erosion as it influences evapotranspiration, biomass production, and residue decomposition process (Pruski and Nearing, 2002; Chien et al., 2013), which might increase or

decrease erosion. The net change in erosion due to changing temperatures is determined by considering both the negative, and positive, effects (O'Neal et al., 2005). The increased CO_2 concentration leads to reduced transpiration as stomatal apertures of plant and therefore the stomatal conductance are reduced, resulting in higher soil water content in the soil profile, increasing the potential for runoff and hence erosion (Schulze, 2000). However, the increase in CO_2 concentration would also lead to increased biomass production, which augments ground cover and decreases erosion (Guo et al., 2019; Nearing et al., 2004).

Erosion Response to Climate Change

The potential change in erosivity in response to a changing climate was investigated by Nearing (2001). Rainfall erosivity was computed for two twenty-year periods of 2040–2059 and 2080–2099, and compared with the value for 2000–2019 in the United States using two climate models: UK Hadley Centre model (HadCM3) and Canadian Global Coupled model (CGCM1). Rainfall erosivity was calculated as a function of: i) average annual precipitation and ii) Fournier coefficient, which depends on average monthly and annual temperature. The results from HadCM3 showed a general increase in erosivity over Eastern and Northern US. The estimated erosivity would decrease in the Southwestern US, including parts of California, Nevada, Utah, and eastern Texas. CGCM1 results showed an increase in erosivity over the Northern US. CGCM1 model also showed a substantial increase in erosivity in the Northeastern and Northwestern US, which was not consistent with the HadCM3 model results. Estimated erosivity would generally increase in the Pacific Northwest except in the case of HadCM3 simulation using average precipitation. The erosivity results from the two methods were generally agreeable for most areas across the US, with inconsistency (or opposite trends) projected for 16–20% of the areas. The change in projected is substantial, with variation in magnitude from region to region,

and average magnitude of change (either increase or decrease) to be 29% and 59% for the two periods.

Pruski and Nearing (2002) estimated the impact of precipitation change on soil erosion rates using WEPP. In their study, change in precipitation was considered as due to i) change in the number of wet days, ii) change in the amount of rainfall per event, and iii) equal change in the number of wet days and in the amount of rain per event. In all three cases, the precipitation was either unchanged (base line), or changed by ±10% and ±20%. The climate inputs for WEPP were created by modifying relevant parameters in the random climate generator (CLIGEN; Nicks et al., 1995). The WEPP simulations were conducted for three locations (West Lafayette, IN; Temple, TX; and Corvallis, OR), with three slope configurations, three soil types, and four crop scenarios (grazing pasture, corn and soybean rotation, winter wheat, and fallow). The results indicate that runoff will increase with an increase in average precipitation regardless of the form of precipitation change. However, runoff was found to be more sensitive to an increase in the average amount of rainfall in a given day than to an increase in the number of wet days. As runoff, soil loss is more sensitive to change in rainfall amount per event with a 2.4% average increase with each percent increase in precipitation, compared to a 0.9% average increase with each percent increase in the number of wet days. This may be because increase in the number of wet days would lead to an increase in biomass production due to the increase in precipitation, which in turn will increase the surface resistance to erosion. However, this effect of increase in biomass production was superseded in the case of increase in rainfall amount per event by the intensified rill and interrill soil detachment processes that depend directly on rainfall amount and intensity and runoff rates.

Nearing et al. (2004) examined long-term erosion (1990–2099) using the WEPP model, and compared future outcomes with the 1990 erosion results for eight locations under corn and wheat management across the US. They showed that the impacts on runoff and erosion of different future climate scenarios would vary depending on location and management. In some locations, erosion will increase with increase in precipitation; in others, erosion will increase with decreasing precipitation. This is because decrease in precipitation resulted in decrease in biomass production due to water stress, which in turn led to decrease in ground cover and an increase in erosion. A few of the scenarios showed an increase in precipitation, decrease in runoff, and increase in erosion. This is because the projected precipitation decreases during the growing season, decreasing runoff and erosion, but the precipitation increases during April and May, causing an increase in runoff and erosion, with a net effect of decreased runoff but increased erosion overall.

Li and Fang (2016) reviewed published work assessing the impact of a changing climate on soil erosion on multiple spatial and temporal scales in the US, China, the United Kingdom, and Germany. Their review was focused on key factors, such as precipitation, temperature, vegetation, and crop management. The authors found that soil erosion could increase or decrease under future climate changes depending on the combined direct and indirect effects of changes in precipitation, temperature, and CO_2 concentration. Climate change could result in a change in vegetation and cropping systems. An increase in precipitation amount would lead to larger amount of runoff and thus larger erosion rate. An increase in rainfall duration reduces solar radiation, thus hindering plant growth and decreasing plant cover, causing an increase in erosion. On the other hand, increased precipitation can increase plant biomass production, increasing canopy cover, thus reducing runoff and erosion. An increase in temperature leads to an increase

in ET and decrease in soil water, which increases soil infiltration capacity and reduces runoff and erosion. Increasing temperature can also cause a longer growing season for some crops, thus increasing vegetative cover for a more extended period and reducing annual runoff and erosion. On the other hand, the increasing temperature can increase residue decomposition rate leading to reduced resistance to runoff and therefore increased erosion. The authors submit that the impact of climate change on soil erosion is best assessed at the regional level accounting for changes in crop management and considering all erosion processes, including rill, gully, and channel erosion.

Borrelli et al. (2020) modeled global soil erosion and predicted the baseline global soil erosion rate to be 3 t ha^{-1} yr^{-1} for 2015, and the combined effect of future land use and climate change to be an increase in erosion by 30%, 51%, and 66% by 2070 for the scenarios of Shared Socioeconomic Pathway and Representative Concentration Pathway (SSP-RCP) 2.6, 4.5, and 8.5 (Pachauri, 2014).

Edwards et al. (2019) studied climate change impacts on wind and water erosion of US rangelands considering changes in climate and management factors that cause erosion. They analyzed the projected changes in future annual and seasonal temperature, precipitation, and wind speed, and submitted that vulnerability to erosion will increase due to projected trend of reduced vegetation cover, and increased rainfall erosivity.

A WEPP simulation study by O'Neal et al. (2005) accounted for the shift in cropping systems from wheat and maize to soybeans, which are projected to be more profitable under climate change. The results indicate an increase in runoff and soil loss in 2040–2059 ranging +10% to +310% and +33% to +274%, respectively, in comparison to 1990–1999.

Garbrecht and Zhang (2015) used WEPP-CO_2 to simulate soil erosion for the period of 2041–2070 for wheat production areas of central Oklahoma using 10 Global Climate Models (GCMs) for the RCP 8.5 scenario and conventional and conservation tillage practices. The results showed a doubling of soil erosion rate on average to 15.3 t ha^{-1} under full conventional tillage compared to current conditions. This increase was associated with intensified storm events and accelerated plant growth from increased temperature and CO_2 concentration, resulting in early harvest and more fallow and bare field areas. The study also projected an average reduction in erosion by 53% (8.5 t ha^{-1}) and 96% (0.6 t ha^{-1}) for reduced tillage and no-till compared to conventional tillage.

Sharratt et al. (2015) used the Water Erosion Prediction System (WEPS) to assess the impact of a changing climate on wind erosion of agricultural lands in the Columbia plateau. Daily climate outputs from 18 GCMs for the RCP 4.5 scenario were used as inputs to WEPS for typical wheat-based rotations under conventional and conservation tillage. Simulations were conducted for historical (1970–1999) and future mid-21st century (2035–2064) and relative changes were compared. A substantial increase in temperature and a minor increase in precipitation were projected for the Columbia Plateau. The authors reported a decrease in wind erosion by 25–84% during the mid-21st century due to greater biomass production in warmer time periods.

Wang et al. (2018) used the macro-scale Variable Infiltration Capacity-Water Erosion Prediction Project (VIC-WEPP) model to estimate soil loss under climate changes for 2000–2100 in the US Great Lakes region. Three models from the Coupled Model Intercomparison Project 3 (CMIP3) were used with three emission scenarios (A2, A1B, B1). The authors simulated three periods: early (2030–2039), middle (2060–2069), and late (2090–2099) futures,

and compared the erosion results with those during the historical period (2000–2009). The simulated seasonal runoff increases in fall and winter because of a rise in air temperature that converts snow to rainfall, and a decrease in spring and summer because of the increasing air temperature that increases ET. The net outcome is a decrease in annual runoff, with the largest decrease of 8.5 mm yr^{-1} (−8.1%) for the middle-future period and A1B scenario, even though precipitation was projected to increase generally. The simulated annual soil loss will decrease ranging 0.43 t ha^{-1} (−5.0%) to 1.8 t ha^{-1} (−21%) for the three emission scenarios and three future periods. The simulated seasonal soil loss follows the simulated runoff pattern, increasing in fall and winter, and decreasing in spring and summer, resulting in an overall decrease annually.

Rationale and Objectives

Few studies have assessed the response of water erosion to changes in future climate in the inland Pacific Northwest. This assessment is necessary to identify sustainable management practices that can tackle erosion problems in the future. The objectives of this study were to (i) assess the changes in water erosion as impacted by the projected future climate using WEPP, and (ii) identify conservation practices to reduce erosion, especially from the "hot spots".

3.2. Methodology

3.2.1. Study Area

Whitman County, one of the largest cereal-grain production counties with historical erosion problems, was chosen as the study area. Whitman County is located in southeastern Washington, with elevation spanning 160– 1250 m a.m.s.l. (USGS, 2019) and a Mediterranean climate characterized by dry summers and wet winters. The area consists of three distinct precipitation zones: low, intermediate, and high, with their respective long-term average annual precipitations of 355 mm, 450 mm, and 533 mm (NCDC, 2022). Conventional tillage is common

within the study area, and conservation tillage (reduced tillage and no-till) has increased since the 1980s (Dahal et al., 2022). Wheat is the main crop, and the crop rotation is dictated by available water. Winter wheat-fallow, winter wheat-spring-barley-fallow, and winter wheat-spring barley-pea are in commonly practiced in the low-, intermediate-, and high-precipitation zones, respectively.

Three HUC-12 watersheds, one for each precipitation zone (same as described in Chap 2), were used for WEPP simulation. The watersheds are the Winn Lake Canyon Watershed for the low-precipitation zone (WLCW-Low), Upper Imbler Creek Watershed (UICW-Intermediate) for the intermediate-precipitation zone, and Spring Flat Creek Watershed (SFCW-High) for the high-precipitation zone.

3.2.2. Climate

Projected climates from different GCMs were grouped based on RCP scenarios. RCPs represent different trajectories of greenhouse gas (GHG) concentrations used to forecast the potential effects of climate change, reflecting future human activities related to GHG emissions (Stocker et al., 2013). Each RCP scenario (+2.6, +4.5, +6.0, +8.5 W/m^2) is defined by its radiative forcing value for the year 2100 compared to levels before the industrial era. RCP 4.5 represents a peak in emission around 2040 and then a decline owing to policies that stabilize GHG emissions whereas RCP 8.5 represents a continuous rise in emission with no efforts to mitigate GHG emissions. These two scenarios were modeled in this study with 20 GCMs.

The GCM outputs were downscaled into finer spatial resolutions, making them more relevant for regional assessment. Specifically, I adopted the downscaled GCM data by Abatzoglou and Brown (2012), from the Climatology Lab (https://www.climatologylab.org/), employing the statistical method Multivariate Adaptive Constructed Analogs (MACA). I

incorporated the downscaled outputs from all 20 GCMs for the historical as well as the future RCP 4.5 and RCP 8.5 scenarios. The primary climate variables examined were precipitation and temperature.

I developed Python scripts to acquire, aggregate, and download the downscaled products. The three model watersheds were used to identify the downscaled product tiles: tiles falling in each watershed were spatially averaged, and a single set of daily climate data was obtained for each watershed for both historical and future periods.

3.2.3. WEPP Inputs

Climate inputs were divided into two 30-year periods: historical (1976–2005) and future (2036–2065). Additional climate data needed for WEPP simulation, including wind velocity, dew-point temperature, and precipitation characteristics, were generated through a stochastic weather generator CLIGEN (v5.0, Srivastava et al., 2019). Slope and soil properties were delineated through WEPPcloud (Lew et al., 2022) and were modified, including adjusting slope length, baseline hydraulic conductivity, interrill and rill erodibility, and critical shear following Dahal et al. (2022). Three tillage practices: intense, reduced, and no-till, were included in WEPP simulations for the historical and future periods. Crop rotations varied by precipitation zones but to isolate the effects of climate on water erosion, for the same precipitation zone, I used the same crop rotations in historical and future scenarios. Wheat-fallow (WF) rotation was used for the low-precipitation zone, wheat-barley-fallow (WBF) was used for the intermediate-precipitation zone, and wheat-barley-pea (WBP) was used for the high-precipitation zone.

3.2.4. WEPP Simulation

WEPP (watershed v.2020.5) was used simulate water erosion following the workflow (Figure 3.1). Hillslopes were discretized into three Overland Flow Elements (OFEs) to better

simulate saturation-excess runoff at the bottom of the hillslopes. Python and r scripts were developed to convert input files from the default single OFE to three OFEs and to conduct WEPP simulations in batch. With three watersheds, 20 GCMs, one historical and two RCP scenarios, and three tillage types, I conducted a total of 540 (3×20×3×3) WEPP runs.

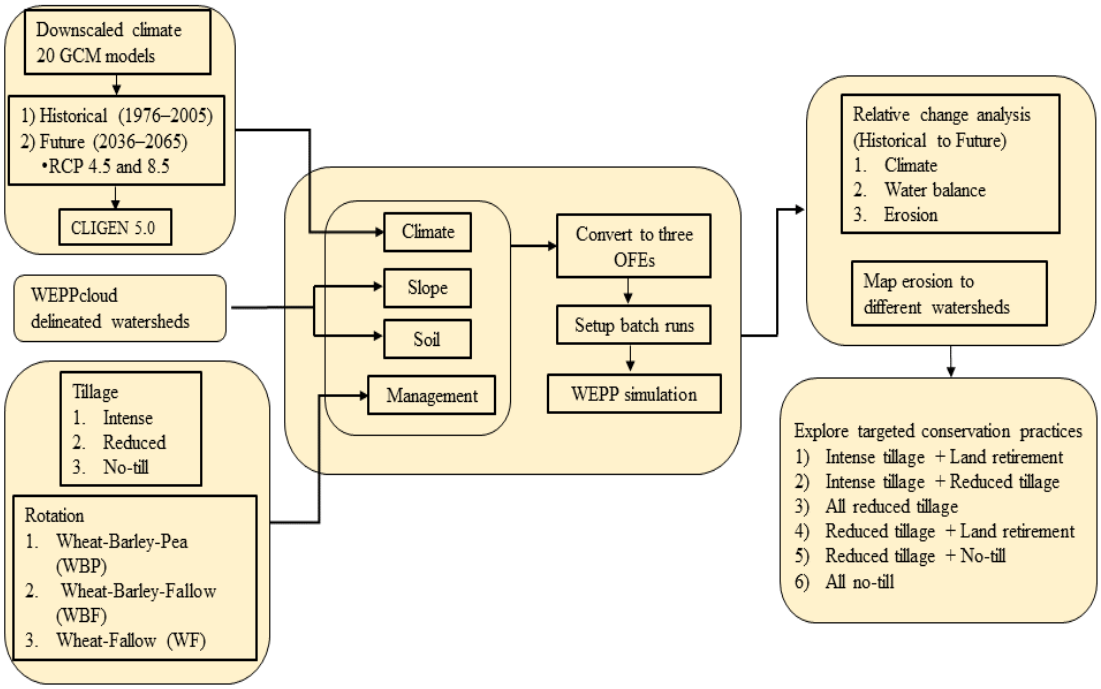

Figure 3.1. Flowchart of WEPP simulations.

2.5. Analysis of Results

Climate variables and WEPP-simulated water balance and erosion results were aggregated as monthly, seasonal, and annual (water year, October 1–September 30 of the following year). The relative change from historical to future in climate, water balance, and erosion under different tillage practices and RCP scenarios for all GCM models were assessed and synthesized. Erosion results for future scenarios were mapped to the model watersheds, and differences in erosion due to hillslope characteristics were determined. (Figure 3.1). The areas in the model watersheds with consistently high erosion (hot spots) were identified, and

implementation of combinations of conservation practices, including reduced tillage, no-till, and land retirement, was assumed for those areas to determine differences in erosion rates.

3.3. Results

3.3.1. Climate

3.3.1.1. Precipitation

Future annual precipitation generated by the models varies, with most models indicating an increase in precipitation (Figure 3.2). The average annual precipitation for all three precipitation zones increases from historical to RCP 4.5 and RCP 8.5 by 4–5% and 5–6%, respectively (Table 3.1). The projected winter precipitation increases markedly for all three precipitation zones with an average increase of 8–10% (8–14 mm) from historical to RCP 4.5 and RCP 8.5, respectively, with the largest increase occurring in the high-precipitation zone. The projected spring precipitation increases by 8–9% (5–12 mm) for the three zones and the two future scenarios. The projected fall precipitation follows a similar trend but the increase is larger under RCP 4.5 than RCP 8.5. Projected summer precipitation decreases from the historical under both RCP 4.5 and RCP 8.5, by 3–4% for the three precipitation zones.

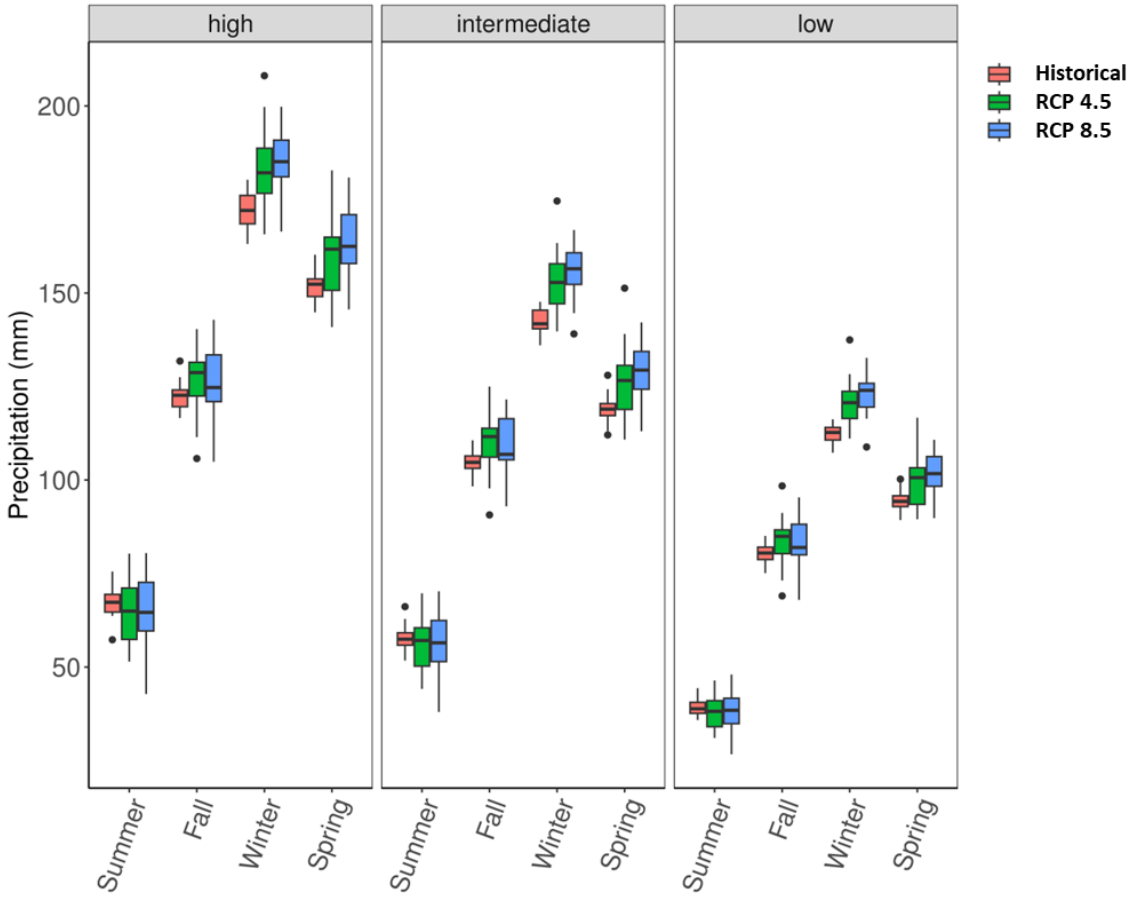

Figure 3.2. Historical and projected future (RCP 4.5 and RCP 8.5) seasonal precipitation from the 20 GCMs for the three precipitation zones.

Table 3.1. Projected future (RCP 4.5 and 8.5) climate change for the three precipitation zones. Values in parentheses are percent changes: (+) indicates increase and (–) indicates decrease.

		Precipitation Zone					
		High		Intermediate		Low	
		RCP 4.5	RCP 8.5	RCP 4.5	RCP 8.5	RCP 4.5	RCP 8.5
Precipitation*	Annual	21 (4)	27 (5)	22 (5)	26 (6)	16 (5)	19 (6)
	Summer	−2 (−4)	−2 (−4)	−2 (−3)	−2 (−3)	−1 (−3)	−1 (−3)
	Fall	5 (3)	4 (3)	6 (4)	5 (4)	4 (3)	3 (3)
	Winter	11 (8)	14 (8)	11 (9)	13 (9)	8 (9)	10 (9)
	Spring	8 (8)	12 (8)	8 (9)	11 (9)	5 (8)	8 (8)
Temperature¶	Daily	2 (24)	3 (31)	2 (24)	3 (31)	2 (19)	3 (25)
	Summer	2 (18)	3 (18)	2 (17)	3 (17)	2 (15)	3 (15)
	Fall	2 (30)	3 (30)	2 (30)	3 (30)	2 (24)	3 (24)
	Winter	2 (4573)	3 (4580)	2 (445)	3 (445)	2 (246)	3 (246)
	Spring	2 (28)	2 (28)	2 (27)	2 (27)	2 (21)	2 (21)

*Precipitation, average annual and seasonal, mm; ¶Temperature, average daily and seasonal, °C

3.3.1.2. Temperature

Projected future temperatures vary, but a consistent warming trend projected across the GCMs is discernible (Figure 3.2). The average daily temperature increases across all three precipitation zones from the historical to future RCP 4.5 and RCP 8.5, by 19–24% and 25–31%, respectively (Table 3.1). Projected winter temperature increases notably across all zones with increase from historical average of ~0 °C to 2–3 ° C. An uptick of 15–28% in temperature across the three zones was projected for spring and summer for the two future scenarios, with a 24–30% hike in temperature projected for fall. Projected maximum and minimum temperatures follow a similar increasing trend as the average daily temperature. The number of days with minimum temperature below 0 °C is expected to decrease on average by 38, 44, and 47 for RCP 4.5 and by 46, 55, and 57 days for RCP 8.5 for the low-, intermediate-, and high-precipitation zones, respectively.

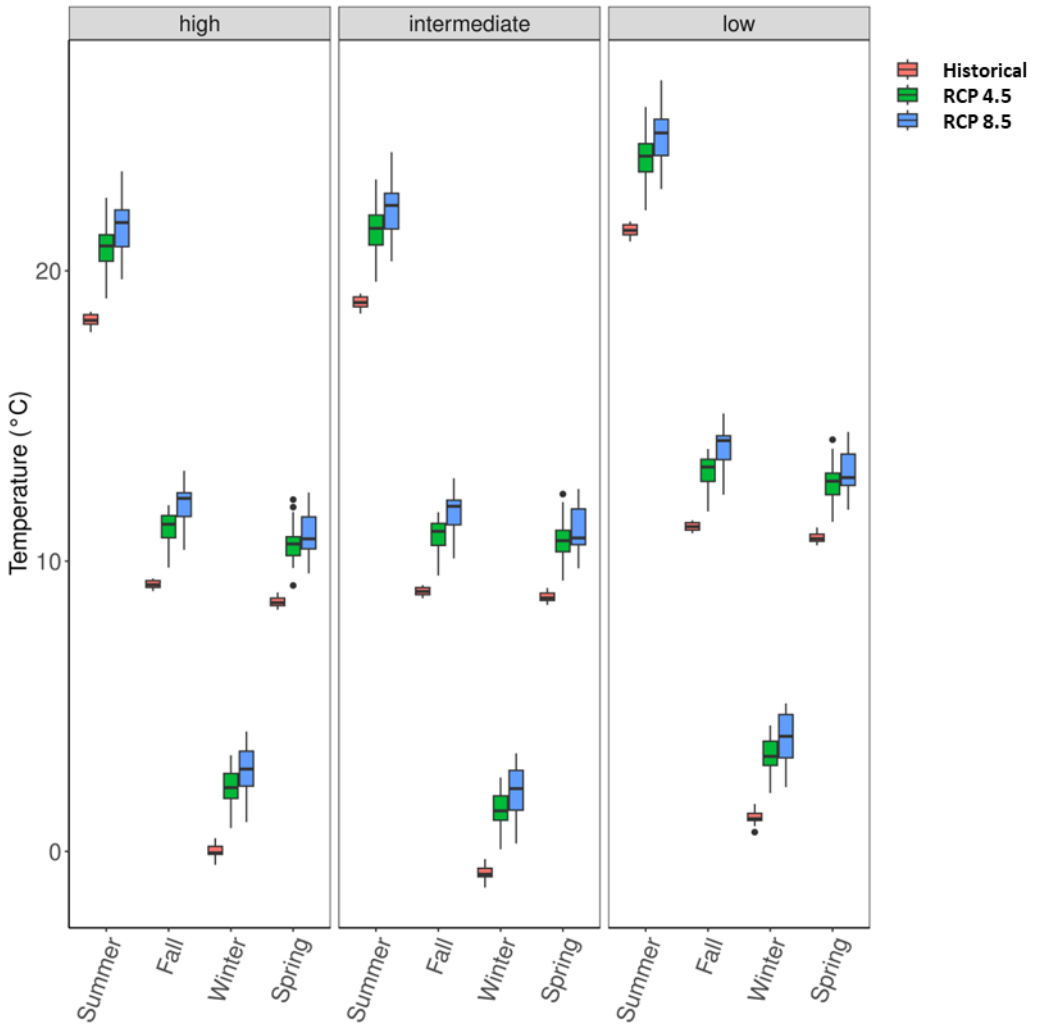

Figure 3.3. Historical and projected future (RCP 4.5 and RCP 8.5) seasonal temperatures by all 20 GCMs for the three precipitation zones.

3.3.2. Water Balance

3.3.2.1. Evapotranspiration (ET)

Evapotranspiration (ET) responses to projected future climate under different tillage practices showcased consistent increase in all precipitation zones from the historical period (Figure 3.4). The increase in annual ET is the most pronounced in the high-precipitation zone, especially under intense tillage (Table 3.2). RCP 8.5 consistently yielded the largest average increase in ET for all tillage practices, with the increase reaching 57 mm (14%) in the high-precipitation zone. The intermediate-precipitation zone mirrored this trajectory, registering a

range of 40–48 mm of increased ET across tillage practices, with little distinction between the results from the two RCPs. The change in annual ET is lowest in the low-precipitation zone, by 22–26 mm.

The summer months had highest ET surges for all precipitation zones (Table 3.2). This highest increase (39 mm, 21%) in summer ET was in the high-precipitation zone under intense tillage in RCP 8.5. Winter ET increases as well (with its relative increase being the highest of all seasons), especially in the intermediate- and high-precipitation zones for both RCPs, irrespective of the tillage method. Changes in spring ET are moderate in comparison to the changes in winter, and changes in fall ET are largely negligible.

Table 3.2. Change in projected future (RCP 4.5 and 8.5) ET (mm) for the three precipitation zones under three tillage practices. Values in parentheses are percent changes; (+) indicates increase and (–) indicates decrease.

		Precipitation Zone					
		High		Intermediate		Low	
Tillage		RCP 4.5	RCP 8.5	RCP 4.5	RCP 8.5	RCP 4.5	RCP 8.5
Intense	Annual	48 (12)	57 (14)	40 (12)	48 (14)	22 (8)	26 (9)
	Summer	34 (19)	39 (21)	22 (18)	26 (21)	4 (8)	4 (9)
	Fall	0 (1)	0 (0)	0 (1)	0 (1)	3 (8)	4 (8)
	Winter	11 (24)	14 (29)	13 (29)	15 (35)	8 (14)	9 (16)
	Spring	3 (2)	6 (4)	6 (4)	8 (6)	7 (5)	9 (6)
Reduced	Annual	41 (9)	48 (11)	41 (11)	47 (13)	21 (7)	24 (8)
	Summer	20 (10)	22 (10)	15 (11)	15 (11)	1 (2)	0 (1)
	Fall	1 (2)	1 (2)	1 (1)	1 (2)	3 (7)	3 (7)
	Winter	11 (27)	14 (33)	12 (31)	15 (38)	10 (18)	12 (21)
	Spring	9 (6)	12 (8)	14 (10)	17 (12)	8 (5)	9 (6)
No-till	Annual	41 (9)	48 (11)	41 (11)	46 (13)	20 (7)	23 (8)
	Summer	19 (9)	20 (10)	15 (11)	14 (10)	0 (1)	0 (0)
	Fall	1 (3)	1 (3)	1 (2)	1 (1)	3 (6)	3 (6)
	Winter	11 (26)	14 (33)	12 (30)	15 (37)	10 (17)	12 (21)
	Spring	10 (7)	13 (9)	14 (10)	17 (12)	8 (5)	9 (6)

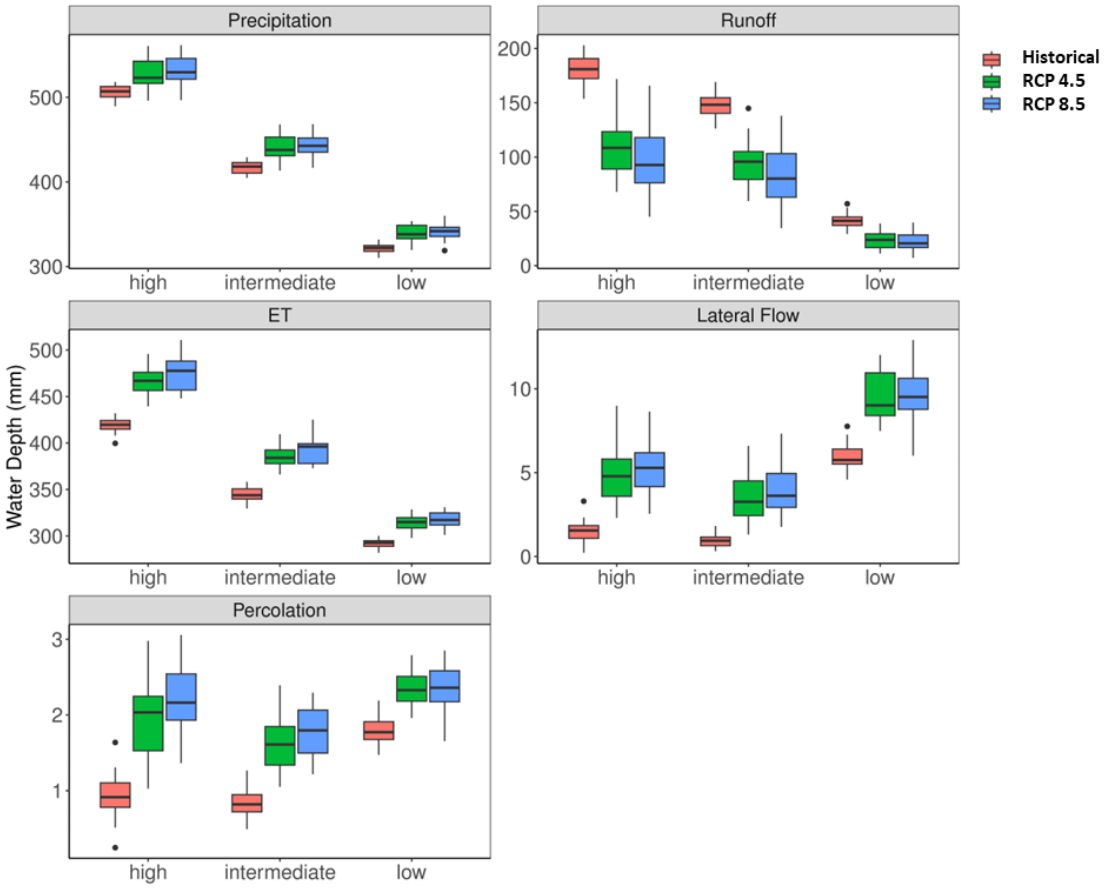

Figure 3.4. Historical and projected future (RCP 4.5 and RCP 8.5) annual water balance for the three precipitation zones from all GCMs.

3.3.2.2. Runoff

Projected runoff consistently decreases from the historical period for all three precipitation zones for all tillage scenarios (Figure 3.4). The most notable reductions in annual runoff are in the high-precipitation zone under intense tillage, especially under RCP 8.5, plummeting by 81 mm (45%) (Table 3.3). Annual runoff for the intermediate zone follows a similar pattern, but the decrease is more moderate ranging 52–64 mm (35–44 %) for intense tillage. The decrease in runoff for the low-precipitation zone, ranging 13–19 mm, with the percent decrease equally high (43–46%)for all scenarios.

Projected seasonalrunoff decreases consistently across all precipitation zones, tillage types, and RCP scenarios (Table 3.3). Winter runoff reductions are the most drastic, especially in

the intermediate- and high-precipitation zones, by up to 72 mm under RCP 8.5. Projected spring runoff decreases as well in all precipitation zones, though at a smaller magnitude. Projected runoff reductions for fall are low, all less than 10 mm. As in the historical period, runoff is minimal in summer in both future scenarios for all precipitation zones.

Table 3.3. Change in projected future (RCP 4.5 and RCP 8.5) runoff (mm) for the three precipitation zones under three tillage practices. Values in parentheses are percent changes; (+) indicates increase and (–) indicates decrease.

		Precipitation Zone					
		High		Intermediate		Low	
Tillage		RCP45	RCP85	RCP45	RCP85	RCP45	RCP85
Intense	Annual	−71 (−39)	−81 (−45)	−52 (−35)	−64 (−44)	−18 (−43)	−19 (−46)
	Summer	0*	0	0	0	0	0
	Fall	−4 (−28)	−6 (−47)	−2 (−4)	−4 (−35)	0	−1 (78)
	Winter	−63 (−39)	−72 (−45)	−44 (−34)	−53 (−41)	−18 (−45)	−19 (−48)
	Spring	−4 (−33)	−4 (−16)	−7 (−72)	−7 (−73)	0	0
Reduced	Annual	−50 (−41)	−54 (−44)	−50 (−43)	−56 (−47)	−15 (−46)	−15 (−46)
	Summer	0	0	0	0	0	0
	Fall	−2 (−2)	−3 (−39)	−1 (19)	−3 (−29)	0	0
	Winter	−46 (−41)	−49 (−44)	−44 (−41)	−48 (−44)	−15 (−48)	−15 (−48)
	Spring	−3 (−21)	−3 (−6)	−5 (−72)	−6 (−76)	0 (310)	0 (628)
No-till	Annual	−49 (−42)	−52 (−45)	−50 (−44)	−54 (−48)	−13 (−46)	−13 (−45)
	Summer	0)	0	0	0	0	0
	Fall	−1 (43)	−2 (−29)	0 (56)	−2 (−13)	0 (1310)	0 (1631)
	Winter	−45 (−43)	−48 (−46)	−44 (−43)	−47 (−45)	−13 (−48)	−13 (−47)
	Spring	−3 (−18)	−3 (−5)	−5 (−71)	−6 (−77)	0 (278)	0 (597)

*For historical runoff of zero, percent change is not calculated.

3.3.3. Erosion

Predicted changes in erosion vary depending on the GCMs, precipitation zone, tillage intensity, and RCP scenario. Annual erosion in the high-precipitation zone decreases notably under intense tillage, more so for RCP 8.5, with a decrease of 4.3 Mg ha^{-1} (Table 3.4.). The projected erosion reduction in the low-precipitation zone closely mirrors the reduction in the high-precipitation zone, decreasing by 3.5 Mg ha^{-1} under RCP 8.5. The erosion reduction in the intermediate zone is minimal.

Table 3.4. Projected future (RCP 4.5 and RCP 8.5) average annual erosion (t ha^{-1}) for the three precipitation zones under three tillage practices; (+) indicates increase and (–) indicates decrease.

		Precipitation Zone					
		High		Intermediate		Low	
		RCP 4.5	RCP 8.5	RCP 4.5	RCP 8.5	RCP 4.5	RCP 8.5
Intense	Annual	−3.1	−4.3	−0.2	−2	−3.2	−3.5
	Summer	0.2	0.4	0.3	0.4	0.2	0.1
	Fall	−0.6	−1.4	−0.4	−1.4	−0.1	−0.2
	Winter	−2.2	−2.9	1.2	0.2	−3.1	−3.4
	Spring	−0.5	−0.4	−1.3	−1.2	0	0
Reduced	Annual	0.4	0.8	0.3	0	−1.4	−1.6
	Summer	0.1	0.3	0.1	0.1	0	0
	Fall	−0.1	−0.3	0	−0.3	0	0
	Winter	0.4	0.8	0.6	0.5	−1.4	−1.6
	Spring	0	0.1	−0.4	−0.3	0	0
No-till	Annual	0.1	0.2	0.2	0.3	−0.3	−0.3
	Summer	0	0.1	0	0.1	0	0
	Fall	0	0	0.1	0	0	0
	Winter	0.1	0.2	0.2	0.4	−0.3	−0.4
	Spring	0	0	−0.1	−0.1	0	0

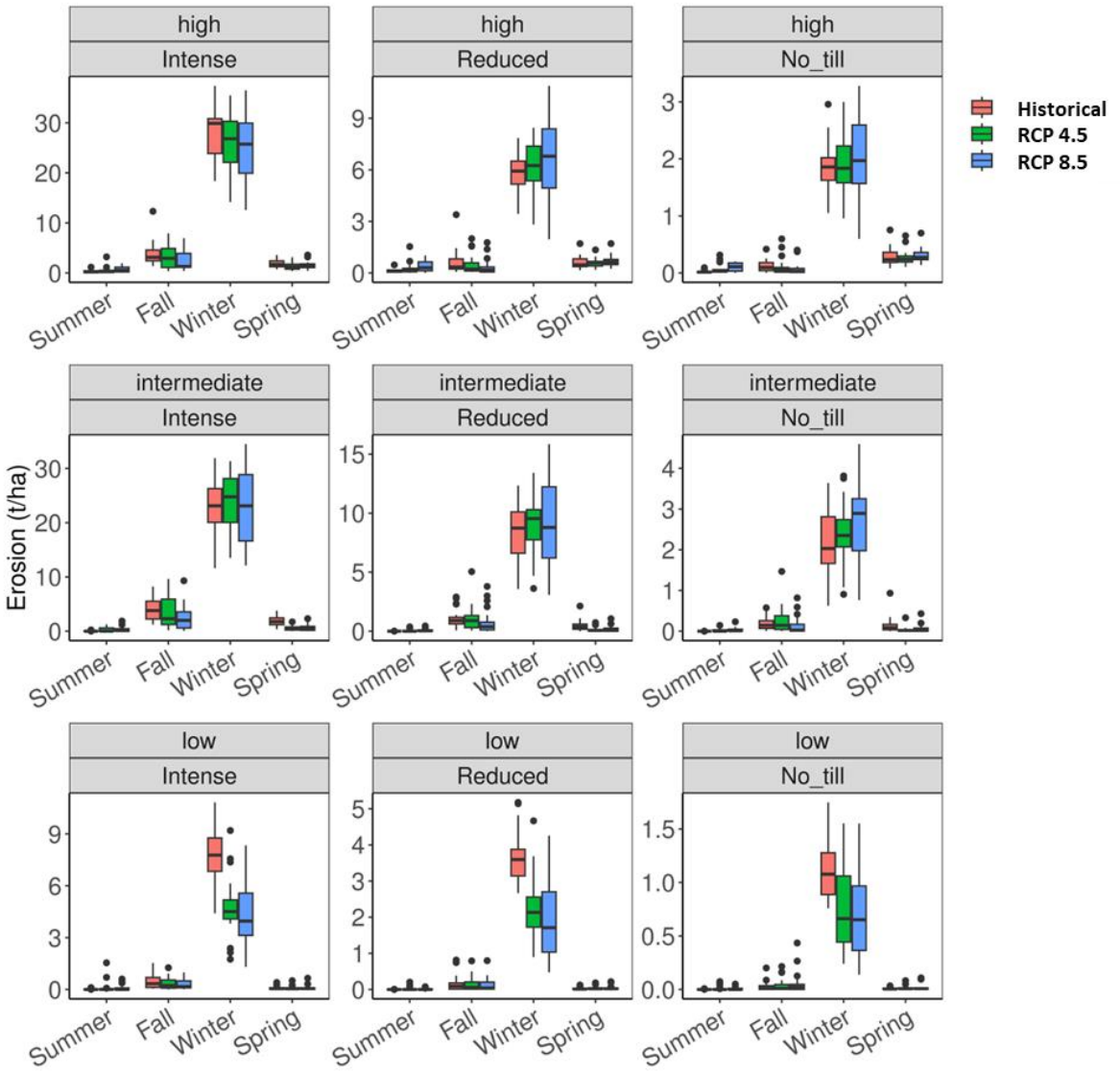

Figure 3.5. Historical and projected future (RCP 4.5 and RCP 8.5, from all GCMs) seasonal erosion for the three precipitation zones under different tillage conditions.

Projected seasonal erosion changes follow a similar trend to annual erosion with marked changes in winter (Figure 3.5). For the high-precipitation zone, winter erosion decrease was most prominent under intense tillage, by 2.2 (4%) and 2.9 Mg ha^{-1} (8%) under the RCP 4.5 and RCP 8.5, respectively (Table 3.4). For the intermediate-precipitation zone, projected winter erosion also decreases but no more than 1.2 Mg ha^{-1}. In the low-precipitation zone, seasonal erosion decreases consistently, most prominent for winter by up to 3.4 Mg ha^{-1} (44%) under intense

tillage and RCP 8.5. For all precipitation zones, fall and spring erosion generally decrease albeit by no more than 1.4 Mg ha^{-1}.

Change in erosion by slope steepness

Projected change in erosion generally increases with increasing slope steepness (Figure 3.6). In the high-precipitation zone, there is a consistent decreasing trend in erosion from historical to future when the slope steepness is lower than 20%. For steeper slopes (>20%) of the high-precipitation zone, projected erosion in the future increases with slope gradient for all tillage conditions and reaches 35–45 Mg ha^{-1} for the slope steepness greater than 30% for intense tillage (Figure 3.6). In the intermediate-precipitation zone, under intense tillage, erosion increases in RCP 4.5, but decreases in RCP 8.5 when the slope steepness is lower than 25% but increases in both future scenarios when slope gradient is greater than 25%. The shift from decrease to increase in future erosion rate also occurs under reduced tillage and no-till for both the intermediate- and high-precipitation zones but at different slope steepness threshold. In the low-precipitation zone, there is a consistent decrease in erosion rate under all tillage intensities across all slope steepness.

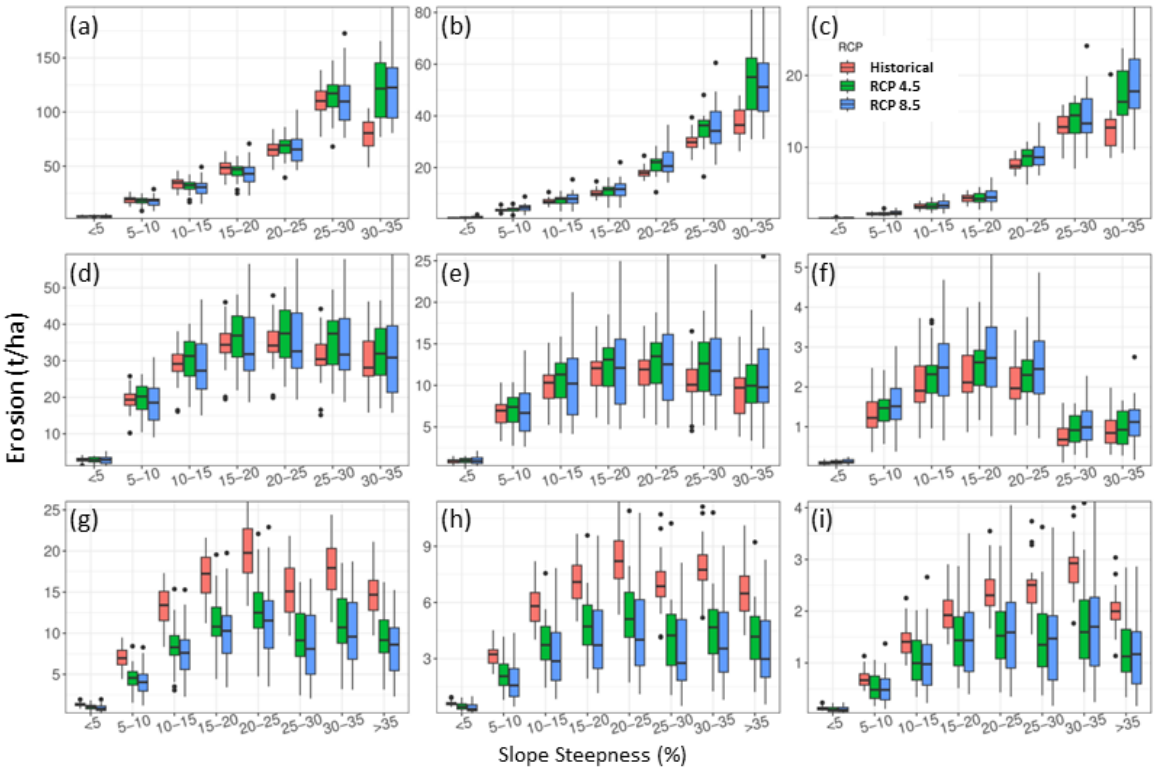

Figure 3.6. Historical and projected future (RCP 4.5 and RCP 8.5, from all GCMs) erosion: (a), (b), and (c) for high-precipitation zone, (d), (e), and (f) for intermediate-precipitation zone, and (g), (h), and (i) for low-precipitation zone, under intense tillage, reduced tillage, and no-till, respectively.

3.4. Discussions

3.4.1. Change in Water Balance Components

Consistent increase in future may be attributed to increase in temperature, precipitation, and biomass density. Increased temperature directly leads to increases in ET and biomass density (Pruski and Nearing, 2002; Chien et al., 2013). An increase in biomass density amplifies crop water use hence increasing ET. This circular effect results in a marked uptick of ET in the summer months from the historical period. Additionally, increase in precipitation means more available soil water, which in turn results in an increase in ET in non-growing season.

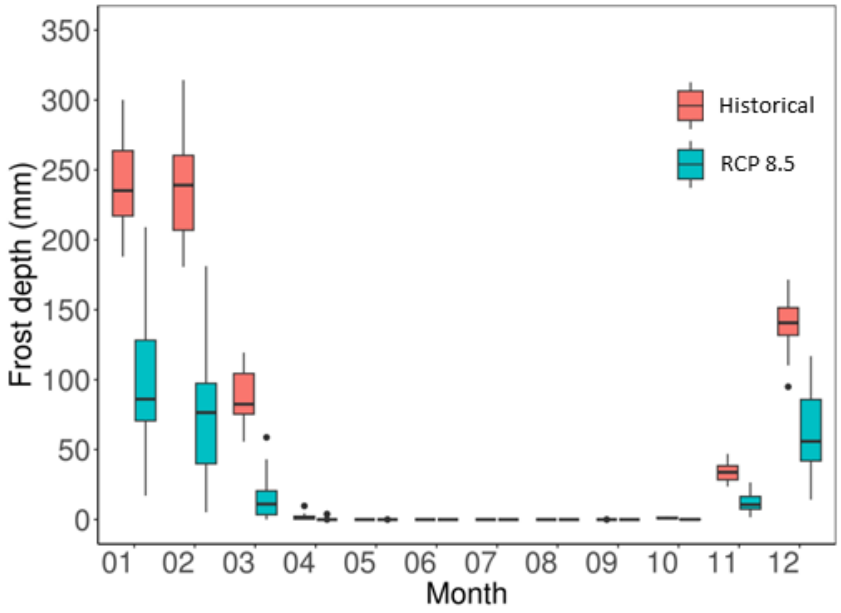

Figure 3.7. Projected future decrease in frost depth for historical and RCP 8.5, high-precipitation zone, under intense tillage.

In contrast, projected future runoff decreases consistently even with an increase in precipitation. This can be attributed to the change in soil freeze-thaw regime due to the increase in temperature. WEPP adjusts the soil hydraulic conductivity based on soil freeze-thaw conditions (Flanagan & Livingston, 1995), decreasing the conductivity when soil is frozen. Projected frost depth in winter decreases from the historical period (Figure 3.7) due to general increase in temperature and decrease in the number of days with T_{min} below 32 °F . This results in increased infiltration capacity during winter months and hence lower runoff.

3.4.2. Change in Erosion

Projected erosion under intense tillage decreases despite a increase in precipitation in the high-precipitation zone. This is largely due to the decrease in projected runoff, especially during the winter season. The increase in temperature will reduce the number of events with rain on frozen and thawing soils resulting in a further decrease in erosion. In the intermediate-precipitation zone, projected erosion increases in winter, albeit by a small margin. This is

because the increase in precipitation counters the effect on erosion due to milder winter conditions, and the overall effect is a slight increase in erosion. Erosion in the low-precipitation zone has been relatively low due to its low precipitation and low runoff (Dahal et Al., 2022). With a further decrease in future runoff the erosion is minimal in all conditions, even lower than the NRCS tolerance limit of 11 t ha^{-1}.

The decreasing erosion trend does not hold true under reduced tillage for the intermediate- and high-precipitation zones, with a small net average increase (~0–1 t ha^{-1}) in the future. The reason could be a faster residue decomposition in the future. Increase in future temperature results in more rapid residue decomposition, less dead biomass on the ground, leading to an increase in erosion (Figure 3.8). Yet the increase in temperature also affects winter conditions in favor of a decrease in erosion, and the overall outcome is a small increase in erosion.

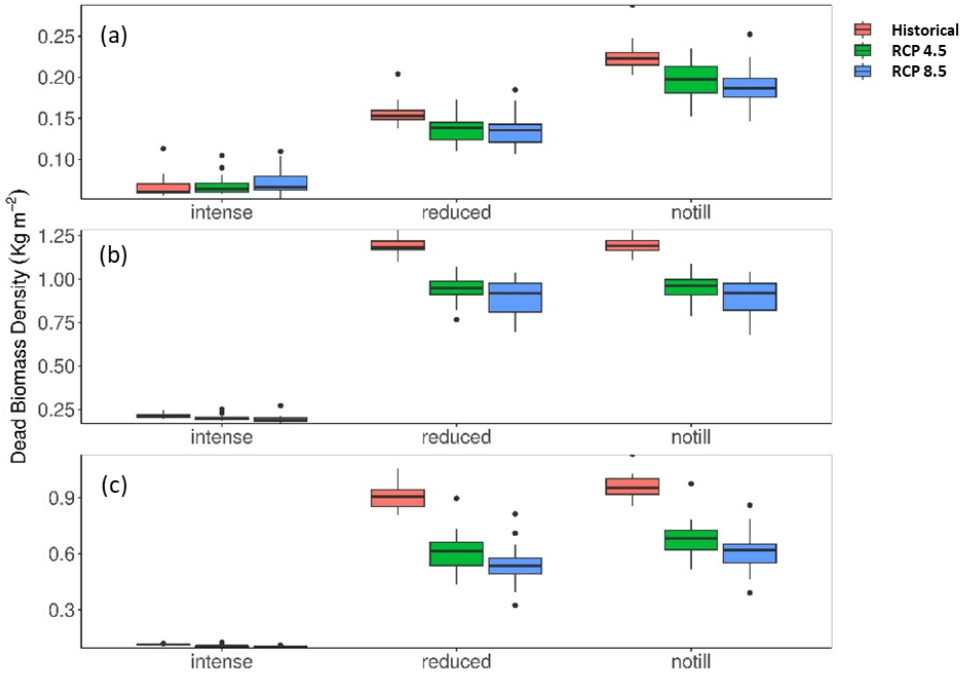

Figure 3.8. Average daily dead biomass by tillage intensity in a) wheat, b) barley, and c) pea for the high-precipitation

zone.

In the high precipitation zone, predicted erosion generally increases on steeper slopes, especially when slope steepness exceeds 20%. This is because steeper slopes generate more runoff and hence causing greater erosion, all other conditions being the same. In WEPP, excess rainfall after infiltration first fills up depression storage before runoff occurs (Flanagan and Livingston, 1995) With the depression storage inversely related to slope steepness (Flanagan and Livingston, 1995). Therefore, steeper slopes have smaller depression storage and hence a higher potential for runoff, other conditions being equal. The intermediate and low precipitation zone didn't follow this trend of increase in erosion in steeper slopes because the impact of slope steepness on erosion could have been nullified by soil properties such as higher soil depth and hydraulic conductivity, lower soil erodibility and higher critical shear resulting in overall decrease in erosion.

3.4.3. Future Erosion Hot Spots and Targeted Management

Despite the decrease in projected future erosion, erosion rates remain high in places, often 2–3 folds higher than the NRCS tolerance limit. Hillslopes with steep gradient, shallow soils under intense tillage, and wheat years all exhibit erosion rates far exceeding 50 Mg ha^{-1} (Figure 3.9).

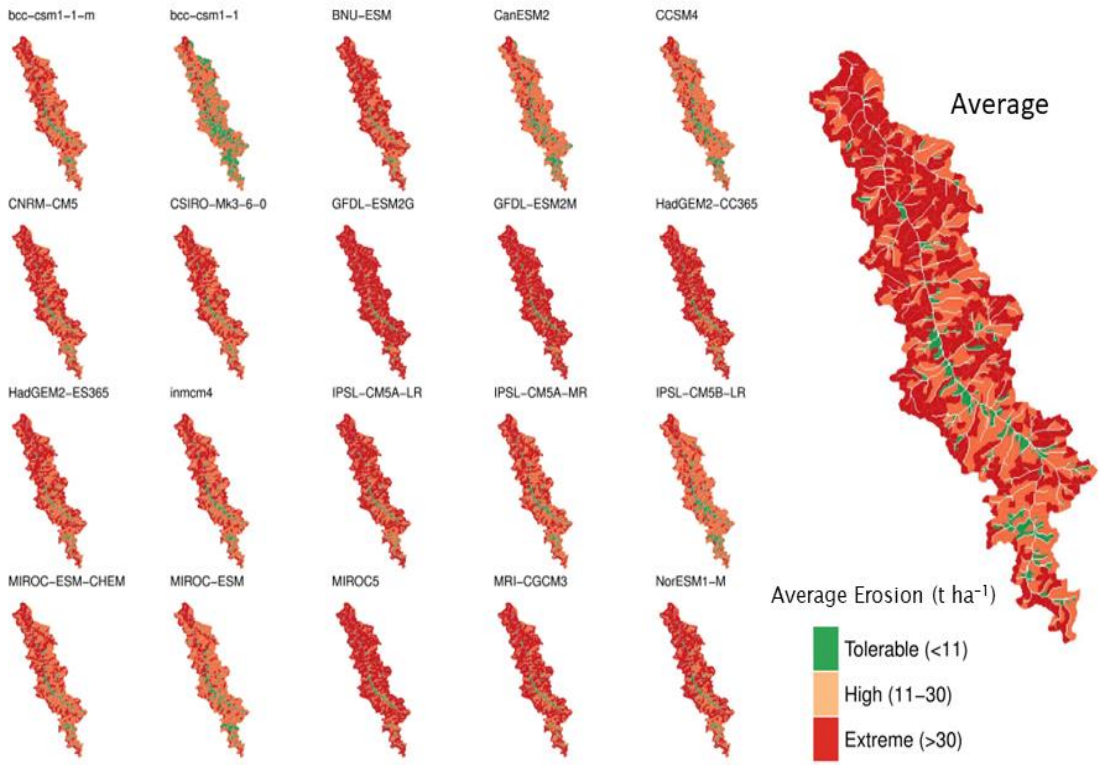

Figure 3.9. Erosion in the high-precipitation zone under intense tillage and RCP 8.5 (from all 20 GCMs).

These problem areas (hot spots) can be targeted for erosion reduction WEPP simulations suggest that targeted management under intense tillage is not effective with only a minor decrease in erosion under conservation scenarios 1 and 3 (Table 3.4). However, reducing tillage for the whole watershed will decrease erosion by 55–74% in the three precipitation zones, and implementation of no-till across the whole watershed will decrease erosion by 85–93% (Table 3.5). Hillslopes with slope steepness >20% constitute less than 4% of the total area of each of the three watersheds yet produce disproportionately high erosion (Figure 3.6). Should these areas be retired (e.g., converted to perennial prairie) and the rest of the watershed be under reduced tillage, erosion would be decreased by 57–77% for the three watersheds (Figure 3.10).

Table 3.5. Projected future average annual erosion under different management conditions.

Management	Precipitation Zone					
	High		Intermediate		Low	
	RCP 4.5	RCP8.5	RCP 4.5	RCP 8.5	RCP 4.5	RCP 8.5
Intense	36.2	35.3	34.3	32.1	6.1	5.7
Reduced	9.1	9.8	12.2	11.8	2.8	2.5
No-till	2.7	2.9	2.9	3.0	0.8	0.8
Conserv. 1*	34.7	33.9	34.0	31.9	5.8	5.4
Conserv. 2⁋	8.8	9.4	12.1	11.7	2.7	2.4
Conserv. 3*	34.1	33.2	33.9	31.8	5.6	5.2
Conserv. 4⁋	8.5	9.2	12.0	11.7	2.6	2.4

*Intense tillage with targeted reduced tillage (Conserv. 1) or land retirement (Conserv. 3) on hillslopes with steepness >20%; ⁋Reduced tillage with targeted no till (Conserv. 2) or land retirement (Conserv. 4) on hillslopes with steepness >20%

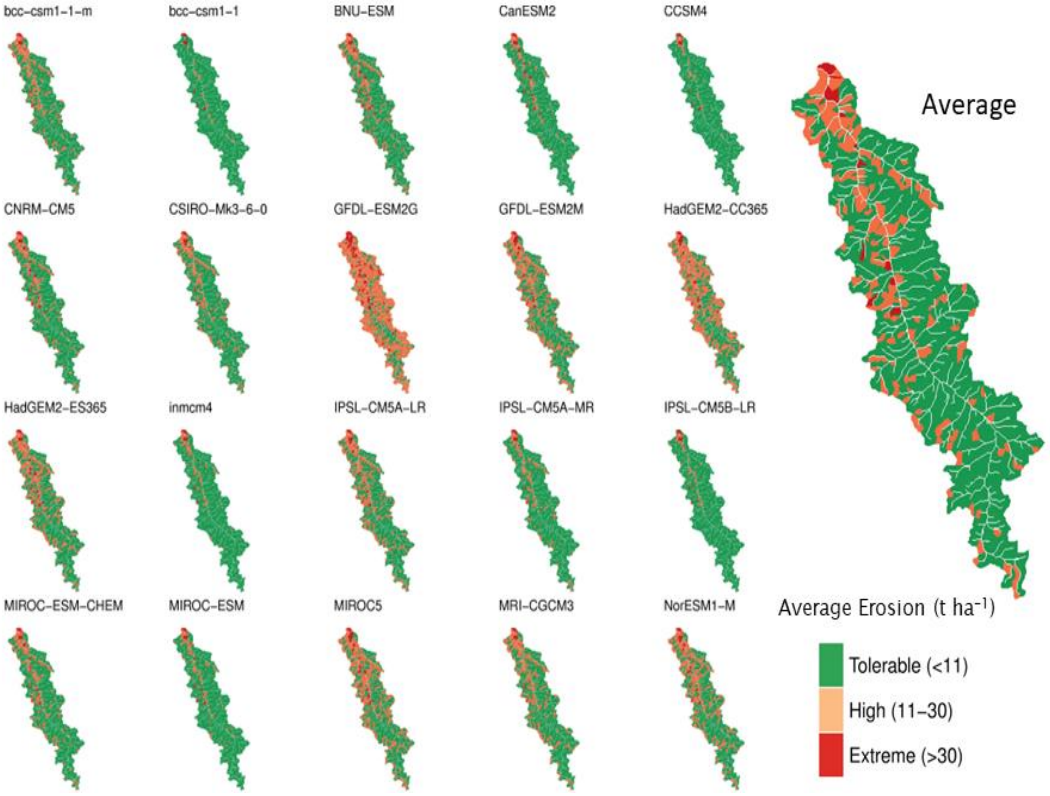

Figure 3.10. Erosion in the high-precipitation zone under targeted conservation practices (scenario 4, reduced tillage with hillslopes with gradient > 20% retired) for RCP 8.5 (from all GCMs).

3.5. Summary and Conclusions

In this study, water erosion was simulated for the historical period and two future climate scenarios for three model watersheds in Whitman County. Downscaled climate data from 20

GCMs for historical (1976–2005) and RCP 4.5 and RCP 8.5 future (2036–2075) scenarios were assimilated and aggregated for the three model watersheds. Relative changes in climate, water balance, and erosion rate for the three model watersheds were assessed. WEPP-simulated water erosion for future scenarios were mapped, hot spots were identified, and select management scenarios were tested. The results highlighted nuanced interplay between climate factors and water erosion, and demonstrated the importance of strategic land management in mitigating future erosion risks. Major conclusions of this study include:

1. There is a general increase in future ET in the three precipitation zones of Whitman County, caused by the projected increase in temperature and precipitation, and in turn, biomass density. There is a general decrease in runoff due to an increase in ET, and projected increased infiltration capacity resulting from a decrease in frost depths in the area.

2. Projected future water balance and erosion were impacted by multiple factors and their interaction, at times offsetting the effects of one another. The predicted future average annual erosion generally decreases in the three precipitation zones of Whitman County due to the decrease in predicted future runoff.

3. The decrease in projected water erosion in the low- and high-precipitation zones occurs mostly in winter months (by 2.2–3.5 Mg ha^{-1}) due to a decrease in runoff and milder winter soil freeze-thaw conditions resulting from an increase in temperature. The projected winter erosion slightly increases in the intermediate-precipitation zone (by 0.2–1.2 Mg ha^{-1}) because of the competing effects of increased temperature and precipitation.

4. Even with the projected decrease in erosion in the low- and high-precipitation zones,

erosion amounts rates remain problematic in places, exceeding 50 Mg ha^{-1} on steeper slopes and shallow soils or during wheat years, especially in the intermediate- and high-precipitation zones.

5. The excessive erosion on hot spots may be mitigated by targeted management. Retiring the areas with slope steepness >20% and reducing the tillage intensity in other areas of the watershed would decrease the erosion rate by 57–77% across all three precipitation zones.

3.6. Acknowledgments

This study is in part supported by USDA AFRI NIFA (Grant No. 2018-68002-27920). I acknowledge the funding support from Puget Sound Partnership (NTA 2018-0704) and Chicona Endowment Assistantship.

REFERENCES

Abatzoglou, J.T., & Brown, T.J. (2012). A comparison of statistical downscaling methods suited for wildfire applications. International Journal of Climatology, 32(5), 772–780.

Abatzoglou, J.T., Rupp, D.E., & Mote, P.W. (2014). Seasonal climate variability and change in the Pacific Northwest of the United States. Journal of Climate, 27(5), 2125–2142.

Adams, R.M., Hurd, B.H., Lenhart, S., & Leary, N. (1998). Effects of global climate change on agriculture: An interpretative review. Climate Research, 11(1), 19–30.

Aydinalp, C., & Cresser, M.S. (2008). The effects of global climate change on agriculture. American-Eurasian Journal of Agricultural & Environmental Sciences, 3(5), 672–676.

Borrelli, P., Robinson, D.A., Panagos, P., Lugato, E., Yang, J.E., Alewell, C., ... & Ballabio, C. (2020). Land use and climate change impacts on global soil erosion by water (2015–2070). Proceedings of the National Academy of Sciences, 117(36), 21994–22001.

Chien, H., Yeh, P.J.F., & Knouft, J.H. (2013). Modeling the potential impacts of climate change on streamflow in agricultural watersheds of the Midwestern United States. Journal of Hydrology, 491, 73–88. https://doi.org/10.1016/j.jhydrol.2013.03.042

Dahal, M.S., Wu, J.Q., Boll, J., Ewing, R.P., & Fowler, A. (2022). Spatial and agronomic assessment of water erosion on inland Pacific Northwest cereal grain cropland. Journal of Soil and Water Conservation, 77(4), 347–364. https://doi.org/10.2489/jswc.2022.00091

Dun, S., Wu, J.Q., Elliot, W.J., Robichaud, P.R., Flanagan, D.C., Frankenberger, J.R., Brown, R. E., & Xu, A.C. (2009). Adapting the Water Erosion Prediction Project (WEPP) model for forest applications. Journal of Hydrology, 366(1–4), 46–54. https://doi.org/10.1016/j.jhydrol.2008.12.019

Edwards, B.L., Webb, N.P., Brown, D.P., Elias, E., Peck, D.E., Pierson, F.B., ... & Herrick, J.E. (2019). Climate change impacts on wind and water erosion on US rangelands. Journal of Soil and Water Conservation, 74(4), 405–418.

Flanagan, D.C., & Livingston, S.J. (Eds.) (1995). WEPP User Summary: USDA-water erosion prediction project. NSERL Report 11. West Lafayette, IN: USDA ARS National Soil Erosion Research Laboratory. Retrieved from https://www.ars.usda.gov/ARSUserFiles/50201000/WEPP/usersum.pdf

Garbrecht, J.D., & Zhang. C.X. (2015). Soil erosion from winter wheat cropland under climate change in Central Oklahoma. Applied Engineering in Agriculture, 31, 439–454. https://doi.org/10.13031/aea.31.10877

Guo, Y., Peng, C., Zhu, Q., Wang, M., Wang, H., Peng, S., & He, H. (2019). Modelling the impacts of climate and land use changes on soil water erosion: Model applications, limitations, and future challenges. Journal of Environmental Management, 250, 109403.

https://doi.org/10.1016/j.jenvman.2019.109403

Henry, H.A. (2008). Climate change and soil freezing dynamics: historical trends and projected changes. Climatic Change, 87(3–4), 421–434.

Karimi, T., Stöckle, C.O., Higgins, S., & Nelson, R. (2018). Climate change and dryland wheat systems in the US Pacific Northwest. Agricultural Systems, 159, 144–156. https://doi.org/10.1016/j.agsy.2017.09.004

Lew, R., Dobre, M., Srivastava, A., Brooks, E.S., Elliot, W.J., Robichaud, P.R., & Flanagan, D.C. (2022). WEPPcloud: An online watershed-scale hydrologic modeling tool. Part I. Model description. J. Hydrol., 608, 127603. https://doi.org/10.1016/j.jhydrol.2022.127603

Li, Z., & Fang, H. (2016). Impacts of climate change on water erosion: A review. Earth Science Review, 163, 94–117.

NCDC (National Climatic Data Center). (2022). NOAA satellite and information service. NCDC. Retrieved from https://www.ncdc.noaa.gov/cdo-web/

Nicks, A. D., Lane, L. J., & Gander, G. A. (1995). Chapter 2. Weather generator. In D. C. Flanagan & M. A. Nearing (Eds.), *USDA-Water Erosion Prediction Project: Hillslope profile and watershed model documentation* (pp. 2.1–2.22). NSERL Report 10. West Lafayette, IN: USDA ARS National Soil Erosion Research Laboratory.

Nearing, M.A. (2001). Potential changes in rainfall erosivity in the US with climate change during the 21st century. Journal of Soil and Water Conservation, 56, 229–232.

Nearing, M.A., Pruski, F.F., & O'Neal, M.R. (2004). Expected climate change impacts on soil erosion rates: A review. Journal of Soil and Water Conservation, 59(1), 43–50.

O'Neal, M.R., Nearing, M.A., Vining, R.C., Southworth, J., & Pfeifer, R.A. (2005). Climate change impacts on soil erosion in Midwest United States with changes in crop management. Catena, 61(2–3), 165–184. https://doi.org/10.1016/j.catena.2005.03.006

Pruski, F.F., & Nearing, M.A. (2002). Runoff and soil-loss responses to changes in precipitation: A computer simulation study. Journal of Soil and Water Conservation, 57, 7–16.

Schulze, R. (2000). Transcending scales of space and time in impact studies of climate and climate change on agrohydrological responses. Agriculture, Ecosystems & Environment, 82, 185–212. https://doi.org/10.1016/S0167-8809(00)00207-6

Sharratt, B.S., Tatarko, J., Abatzoglou, J.T., Fox, F.A., & Huggins, D. (2015). Implications of climate change on wind erosion of agricultural lands in the Columbia plateau. Weather and Climate Extremes, 10, 20–31.

Srivastava, A., Flanagan, D.C., Frankenberger, J.R., & Engel, B.A. (2019). Updated climate database and impacts on WEPP model predictions. Journal of Soil and Water Conservation,

74(4), 334–349.

Stocker, T.F., Dahe, Q., & Plattner, G. (2013). Climate Change 2013, The Physical Science Basis. In Fifth Assessment Report of the intergovernmental panel on climate change, 33–115. Cambridge University Press, Cambridge, NY, USA.

US Geological Survey. (2019). USGS NED 1 arc-second ArcGrid 2019. USGS. Retrieved from https://apps.nationalmap.gov/downloader/

Wang, L., Cherkauer, K.A., & Flanagan, D.C. (2018). Impacts of climate change on soil erosion in the Great Lakes region. Water, 10, 715. https://doi.org/10.3390/w10060715

4. IDENTIFYING PRIORITY SITES FOR RAIN GARDENS IN THE LOWER PUYALLUP RIVER WATERSHED

4.1. Introduction

Impervious surfaces in urban areas hinder infiltration, reduce evapotranspiration (ET), and increase the rate and quantity of runoff (Tsihrintzis and Hamid, 1997; Walsh, 2012). Runoff across roads, parking lots, and roofs carry various chemicals, including nutrients and heavy metals, such as phosphorus, lead, zinc, potassium, and calcium (Tsihrintzis and Hamid, 1997; Bjorkuland et al., 2018). Pollutant-laden stormwater runoff adversely impacts the water quality of the receiving water bodies (ponds, lakes, and streams) (Paul and Meyer, 2001; Lee et al., 2007; Muller et al., 2020). This impairment contributes to degraded aquatic habitat and endangers species in the aquatic ecosystem (Booth and Jackson, 1997; Palmer, 2008). For example, toxic stormwater runoff in the Pacific Northwest has increased the mortality of juvenile coho salmon (Sandahl et al., 2007; McIntyre et al., 2018).

Green Stormwater Infrastructure (GSI)

Stormwater pollution can be mitigated by slowing and retaining runoff and treating its associated pollutants (Schueler et al., 1992; USEPA, 2022). Green Stormwater Infrastructures (GSIs) are Best Management Practices (BMPs) that intercept and retain urban runoff by enhancing infiltration and ET (Grumbles, 2007; Chini, 2017; Taguchi et al., 2020). Vacant areas in urban watersheds can be used to install these structures to improve stormwater management, create open space for neighborhood recreational activity, and increase biodiversity (Chini, 2017).

Rain gardens are common small-scale GSI that serve as a stormwater sink comprising a plant-soil system where water retention is enhanced through infiltration and storage (Shuster et al., 2017; Taguchi et al., 2020; USEPA, 2022; Martin-Mikle et al., 2015). Rain gardens collect

runoff from nearby rooftops, yards, sidewalks, and parking lots (Taguchi et al., 2020; USEPA, 2022), capturing pollutants and reducing their loads through mechanisms such as sedimentation, adsorption, microbial breakdown, and plant uptake (Woodward et al., 2009; Winston et al., 2010). Jennings (2016) tested rain gardens at 35 locations in the contiguous United States and found that runoff reductions ranged from 52% to 100%. Dietz and Clausen (2005) evaluated the performance of two rain gardens in Haddam, CT, USA, and found that the rain gardens markedly increased the lag time of runoff and reduced the peak flow rate. Additionally, ammonia nitrogen (NH_3-N) and total nitrogen concentrations in the rain gardens' outlet were considerably lower than what was going into the rain gardens.

The effectiveness of rain gardens depends on their design, construction, and landscape position (Shuster et al., 2017). Critical parameters for rain garden design include the drainage area contributing to runoff and the soil characteristics in which the rain garden is to be constructed (WSDE, 2014). If the rain garden is not sized correctly, runoff from the contributing drainage area could overwhelm it, limiting its ability to store, infiltrate, and treat stormwater (Guo et al., 2021). Soil with adequate permeability and storage capacity is essential to maximizing the rain garden's performance (Jennings, 2016; Shuster et al., 2017). Soils of extremely high permeability offer a shorter retention time for pollutant treatment. In contrast, those of low permeability impede infiltration and could generate more runoff, leading to a rain garden's failure (Shuster et al., 2017). Another critical factor is the cost-effectiveness of installing a rain garden (Martin-Mikle et al., 2015)—given the limitation of resources, GSIs should be placed where they will be most effective to justify the cost of installment.

Placement of GSI

Shojaeizadeh et al. (2020) developed a placement tool for GSI using Storm Water Management Model (SWMM) at a sub-basin scale. This approach placed different GSIs in optimal locations, meeting the targeted flow and pollutant reduction while minimizing the cost. The hydrological and water quality estimation capabilities of SWMM were coupled with performance, cost, and optimization framework to develop a new interface that could identify the optimal number and type of GSI for each sub-basin to meet the target runoff and pollutant reduction while also minimizing the cost. Various other studies have also used SWMM coupled with optimization algorithms to place GSI at the sub-basin scale (Macro et al., 2019; Wu et al., 2019).

Kaykhosravi et al. (2019) proposed an approach to meeting the low-impact development (LID) demand for the city of Toronto, which included environmental and socioeconomic indices as decision-making criteria to complement the hydrological index. The hydrological index was calculated based on rainfall intensity, slope, hydraulic conductivity, and soil depth. It was used to rank sub-areas within the study area for their propensity to generate runoff. The priority of LID installation within an individual sub-area was then further ranked in terms of environmental and socioeconomic needs. The adequacy of the resulting map was assessed based on the runoff volume estimated by the Hydrological Engineering Center-Hydrological Modeling System model (HEC-HMS; USACE-HEC, 1998). The indexing method and the HEC-HMS model yielded generally agreeable results except for flat areas. The reason may be that the hydrological index method is primarily dependent on, and therefore sensitive to, slope steepness.

Guo et al. (2021) used the WEPP model to evaluate the efficiencies of various LIDs in an urban watershed of Austin, Texas. The urban watershed was delineated through the WEPP cloud,

and was simulated to obtain soil loss for each hillslope. Select hillslopes producing the most significant soil loss were identified as the most suitable for placing LIDs, such as native planting, permeable pavement, rain gardens, and detention ponds. LIDs were placed in select hillslopes separately and in combination, and the WEPP was run for various scenarios to reassess the impact on runoff reduction. The average annual surface runoff was reduced from 15–56 % in all scenarios except detention ponds, where the primary function is to delay the stormwater and is not expected to reduce surface runoff. The scenarios with native planting performed best, reducing average annual runoff depths by 54–56 %.

Hydrologically-Sensitive Area Approach

Another approach to prioritizing locations for rain gardens in an urban setting is based on identifying Hydrologically-Sensitive Areas (HSAs), which are those areas within a watershed that are more prone to generate runoff (Walter et al., 2000; Bueno and Alves, 2017). Kirkby and Beven (1979) proposed a condition for identifying saturated areas in a watershed based on the equation:

$$\ln\left(\frac{\alpha}{\tan\beta}\right) > \frac{\bar{D}}{m} - \lambda \quad (4.1.1)$$

where $\overline{\mathrm{D}}$ is the mean storage deficit (range $-\infty$ to $+\infty$) of the watershed, α is the contributing area per unit length, β is the slope steepness, λ is the areal average of $\ln(\alpha/\tan\beta)$, and *m* is a watershed-specific constant in relation to subsurface storage. Equation 4.1.1 implies that soil moisture in any area of the watershed can be tracked based on its topographical feature $\ln(\alpha/\tan\beta)$ and soil storage capacity ($\bar{D}/m$). In other words, if the quantity of runoff from the upland contributing area into a location is greater than that location's soil water storage deficit, then the location can be considered saturated. The underlying assumptions of this condition are

that transmissivity of the soil profile is homogeneous, and all points with the same ($\alpha/\tan\beta$), value are hydrologically similar (Beven, 1987). It follows that mapping the topographic index $\ln(\alpha/\tan\beta)$ will indicate the saturation areas within a watershed (Kirkby and Beven, 1979; Beven, 1987). This concept can be extended to heterogeneous soil profiles by including soil transmissivity (*KD*, with *K* being hydraulic conductivity and *D* soil depth) into the index as $\ln(\alpha/KD\tan\beta)$ (Ambroise et al., 1996; Walter et al., 2002; Beven et al., 2021).

Following Kirkby and Beven (1979), Qiu (2009) proposed an indexing method to identify HSAs by calculating two different indices. The first, the Topographic Wetness Index (λ_{TWI}; Eq. 4.1.2), is a function of slope steepness and runoff contributing area. The second, the Soil Water Storage Capacity (λ_{SWSC}; Eq. 4.1.3a), is a function of soil hydraulic conductivity and soil depth modified by percent impervious areas (Eq. 4.1.3b; Qiu, 2009; Martin-Mikle et al., (2015)). Subtracting λ_{SWSC} from λ_{TWI} yields the Hydrologic Sensitivity Index (λ_{HSI}; Eq. 4.1.4). A location is considered hydrologically sensitive if its λ_{HSI} value exceeds some threshold (Qiu et al., 2020), for example, 10 (Qiu, 2009), 9 (Bueno and Alves, 2017), or 1.5 standard deviations greater than the mean (Martin-Mikle et al., 2015).

$$\lambda_{TWI} = \ln\left(\frac{\alpha}{\tan\beta}\right) \qquad (4.1.2)$$

$$\lambda_{SWSC} = \ln(K_s D_m) \qquad (4.1.3a)$$

$$D_m = D \times I \qquad (4.1.3b)$$

$$\lambda_{HSI} = \lambda_{TWI} - \lambda_{SWSC} \qquad (4.1.4)$$

Qiu et al. (2020) examined various topographic index thresholds to determine the best threshold for delineating hydrologically sensitive areas (HSAs) in New Jersey and its five water

regions (Lower Delaware, Upper Delaware, Raritan, Atlantic Coast, and Northeast). The HSA was delineated in these six regions separately for the Topographic Wetness Index (TWI) and Hydrologic Sensitivity Index (HSI). The study used 14 different thresholds of HSI and TWI from 8 to 14.5 with an interval of 0.5 to delineate HSAs, resulting in 168 HSA maps. These HSA maps were compared with the FEMA 100-year floodplain map, and the suitability of various thresholds was assessed. The most suitable was the threshold that led to the most agreeable spatial patterns with the FEMA floodplain. The statewide threshold for HSA delineation was determined to be 10.5 for TWI and 10 for HSI, but the most suitable threshold varied among the five water regions. The authors found that using a TWI threshold produced better agreement in delineating HSAs for areas with shallow water tables and areas where flow path distribution is dominated by topographical convergence. The HSI threshold produced better accuracy in areas where restrictive soil layers dictate the interflow movement of water, and flow path distribution is limited by soil transmissivity.

Martin-Mikle et al. (2015) applied this approach to a mixed-land use watershed in central Oklahoma, USA, and identified sites with an accuracy of 94±5.7% as verified through field visits which assessed the feasibility of LID construction based on open-space availability and topographic suitability. Vittorio and Ahiablame (2015) cautioned that the effectiveness of GSIs on a watershed scale is not always clear, and future research should clarify the spatial translation and downstream effectiveness of installing these structures.

The Puget Sound region in the US Pacific Northwest includes several metropolitan areas, forest-, range-, and croplands encompassing complex ecosystems (PSP, 2021). Situated in the South Puget Sound, the lower Puyallup River watershed is one of the fastest developing areas in the state. The watershed contains multiple aquatic habitats to which Chinook and Coho salmon

return for spawning during the rainy season (Marks and Laley, 2011; Reinelt, 2013). These species are susceptible to harm from toxic stormwater (French et al., 2022).

Rationale and Objectives

Various approaches are available for the placement of GSI and evaluation of their effectiveness, but their use is limited by their low spatial resolutions, cost, and steep learning curve (Jayasooriya et al., 2014; Dovel et al., 2015; Martin-Mikle et al., 2015). There is a need for a simplified approach that can serve as a quick assessment and decision -support tool for stakeholders to identify problem areas in the watershed (Ahiablame et al., 2012). In this study, we aimed to adapt the hydrological sensitivity approach method using publicly available data for placing GSI in the lower Puyallup watershed. The objectives of this study were to (i) identify optimum locations for placement of rain gardens in the lower Puyallup watershed based on the HSI method and (ii) assess the adequacy of the method through hydrological modeling using WEPP.

4.2. Methodology

4.2.1. Study Area

The study area is the Lower Puyallup Watershed in the South Puget Sound, western Washington (Figure 4.1). The watershed measures 128 km^2 and comprises several cities, including Puyallup and Tacoma in Pierce County, with approximately 60% residential area (WSDE, 2010). The impervious area accounts for 29% (USGS, 2023). High-intensity development is clustered in the central part from north to south where downtown Puyallup and South Hill are located, and towards the northwestern part including downtown Tacoma. Forests are spread throughout the watershed in natural parks and other wilderness areas while agricultural fields are located towards the north on the Puyallup River floodplains. Various

wetlands, parks, and water bodies are spread throughout the watershed. Several tributaries containing salmon spawning habitats flow south to north and join Puyallup River along the northern boundary of the watershed draining directly into the Puget Sound. The study area is most commonly underlain by glacial sediment deposits called the Vashon till, which overlays sedimentary and volcanic bedrock deposits (Welch et al., 2015).

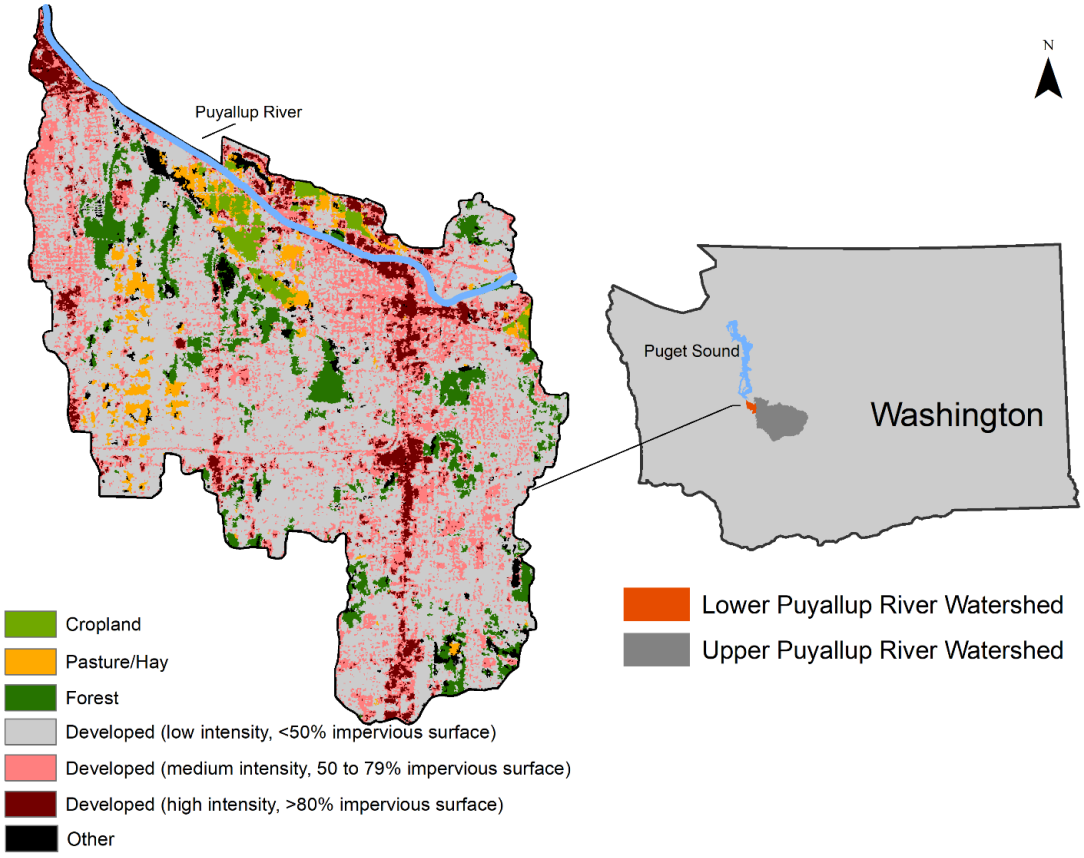

Figure 4.1. Lower Puyallup River Watershed

The area exhibits a Mediterranean climate with warm summer and wet winter. The average annual precipitation of the area is 992 mm, and the average daily temperature is 10.5 °C based on the long-term (1914–2022) weather records (NOAA, 2023). Elevation ranges from −9 m to 200 m a.m.s.l. and increases from the Puyallup River towards the south. Within the watershed, areas are flat towards the north and are hilly and steep towards the central and south

(Figure 4.2a). The predominant soil is the Kapowsin gravelly loam, which is moderately deep, permeable, and mostly found in the central part of the watershed (NRCS, 2023). Shallow, less permeable soils occur in the west-central part of the watershed while deep, highly permeable soils are found in the southern part of the watershed (Figure 4.2b, c; NRCS, 2023).

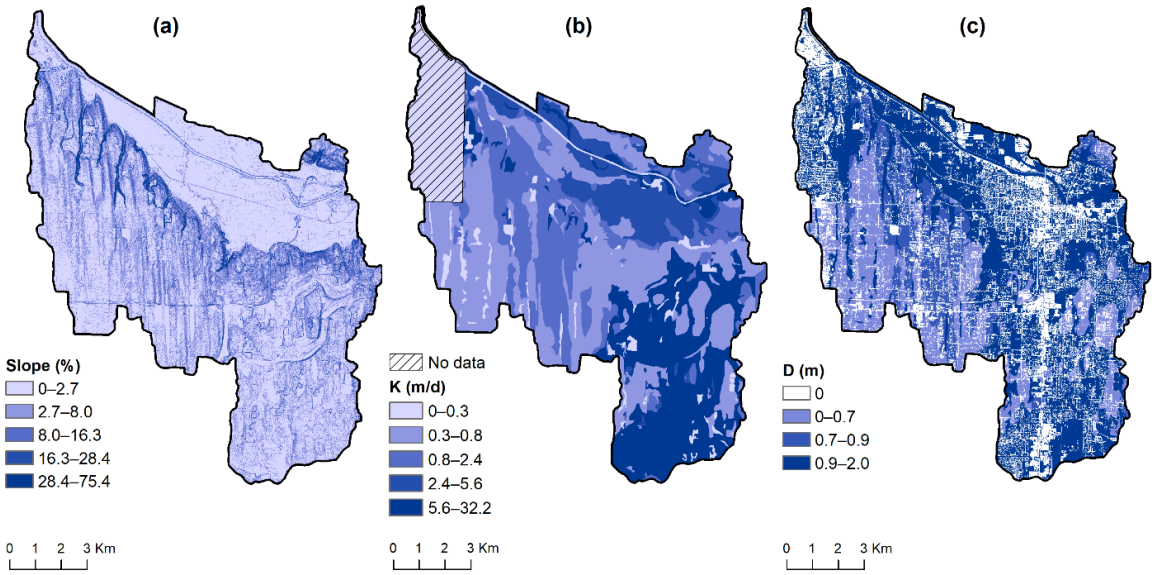

Figure 4.2. Slope (a) and soil characteristics (hydraulic conductivity, b; soil depth, c) of the study area

4.2.2. Data

All the data for this study were compiled from publicly available sources (Table 4.1). The elevation data were LiDAR data of 6-ft/1.8-m resolution (WA DNR, 2023). Soil data were extracted from the SSURGO database (NRCS, 2023). The impervious area layer was derived from National Agriculture Imagery Program (NAIP) imagery (USGS, 2023). Areas unsuitable for rain garden per EPA and state ordinances were extracted from the Pierce County (2023) website.

Table 4.1. Data layers used in this study

GIS Layer	Resolution/format	Source	Citation
Elevation	6-ft/raster	Washington State Department of Natural Resources	(WA DNR, 2023)
Impervious areas	6-ft/raster	National Agriculture Imagery Program	(USGS, 2023)
Unsuitable areas (roads, wetlands, erosion and landslide hazard areas)	polygon	Pierce County Open Geospatial Data Portal	(Pierce County, 2023)
Soil data (depth, hydraulic conductivity)	polygon	United State Department of Agriculture (USDA), Soil survey	(NRCS, 2023)
Watershed boundary, Water bodies	polygon	United States Geological Survey (USGS)	(USGS, 2023)

4.2.3. Computing Hydrologic Sensitivity Index (λ_{HSI})

We computed Hydrologic Sensitivity Index in ArcGIS (ESRI, 2020) using Digital Elevation Model (DEM), soil depth, saturated hydraulic conductivity, and impervious areas. Specifically, slope steepness was computed using the DEM after removing sinks. Grid cells with slope gradient of zero were assigned a small value of 0.0001 following Qiu (2009). D-infinity algorithm (Jenson and Domingue, 1988) was used to compute the flow direction, flow accumulation, and contributing drainage areas (α) from the filled DEM. λ_{TWI} was then computed using Eq. 4.1.2.The impact of impervious surface is taken into account by adjusting the depth to the restrictive layer (Eq. 4.1.3a). λ_{SWSC} was computed following Eq. 4.1.3b, and λ_{HSI}, Eq. 4.1.4. The spatial patterns of λ_{HSI} and the effects of landscape characteristics on λ_{HSI} were analyzed using ArcPy. All post-processing was carried out using R (R Core Team, 2023).

4.2.4. Identifying Areas Suitable for Rain Garden

Areas within the watershed that are unsuitable for rain gardens were excluded following engineering criteria provided in federal and state ordinances (WA DOE, 2019; EPA, 2023). These areas include impervious areas, regulated flood plains, wetlands, water bodies (with a 30-m buffer), landslide and erosion hazard areas, parks, and forests.

Engineering criteria for constructing rain gardens primarily concern size (area), soil depth, and hydraulic conductivity (EPA, 2023). Rain gardens are typically sized to be about 5% of their contributing area at sites where the soil depth exceeds 2 m and saturated hydraulic conductivity ranges between 0.18 to 5.5 m/d (Pierce County Stormwater Manual, 2015). After consulting with local experts, we selected the Maximum rain garden size as 140 m^2 (1500 sq. ft) and 2800 m^2 (30000 sq feet) as the maximum contributing area for rain gardens. (WA DOE, 2019; Pierce County Stormwater Manual, 2015). Areas not meeting these engineering requirements were excluded from consideration.

4.2.5. Adjustment to λ_{HSI}

We converted the λ_{HSI} map from grid- to lot-scale using a 100 ft×100 ft "fishnet", and the λ_{HSI} values were arbitrarily classified into five classes of equal interval to evaluate the association of λ_{HSI} and runoff generation and therefore areas most suitable for rain garden. Impervious areas affect the movement of stormwater runoff in various manners. Residential driveways may be constructed with little change to the natural landscape with minimal effect on runoff flow paths. On the other hand, large-scale industrial and commercial development is subject to state stormwater management regulations where stormwater infrastructure may alter the natural flow paths, e.g., stormwater runoff is collected and removed through storm drains. To account for these potential disruptive effects of impervious areas to natural drainage pathways, we assumed two cases: (i) flow was not, and (ii) flow was, disrupted by impervious areas. For the second case, we adjusted flow accumulation using weighting factors (0 for impervious areas, and 1 for pervious areas) to obtain a new set of λ_{TWI} and λ_{HSI}. Figure 4.3 shows the framework and steps to identify suitable areas for rain garden with or without flow accumulation adjustment.

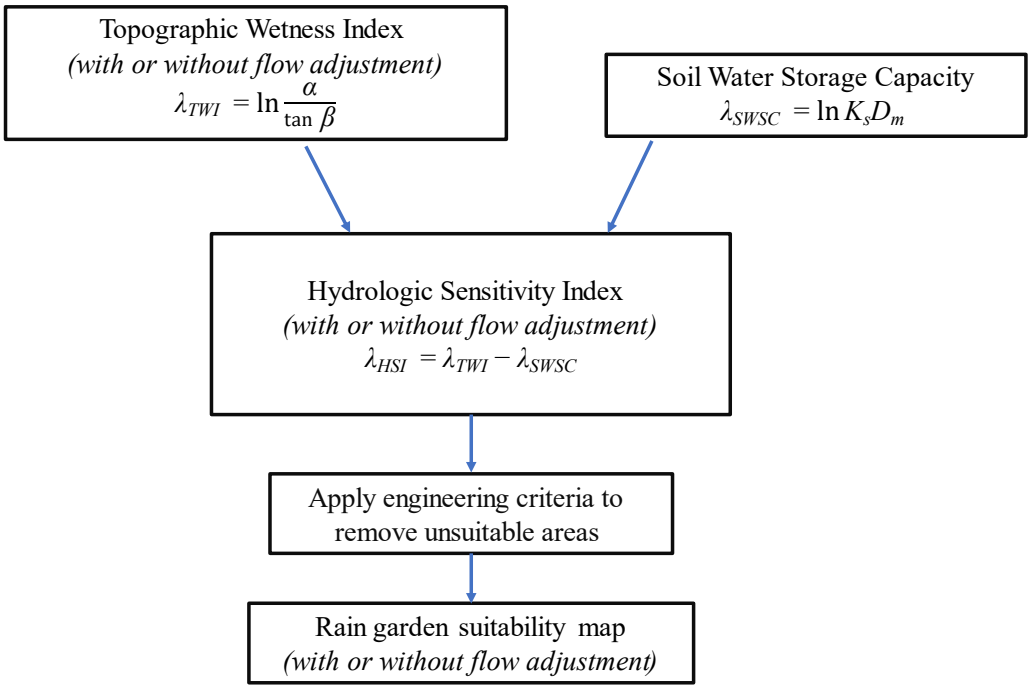

Figure 4.3. Schematic identifying suitable areas for rain garden where with or without flow adjustment due to impervious areas was considered.

4.2.6. Hydrological Analysis

Hydrological modeling was conducted to quantify water balance and assess runoff in relation to λ_{HSI}. This analysis used the Water Erosion Prediction Project (WEPP) model (hillslope version 2012.8). WEPP is a physically-based, distributed-parameter, and continuous-simulation model for hydrology and water erosion (Flanagan et al., 1995). WEPP simulates major hydrological processes, including runoff, infiltration, evapotranspiration (ET), subsurface lateral flow, and deep percolation (Dun et al., 2009; Guo et al., 2019, Dahal et al., 2021). It requires climate, slope, soil, and management inputs and uses the Overland Flow Element (OFE) as the smallest hydrological response unit to represent a unique combination of slope, soil, climate, and management settings.

A conceptual hillslope was designed with three OFEs comprising the top, middle, and toe of a hillslope (Figure 4.4). We used the observed precipitation and temperature from the weather

station within the watershed (McMillin Reservoir, WA; NCDC, 2022) and other climate inputs, such as wind speed and direction, dew-point temperature, and solar radiation generated with CLIGEN, the auxiliary stochastic weather generator (Nicks et al., 1995) and the climate input was built for latest 10 years.

The soil inputs were built based on the properties of the Kapowsin gravelly loam, the most predominant soil series within the study watershed. We varied the slope steepness and lengths for the same soil properties and conducted multiple simulation to assess their effects on runoff generation (Table 4.2). Similarly, we varied the soil depth and hydraulic conductivity for the same slope steepness and length to determine the effect of soil characteristics on runoff generation (Table 4.2). Bromegrass was used as vegetation for the hillslopes for all scenarios following WEPPcloud watershed delineation for the study area, whose growth parameters were selected following Flanagan & Livingston (1995). We modeled hillslopes with pavement and underdrain at the top of the hillslope to assess the effect of developed areas on runoff. Additionally, we computed λ_{HSI} for all combinations of the hillslope properties to evaluate their relationships with the simulated runoff.

Table 4.2. Varying hillslope characteristics (slope length and steepness) and soil properties (depth and saturated hydraulic conductivity) for WEPP simulations

Varying Slope Characteristics[¶,†]		Varying Soil Characteristics[¶,†]	
D, 1.0 m and *K*, 20 mm/hr		tan *β*, 0.075 and *L*, 100 m	
Slope (tan *β*)	Slope Length (*L*, m)	Soil Depth (*D*, m)	Sat. Hydraulic Conductivity (*K*, mm/hr)
0	25	0.5	5
0.075	50	1.0	10
0.15	100	1.5	15
	200	2.0	20
			25

[¶]When changing slope (soil) characteristics, soil (slope) characteristics were held constant

[†]Slope (Soil) characteristics were changed by combining slope steepness and length (soil depth and hydraulic conductivity)

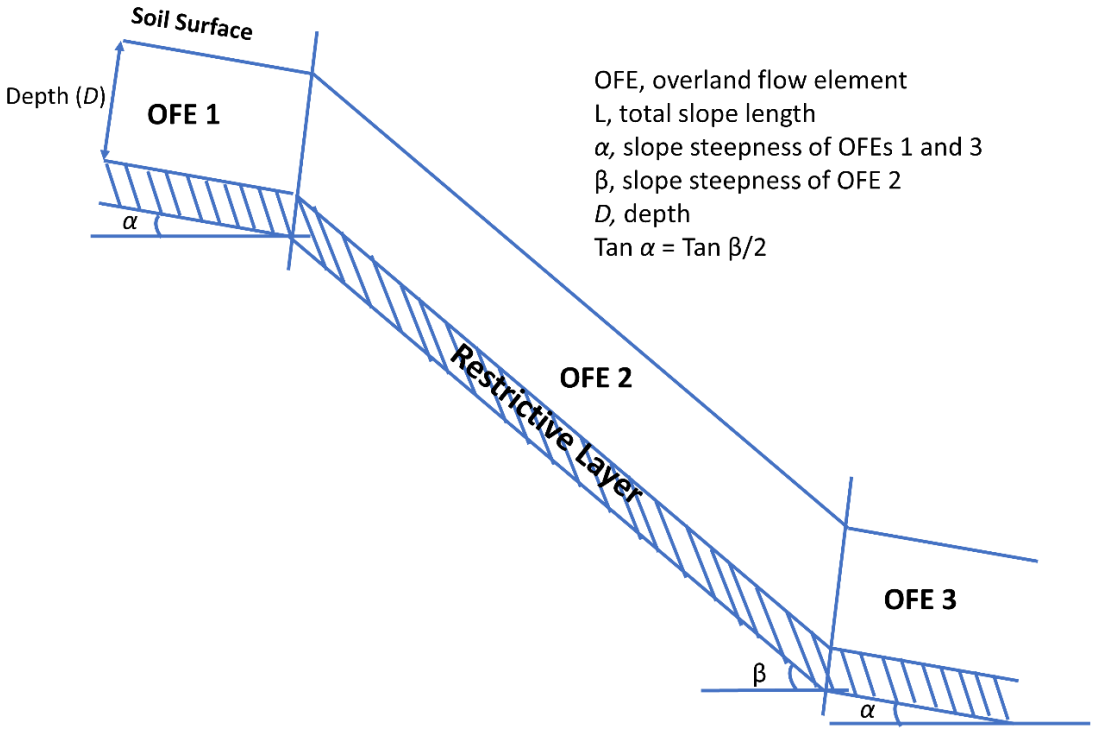

Figure 4.4. Conceptual hillslope comprising three (top, middle, toe) Overland Flow Elements (OFEs) for hydrological analysis.

4.3. Results and Discussion

4.3.1. Distribution of λ_{TWI} and λ_{SWSC}

The λ_{TWI} values ranged from −0.2 to 30, with high-λ_{TWI} areas distributed across the watershed near depressions, wetlands, and the end of flow paths. High-λ_{TWI} areas also clustered at lower elevation in the northwest of the watershed. The λ_{SWSC} ranged from −3.4 to 4.2, with high values more common for the southern part of the watershed because of the larger hydraulic conductivities and deeper soils of that area.

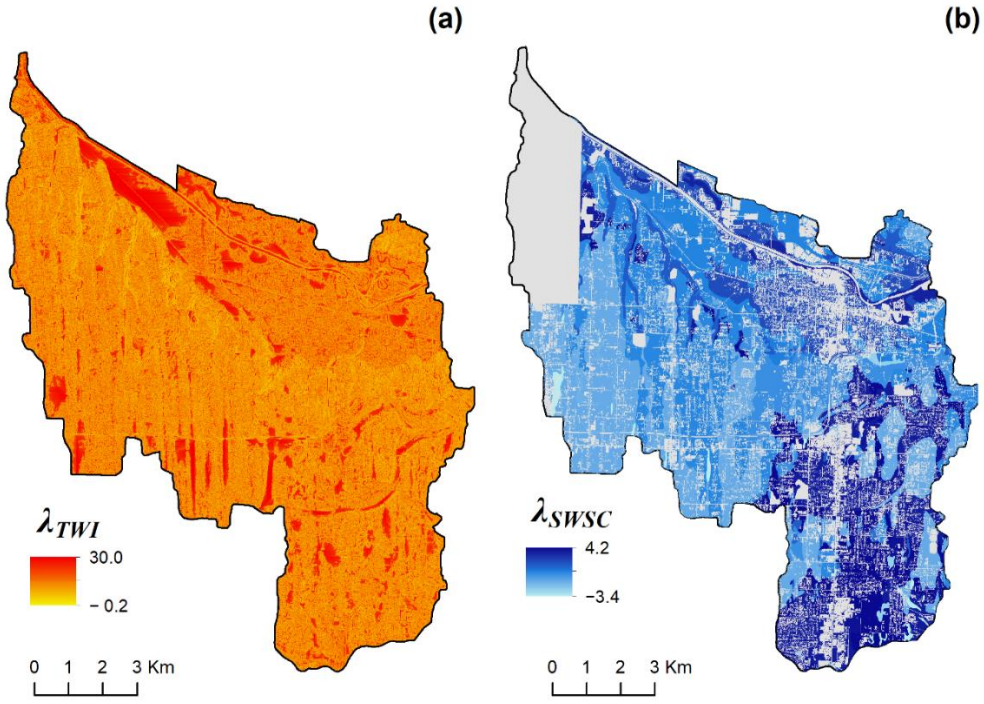

Figure 4.5. Variation of the Topographic Wetness Index (λ_{TWI}) and Soil Water Storage Capacity (λ_{SWSC}) indices within the Lower Puyallup River Watershed

4.3.2. Distribution of λ_{HSI}

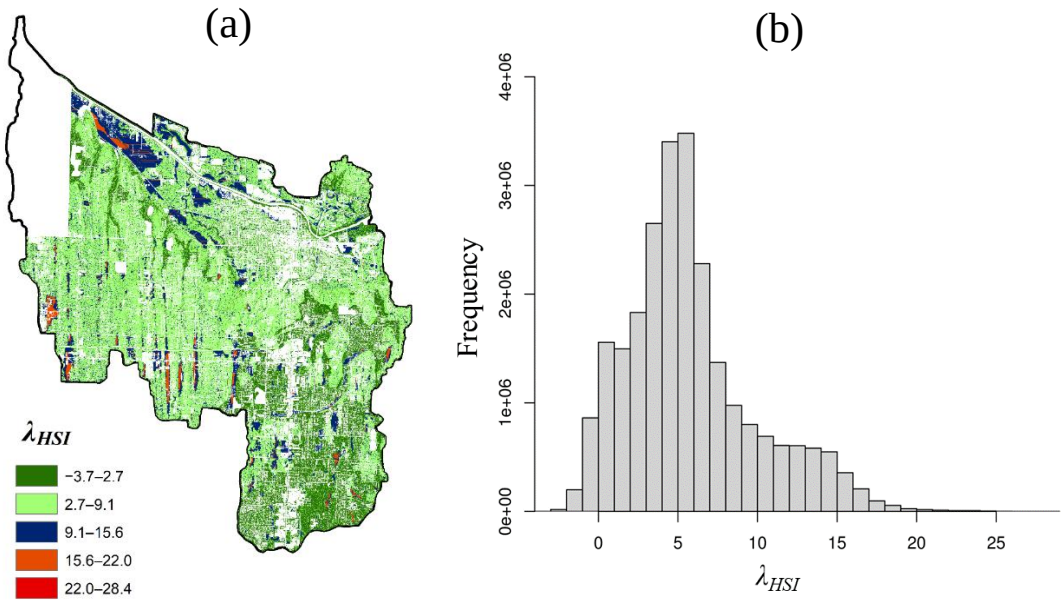

Figure 4.6. (a) Hydrologic Sensitivity Index (λ_{HSI}) and (b) distribution within the Lower Puyallup River Watershed

The λ_{HSI} (range:−3.8 to 28.4, median 5.1, standard deviation 4.1) was divided into five equal interval classes (Figure 4.6, Table 4.3). λ_{HSI} values were skewed towards the right and not normally distributed (W=0.956, p<0.0001). Areas with high λ_{HSI} values were concentrated in the central-western portion of the watershed, primarily due to the presence of elevated λ_{TWI} in these parts. The low-λ_{HSI} areas were primarily located in the southern part of the watershed, resulting from the combination of high λ_{SWSC} and low λ_{TWI} for those areas. Areas not meeting the state ordinances and engineering criteria for rain gardens were excluded from consideration (Figure 4.7a), resulting in 18% of the watershed meeting commonly adopted criteria for siting rain gardens (Figure 4.7b).

Table 4.3. Different classes of HSI

HSI class	λ_{HSI}
Class 1	−3.7–2.7
Class 2	2.7–9.1
Class 3	9.1–15.6
Class 4	15.6–22.0
Class 5	22.0–28.4

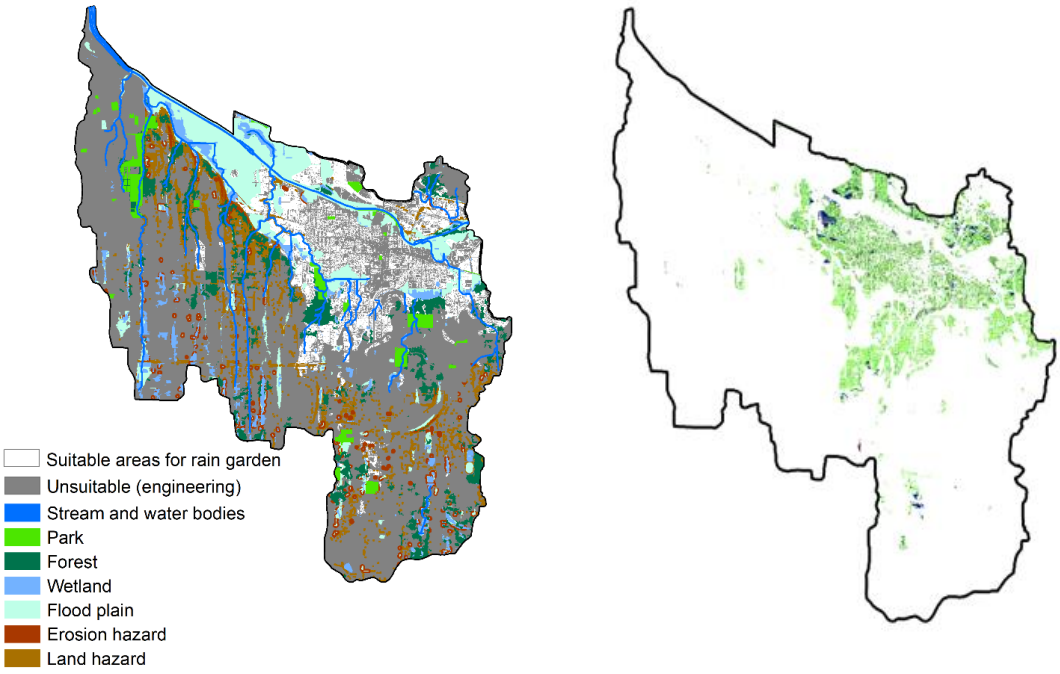

Figure 4.7. (a) Unsuitable areas for rain gardens and (b) suitable areas for rain gardens

4.3.3. λ_{HSI} Variability

λ_{HSI} within the study area varies with contributing area, slope gradient, and soil depth and hydraulic conductivity (Figure 4.8). λ_{HSI} increases with increasing contributing area and decreases with increasing slope steepness; λ_{HSI} decreases with increasing soil depth and hydraulic conductivity.

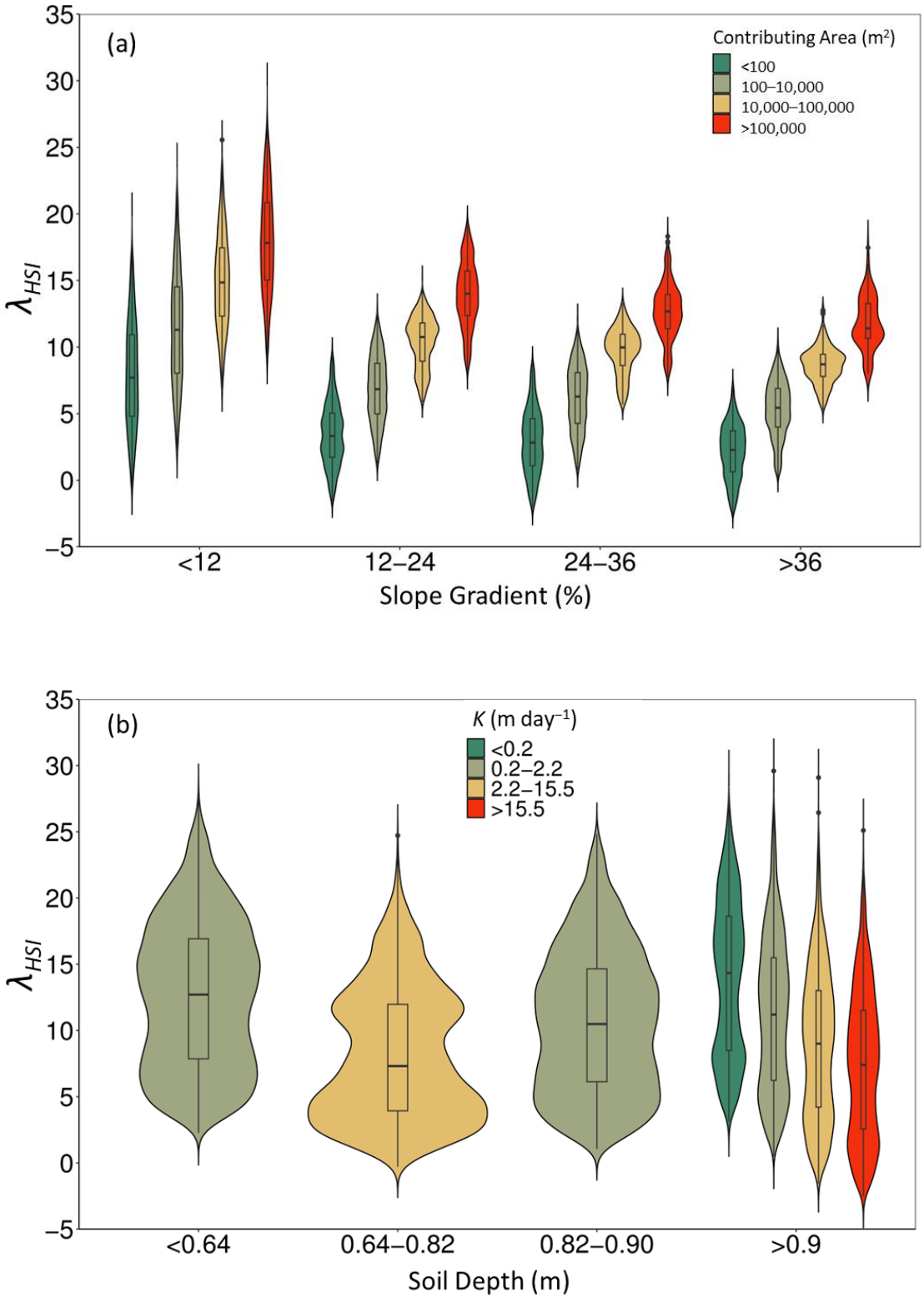

Figure 4.8. Distribution of hydrologic Sensitivity Index λ_{HSI} as influenced by (a) contributing area and slope gradient, and (b) soil hydraulic conductivity and depth

4.3.4. Adjusted λ_{HSI}

Adjusting the effect of impervious areas on runoff resulted in a slightly different flow accumulation and λ_{HSI} with minimal change in most areas of the watershed (Figure 4.9, Table 4.4). This also resulted in differences in λ_{HSI} values across the watershed. in absolute values, the differences were 1 for 61%, between 1 and 4 for 32%, and greater than 4 for 7% of the total watershed area (Figure 4.9b).

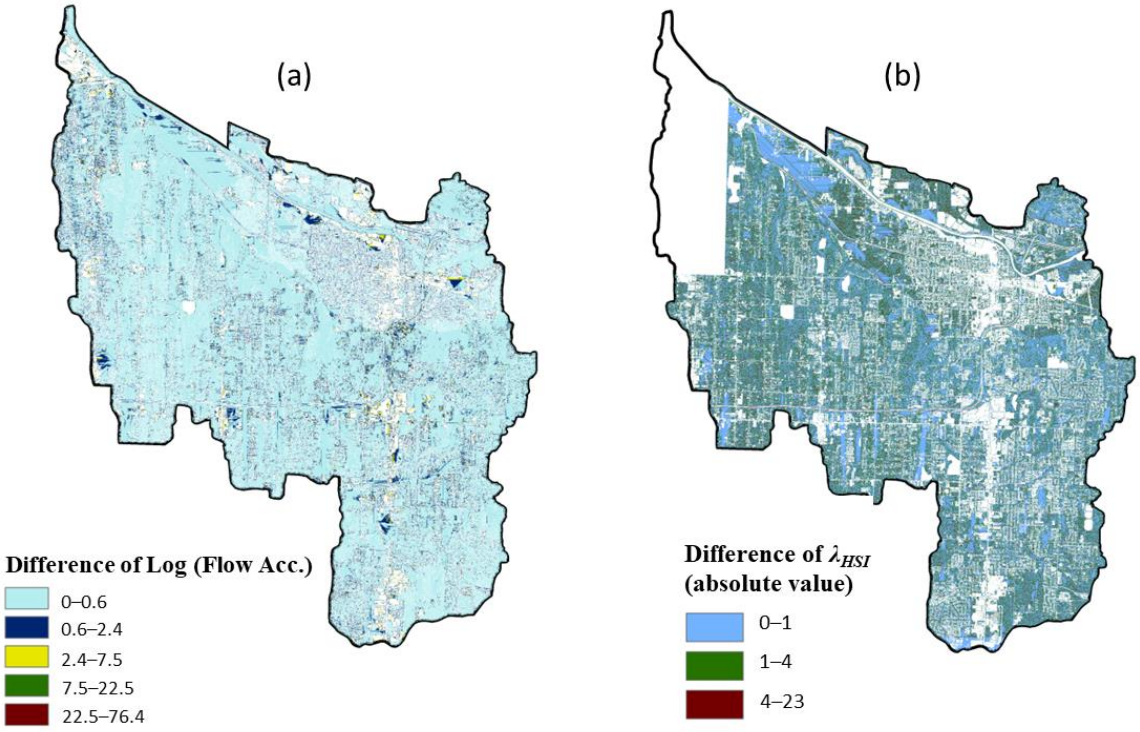

Figure 4.9 Difference in flow accumulation (a) and HSI (b) in the two methods

Table 4.4. Ranges of difference in flow accumulation (in log scale) and λ_{HSI} with or without adjusting for stormwater removal from impervious areas and corresponding percent areas of the watershed (in parentheses)

Flow Accumulation*	λ_{HSI}†
0–0.6 (83%)	−23 to −4 (3%)
0.6–2.4 (14%)	−4 to −1 (14%)
2.4–7.5 (2.3%)	−1 to 1 (61%)
7.5–22.5 (0.15%)	1–4 (18%)
22.5–76.4 (0.01%)	4–23 (4%)

*Log of flow accumulation was computed with or without adjusting for infrastructure removing runoff, and the difference was computed; †difference in λ_{HSI} was computed similarly

4.3.5. Hydrologic Analysis

As expected, WEPP-simulated runoff varied with topographic and soil conditions. WEPP routes water satisfying depression storage as runoff. Lateral flow occurs when the soil water content exceeds field capacity after correcting for entrapped air and is calculated using Darcy's law, dictated by the slope gradient and effective hydraulic conductivity. Consequently, runoff from flat areas (0% steepness) was high, as there was no lateral flow and much of the infiltrated water became saturation-excess runoff. Runoff decreased with increasing slope gradient as lateral flow increased, and increased with increasing slope length as lateral flow decreased (Figure 4.10). ET decreased with increasing slope gradient as more lateral flow occurred. Increasing soil depth promotes infiltration, increasing ET and subsurface lateral flow, resulting in less runoff (Figure 4.11). Similarly, increase in hydraulic conductivity augments infiltration capacity and reduces runoff.

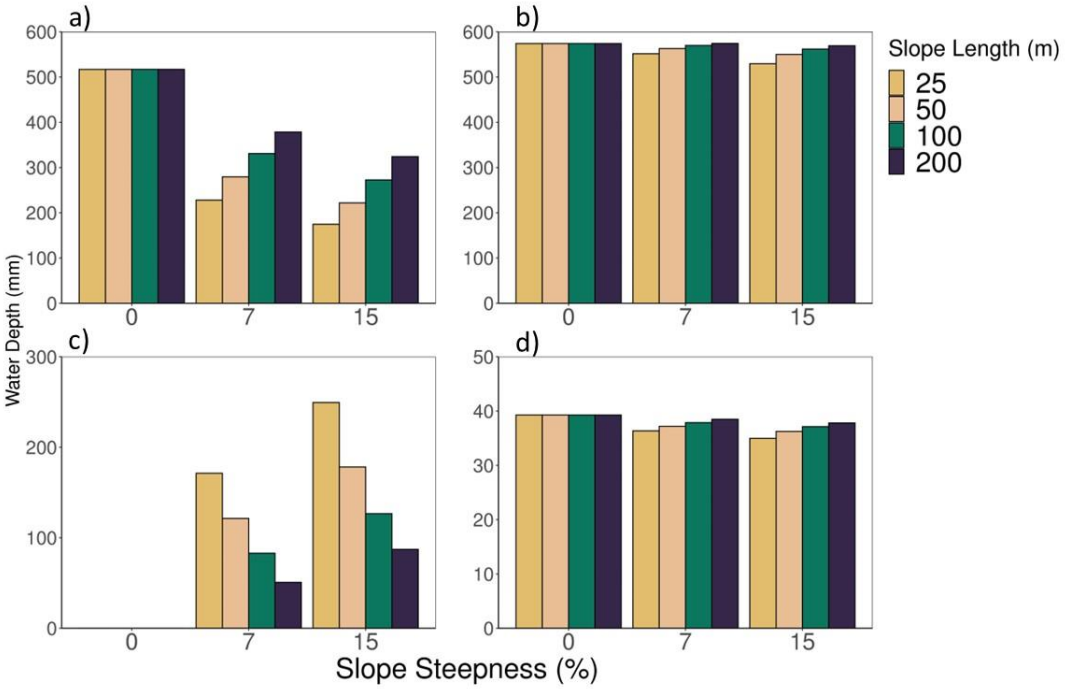

Figure 4.10. WEPP-simulated water balance for the conceptual hillslope as influenced by slope length and gradient. (a) Runoff, (b) ET, (c) subsurface lateral flow, and (d) deep percolation.

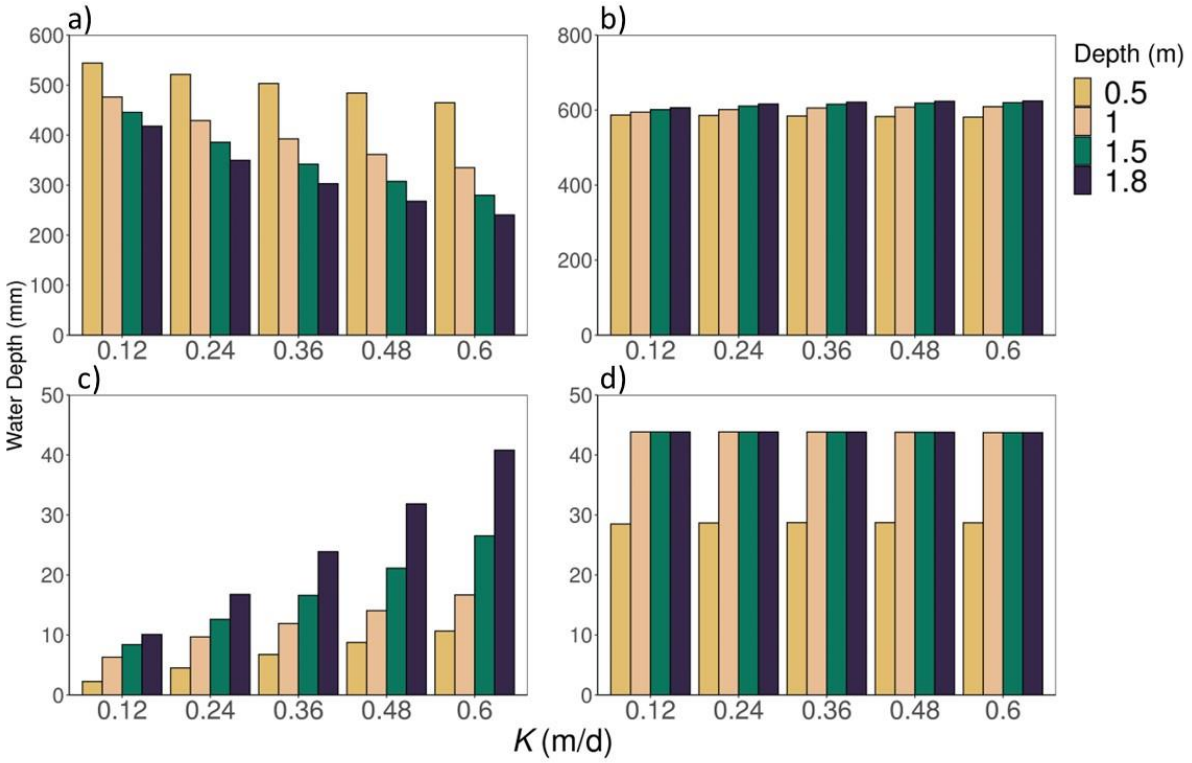

Figure 4.11. Water balance of the study watershed as influenced by hydraulic conductivity and soil depth. (a) runoff,(b) ET, (c) lateral subsurface flow, and (d) deep percolation.

4.3.5.1 Influence of paved areas

With pavement covering the OFE at the hilltop (OFE 1), its lateral flow and ET were reduced, leading to an increase in runoff for this OFE and those downslopes (Figure 4.12), compared to the no-pavement scenario. The area's urban development altered the flow path, exacerbating runoff accumulation at the bottom of the hillslope and necessitating treatment for runoff reduction via GSI. Implementing drainage systems to divert runoff away from the hillslope reduced all water balance components, leading to decreased water accumulation at the bottom of the hillslope.

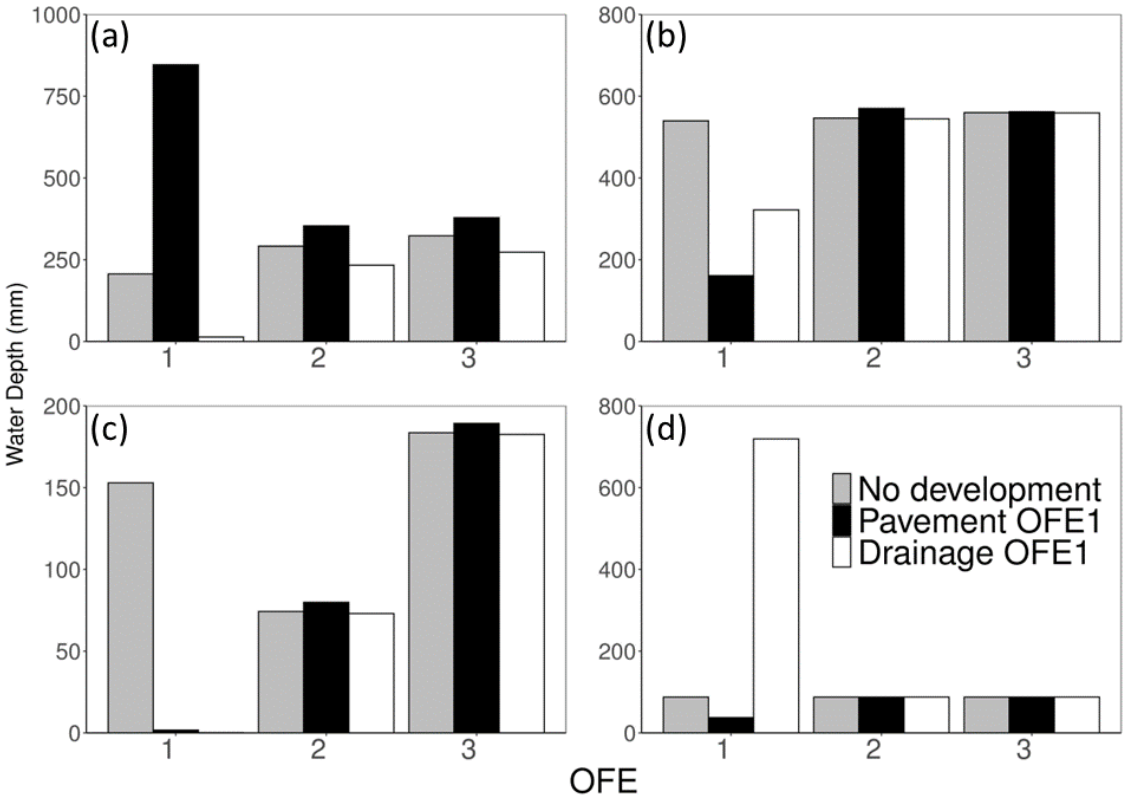

Figure 4.12. Water balance of the design hillslope as impacted by pavement and drainage installation at the hilltop. (a) runoff, (b) ET, (c) lateral subsurface flow, and (d) deep percolation. Note ET from the paved OFE 1 is only soil evaporation and no transpiration.

4.3.6. Variation of Runoff with λ_{HSI}

WEPP-simulated average annual runoff was positively related to λ_{HSI} (0.96, $p<0.0001$). , The intermediate- and lowest-λ_{HSI} scenarios had a 44% and 99% decrease in simulated average annual runoff, respectively, compared to the highest-λ_{HSI} scenario. The areas with the high λ_{HSI} generally had large contributing areas, low slope gradients, shallow soil depths, and low hydraulic conductivity, producing more runoff. Soils with low hydraulic conductivity and shallow depth impeded infiltration and lacked water storage. For a GSI, such as a rain garden, adequate hydraulic conductivity, and soil depth are required to facilitate infiltration and retain the infiltrated water. Additionally, rain gardens are a relatively small-scale GSI that cannot hold all

the runoff from a large contributing area. Therefore, placing rain gardens in high-λ_{HSI} areas will be ineffective.

Areas with low λ_{HSI} had low contributing areas, large slope gradients, extensive soil depths, and hydraulic conductivity. When the soil water storage capacity exceeded the topographic wetness, λ_{HSI} was negative. Areas with low (or even negative) λ_{HSI} were "self-sufficient" in facilitating infiltration and storing water and did not need additional mitigation by GSI. Hence, the most cost-effective areas for rain gardens are those with moderate λ_{HSI} values, where the contributing areas are moderate, and the soil depth and hydraulic conductivity are adequate for receiving and storing infiltrated water.

The WEPP simulation also illustrated that various combination of slope and soil characteristics might result in same λ_{HSI} value and exhibiting equifinality when using λ_{HSI} to guide GSI siting. Areas with different combinations of landscape characteristics may have the same λ_{HSI} value yet may generate different runoff (Figure 4.13). For instance, a soil profile 0.5 m deep with a 4 m/d hydraulic conductivity may generate a different amount of runoff from a soil profile 1 m deep with a 2 m/d hydraulic conductivity despite having the same λ_{HSI}. The reasons are a multitude, including that the effects of soil depth and hydraulic conductivity on runoff differ, the former reflecting storage and the latter transmissivity, and both interacting with other factors (patterns of precipitation events, topographic conditions, and hydraulic properties of underlying geological materials) in runoff generation. Therefore, it is essential to assess further the suitability of the areas with similar or identical λ_{HSI} values through on-site evaluation or alternative modeling techniques.

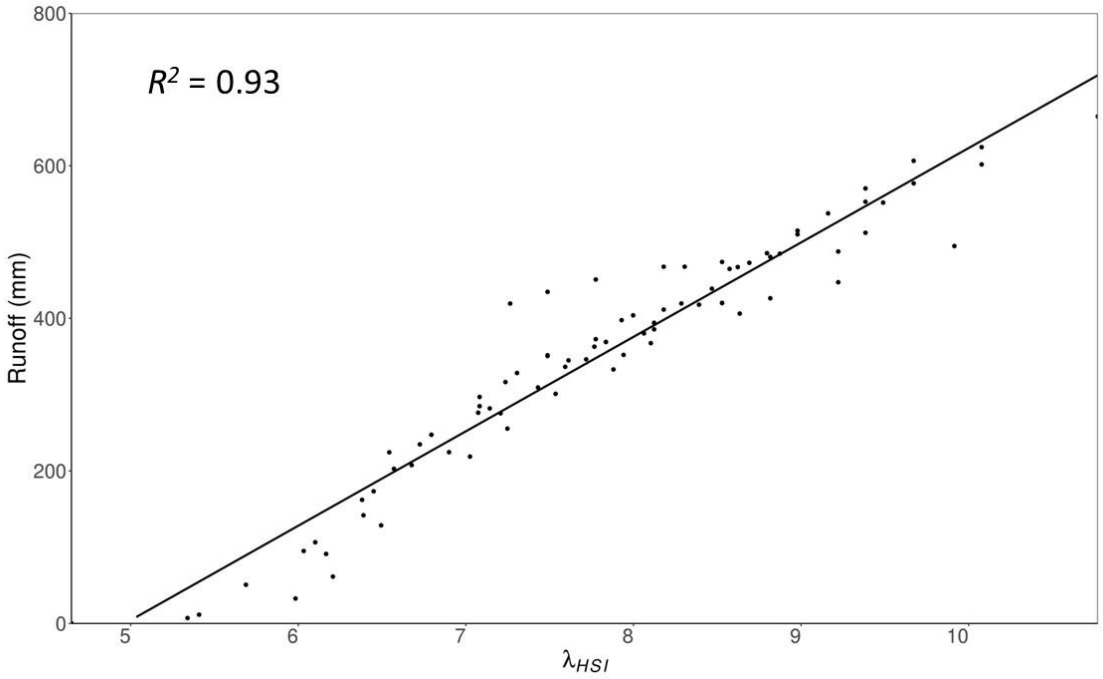

Figure 4.13. Relationship between WEPP-simulated runoff and Hydrologic Sensitivity Index (λ_{HSI}) for representative hillslopes.

4.3.7. Optimizing Placement of Rain Gardens

The suitable areas for rain gardens obtained with or without flow adjustment were similar, and the suitability maps differences were not discernable. Areas of the highest suitability for rain gardens are shown on the lot-scale λ_{HSI} maps (converted from grid-scale) (Figure 4.14), which are the areas with moderate λ_{HSI} values (Class 3). The areas with one interval of λ_{HSI} larger or smaller (Class 2 or 4) were considered less preferable for rain gardens. Areas with the lowest and highest λ_{HSI} values (Class 1 or 5) were considered least preferable. The areas of highest suitability covered 0.98% (0.96% with adjusted flow accumulation) of the watershed. These areas were unevenly distributed across the watershed, with the majority clustered in the northeastern and north-central parts, particularly in the low-lying areas near the Puyallup River. Meanwhile, high suitability areas covered 17% of the watershed both with and without flow

accumulation adjustment, and the moderate suitability areas were the rarest, covering 0.5% (0.7% with flow accumulation adjustment) of the watershed.

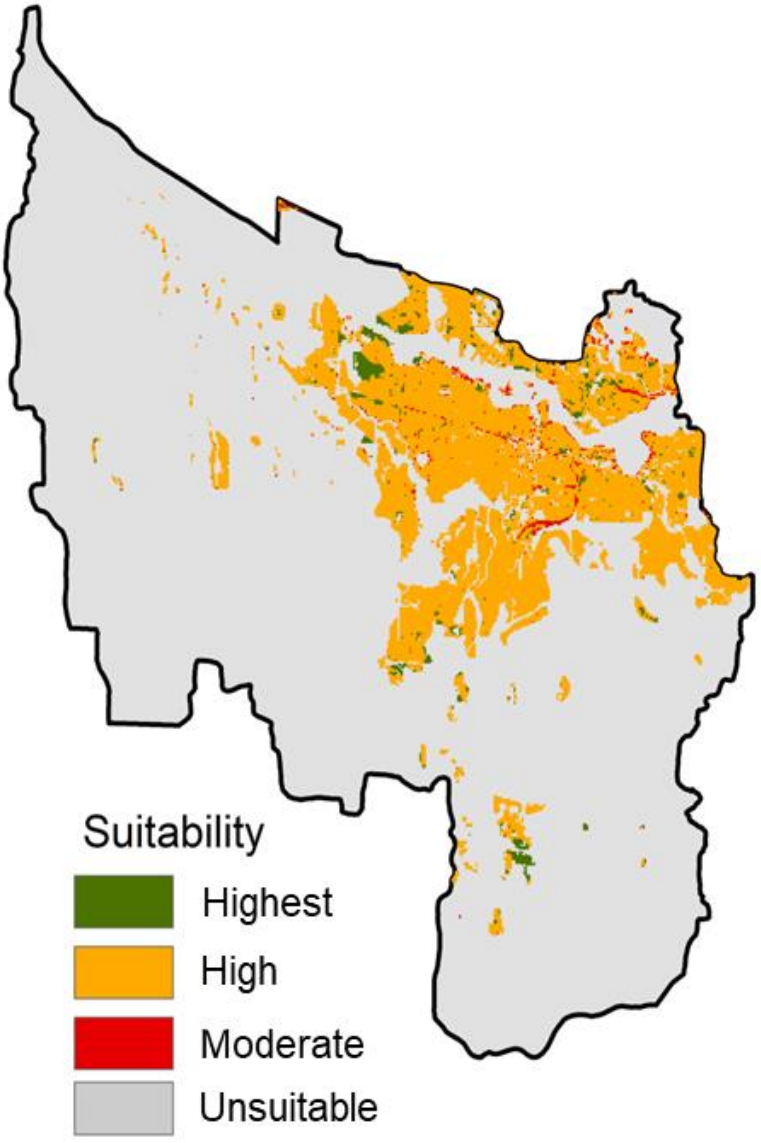

Figure 4.14. Suitable areas for rain gardens (without flow accumulation adjustment).

4.4. Conclusions

This study used the Hydrological Sensitivity Index Approach to identify suitable areas for siting rain gardens, a small-scale Green Stormwater Infrastructure (GSI). Publicly available datasets were used in ArcGIS to compute the three indices: Topographic Wetness Index (λ_{TWI}), Soil Water Storage Capacity Index (λ_{SWSC}), and Hydrologic Sensitivity Index (λ_{HSI}), for the Lower Puyallup River Watershed. Drainage area (α), slope gradient (β), soil depth (D), saturated hydraulic conductivity (K), and impervious areas were used to compute the indices, which describe the propensity of local saturation and runoff generation. Topographic characteristics were derived from the Digital Elevation Model (DEM), and soil properties were extracted from the SSURGO database. Areas unsuitable for rain gardens were excluded following EPA guidelines and state ordinances. The λ_{HSI} and resultant suitability maps were created with or without flow accumulation adjustment using the impervious layer as a weighting factor (0 for impervious areas and 1 for pervious areas). The suitability map was further classified into three suitability levels for rain gardens.

To evaluate the adequacy of the Hydrologic Sensitivity Index method, we applied a physically based hydrologic model WEPP to a design hillslope to explore the relationship between runoff and λ_{HSI} in various combinations of contributing area, slope gradient, soil depth, and soil hydraulic conductivity, as well as the effect of development (pavement and storm drainage infrastructure) on runoff. λ_{HSI} was calculated for all design hillslope conditions, and the correlation between WEPP-simulated runoff and λ_{HSI} was obtained.

Findings from this study demonstrate the adequacy and cost-effectiveness of the Hydrologic Sensitivity Index method. The study provides a strategy for local practitioners in optimizing the placement of rain gardens. The major takeaways from this study are:

1. For the Lower Puyallup River Watershed, λ_{HSI} ranged from −3.8 to 28.4. The high-λ_{HSI} areas more prone to runoff generation were clustered in the central-western flat portion of the watershed. The low-λ_{HSI} areas are in the southern part of the watershed with steeper slopes and deeper soils.
2. The resultant λ_{HSI} maps with or without flow accumulation adjustment exhibited negligible differences, leading to identical rain garden suitability maps illustrating equifinality.
3. The WEPP-simulated runoff was significant and positively correlated with λ_{HSI}. WEPP-simulated runoff increased with the contributing area and decreased with hillslope gradient, soil depth, and hydraulic conductivity. Compared to the highest-λ_{HSI} scenario, the moderate- and lowest-λ_{HSI} scenarios had a 44% and 99% decrease in simulated runoff.
4. When hillslopes were modeled with impervious pavement at the top of the slope, the simulated ET was reduced, leading to an increase in runoff both at the hilltop and at the bottom of the hillslope compared to the no-development scenario suggesting that installing GSI practices for runoff reduction was necessary.
5. Areas with moderate-λ_{HSI} values were the most appropriate for siting rain gardens because these areas did not generate large runoff volumes (exceeding the holding capacity of rain gardens) and had adequate soil storage to receive and retain runoff.
6. Approximately 1% of the study watershed was deemed most suitable for siting rain gardens. These areas were concentrated in the northeastern and north-central regions of the study area, in the low-lying floodplain adjacent areas of the Puyallup River.
7. Future efforts may be devoted to (i) examining seasonal changes in soil saturation to

corroborate further the adequacy of the index method, e.g., through ground-truthing or analysis of remotely sensed images, and (ii) overcoming the equifinality issue to improve the index method. Future efforts may also include rain garden siting based on the Hydrologic Sensitivity Index method with the results from urban rainfall-runoff models.

4.5. Acknowledgments

This study is in part supported by USDA AFRI NIFA (Grant No. 2018-68002-27920). I acknowledge the funding support from Puget Sound Partnership (NTA 2018-0704) and Chicona Endowment Assistantship.

REFERENCES

Ahiablame, L. M., Engel, B. A., & Chaubey, I. (2012). Effectiveness of low impact development practices: Literature review and suggestions for future research. *Water, Air, & Soil Pollution*, 223, 4253–4273.

Björklund, K., Bondelind, M., Karlsson, A., Karlsson, D., & Sokolova, E. (2018). Hydrodynamic modelling of the influence of stormwater and combined sewer overflows on receiving water quality: Benzo(a)pyrene and copper risks to recreational water. *Journal of Environmental Management*, 207, 32–42.

Booth, D. B., & Jackson, C. R. (1997). Urbanization of aquatic systems: Degradation thresholds, stormwater detection, and the limits of mitigation. *Journal of the American Water Resources Association*, 33(5), 1077–1090.

Bueno, P. H. O., & Alves, C. D. M. A. (2017). Proposed methodology to identify priority areas for stormwater management practices based on the identification of hydrologically sensitive areas. In *World Environmental and Water Resources Congress 2017* (pp. 241–252).

Chini, C. M., Canning, J. F., Schreiber, K. L., Peschel, J. M., & Stillwell, A. S. (2017). The green experiment: Cities, green stormwater infrastructure, and sustainability. *Sustainability (Switzerland)*, 9, 1–21.

Dahal, M. S., Wu, J. Q., Boll, J., Ewing, R. P., & Fowler, A. (2022). Spatial and agronomic assessment of water erosion on inland Pacific Northwest cereal grain cropland. *J. Soil Water Conserv.*, 77(4), 347–364. https://doi.org/10.2489/jswc.2022.00091

Dun, S., Wu, J.Q., Elliot, W.J., Robichaud, P.R., Flanagan, D.C., Frankenberger, J. R., ... & Xu, A. C. (2009). Adapting the Water Erosion Prediction Project (WEPP) model for forest applications. *Journal of Hydrology*, 366(1–4), 46–54. https://doi.org/10.1016/j.jhydrol.2008.12.019

Dietz, M. E., & Clausen, J. C. (2005). A field evaluation of rain garden flow and pollutant treatment. *Water, Air, and Soil Pollution*, 167, 123–138. https://doi.org/10.1007/s11270-005-8266-8

Di Vittorio, D., & Ahiablame, L. (2015). Spatial translation and scaling up of low impact development designs in an urban watershed. *Journal of Water Management Modeling*, 23, 1–9.

Dovel, E. L., Kemp, S. J., & Welker, A. L. (2015). Predicting ecological effects of watershed-wide rain garden implementation using a low-cost methodology. *Journal of Environmental Engineering*, 141(3), 04014063.

ESRI. (2022). Available online at https://www.esri.com/en-us/what-is-gis/overview. Accessed 07/05/2022.

French, B. F., Baldwin, D. H., Cameron, J., Prat, J., King, K., Davis, J. W., ... & Scholz, N. L. (2022). Urban roadway runoff is lethal to juvenile coho, steelhead, and chinook salmonids, but

not congeneric sockeye. *Environmental Science & Technology Letters*, 9(4), 232–240. https://doi.org/10.1021/acs.estlett.2c00006

Flanagan, D. C. & Livingston, S. J. (Eds.). (1995). *WEPP User Summary: USDA-water erosion prediction project*. NSERL Report 11. West Lafayette, IN: USDA ARS National Soil Erosion Research Laboratory. Retrieved from https://www.ars.usda.gov/ARSUserFiles/50201000/WEPP/usersum.pdf

Flanagan, D. C. & Nearing, M. A. (Eds.). (1995). *Water Erosion Prediction Project Hillslope Profile and Watershed Model Documentation*. NSERL Report 10. West Lafayette, IN: USDA ARS National Soil Erosion Research Laboratory.

Grumbes, B. H. (2007). Using green infrastructure to protect water quality in stormwater, CSO, nonpoint source and other water programs. United States Environmental Protection Agency (EPA). Available Online: https://www.epa.gov/sites/default/files/2015-10/documents/greeninfrastructure_h2oprograms_07.pdf (accessed on July 2022).

Guo, T., Srivastava, A., Flanagan, D. C., Liu, Y., Engel, B. A., & McIntosh, M. M. (2021). Evaluation of costs and efficiencies of urban Low Impact Development (LID) practices on stormwater runoff and soil erosion in an urban watershed using the Water Erosion Prediction Project (WEPP) model. *Water, 13*(15), 2076.

Jayasooriya, V. M., & Ng, A. W. M. (2014). Tools for Modeling of Stormwater Management and Economics of Green Infrastructure Practices: A Review. *Water, Air, and Soil Pollution, 225*(1-2055), 1–20. https://doi.org/10.1007/s11270-014-2055-1

Jenson, S. K., & Domingue, J. O. (1988). Extracting Topographic Structure from Digital Elevation Data for Geographic Information System Analysis. *Photogrammetric Engineering and Remote Sensing, 54*(11), 1593–1600.

Kaykhosravi, S., Abogadil, K., Khan, U. T., & Jadidi, M. A. (2019). The low-impact development demand index: A new approach to identifying locations for LID. *Water, 11*, 2341.

Kirkby, M. J., & Beven, K. J. (1979). A physically based, variable contributing area model of basin hydrology. *Hydrological Sciences Journal, 24*, 43–69.

Lew, R., Dobre, M., Srivastava, A., Brooks, E. S., Elliot, W. J., Robichaud, P. R., ... & Flanagan, D. C. (2022). WEPPcloud: An online watershed-scale hydrologic modeling tool. Part I. Model description. *J. Hydrol., 608*, 127603. https://doi.org/10.1016/j.jhydrol.2022.127603

Macro, K., Matott, L. S., Rabideau, A., Ghodsi, S. H., & Zhu, Z. (2019). OSTRICH-SWMM: A new multi-objective optimization tool for green infrastructure planning with SWMM. *Environmental Modelling & Software, 113*, 42–47.

Martin-Mikle, C. J., de Beurs, K. M., Julian, J. P., & Mayer, P. M. (2015). Identifying priority sites for low impact development (LID) in a mixed-use watershed. *Landscape and Urban Planning, 140*, 29–41. https://doi.org/10.1016/j.landurbplan.2015.04.002

McIntyre, J. K., Lundin, J. I., Cameron, J. R., Chow, M. I., Davis, J. W., Incardona, J. P., & Scholz, N. L. (2018). Interspecies variation in the susceptibility of adult Pacific salmon to toxic urban stormwater runoff. *Environmental Pollution*, 238, 196–203.

Minton, G. R., Blosser, M., & Schaefer, M. (2002). Summer Strategy for Stormwater Treatment in the Puget Sound Watershed. In *Global Solutions for Urban Drainage* (pp. 1–10).

Müller, A., Österlund, H., Marsalek, J., & Viklander, M. (2020). The pollution conveyed by urban runoff: A review of sources. *Science of the Total Environment*, 709, 136125.

Nicks, A. D., Lane, L. J., & Gander, G. A. (1995). Chapter 2. Weather generator. In D. C. Flanagan & M. A. Nearing (Eds.), *USDA-Water Erosion Prediction Project: Hillslope profile and watershed model documentation* (pp. 2.1–2.22). NSERL Report 10. West Lafayette, IN: USDA ARS National Soil Erosion Research Laboratory.

NOAA. (2023). Available online at https://www.ncei.noaa.gov/cdo-web/datatools/selectlocation. Accessed 06/09/2022.

NRCS. (2023). Soil survey geographic (SSURGO) database. Available online at https://websoilsurvey.nrcs.usda.gov/. Accessed 07/18/2023.

Paul, M. J., & Meyer, J. L. (2008). Streams in the urban landscape. In *Urban ecology* (pp. 207–231). Springer, Boston, MA.

Pierce County. (2021). Pierce County Open Geospatial Data Portal. Accessed January 2021. https://gisdata-piercecowa.opendata.arcgis.com/

Pierce County Surface Water Management (PCSWM). (2015). Pierce County Stormwater Management and Site Development Manual. https://www.piercecountywa.gov/ArchiveCenter/ViewFile/Item/4573

Pierce County. (2023). Available online at https://matterhornwab.co.pierce.wa.us/publicgis/. Accessed 07/18/2021.

Puget Sound Partnership (PSP). (2021). Puget sound watersheds. Accessed on October 2021. https://www.psp.wa.gov/salmon-recovery-watersheds.php

Qiu, Z. (2009). Assessing critical source areas in watersheds for conservation buffer planning and riparian restoration. *Environmental Management*, 44, 968-980. https://doi.org/10.1007/s00267-009-9380-y

Qiu, Z., Lyon, S.W., & Creveling, E. (2020). Defining a topographic index threshold to delineate hydrologically sensitive areas for water resources planning and management. *Water Resources Management*, 34, 3675–3688.

Reinelt, L. (2013). "Puyallup Watershed Assessment". https://www.piercecountywa.gov/AgendaCenter/ViewFile/Item/412?fileID=472

Sandahl, J. F., Baldwin, D. H., Jenkins, J. J., & Scholz, N. L. (2007). A sensory system at the interface between urban stormwater runoff and salmon survival. *Environmental Science & Technology*, 41(8), 2998–3004.

Schueler, T. R., Galli, J., Herson, L., Kumble, P., & Shepp, D. (1992). Developing Effective BMP Systems for Urban Watersheds: Analysis of Urban BMP Performance and Longevity. Metropolitan Washington Council of Governments. Department of Environment Programs.

Shojaeizadeh, A., Geza, M., & Hogue, T. S. (2021). GIP-SWMM: A new green infrastructure placement tool coupled with SWMM. *Journal of Environmental Management*, 277, 111409.

Shuster, W.D., Darner, R.A., Schifman, L.A., & Herrmann, D.L. (2017). Factors contributing to the hydrologic effectiveness of a rain garden network (Cincinnati Oh USA). *Infrastructures*, 2, 1–14. https://doi.org/10.3390/infrastructures2030011

Taguchi, V. J., Weiss, P. T., Gulliver, J. S., Klein, M. R., Hozalski, R. M., Baker, L. A., ... & Nieber, J. L. (2020). It is not easy being green: Recognizing unintended consequences of green stormwater infrastructure. *Water*, 12(2), 522.

Tsihrintzis, V. A., & Hamid, R. (1997). Modeling and management of urban stormwater runoff quality: a review. *Water Resources Management*, 11(2), 136–164.

U.S. Army Corps of Engineers Hydrologic Engineering Center (USACEHEC). (1998). HEC-HMS Hydrologic Modeling System user's manual, USACE-HEC, Davis, Calif.

United States Department of Agriculture (USDA). (2020). Web Soil Survey. https://websoilsurvey.sc.egov.usda.gov/App/HomePage.htm. Accessed September 2020.

United States Environmental Protection Agency. (n.d.). What is Green Infrastructure? https://www.epa.gov/green-infrastructure/what-green-infrastructure. Last Accessed July 2022.

USEPA. (2023). Bioretention (Rain Gardens). In Stormwater Best Management Practice. https://www.epa.gov/system/files/documents/2021-11/bmp-bioretention-rain-gardens.pdf. Accessed in August 2023.

USGS. (2021). Available online at https://www.usgs.gov/centers/eros/science/usgs-eros-archive-aerial-photography-national-agriculture-imagery-program-naip. Assessed 02/01/2021.

United States Geological Survey (USGS). (2020). The National Map. https://apps.nationalmap.gov/downloader/#/. Accessed September 2020.

WA DOE (Washington State Department of Ecology). (2019). Stormwater Management Manual for Western Washington Pub. No. 19-10-021.

WA DNR (Department of Natural Resources). (2021). Available online at https://www.dnr.wa.gov/lidar. Accessed 02/01/2021.

Walsh, C.J., Fletcher, T.D., & Ladson, A.R. (2005). Stream restoration in urban catchments through redesigning stormwater systems: Looking to the catchment to save the stream. *Journal of the North American Benthological Society*, 24, 690-705. https://doi.org/10.1899/04-020.1

Walsh, C.J., Fletcher, T.D., & Burns, M.J. (2012). Urban Stormwater Runoff: A New Class of Environmental Flow Problem. *PLoS ONE*, 7(9). https://doi.org/10.1371/journal.pone.0045814

Walter, M.T., Walter, M.F., Brooks, E.S., Steenhuis, T.S., Boll, J., & Weiler, K. (2000). Hydrologically sensitive areas: Variable source area hydrology implications for water quality risk assessment. *Journal of Soil and Water Conservation*, 55, 277–284.

Washington State Department of Ecology (WSDE). (2010). 2010 Statewide Landuse. WSDE, Olympia, WA. https://fortress.wa.gov/ecy/gispublic/DataDownload/ECY_CAD_Landuse2010.htm

Washington State Department of Ecology (WSDE). (2014). Stormwater Management Manual for Western Washington. Washington DC: Washington State Department of Ecology. https://fortress.wa.gov/ecy/madcap/wq/2014SWMMWWinteractive/Content/Resources/DocsForDownload/2014SWMMWW.pdf

Washington State Department of Ecology (WSDE). Water quality standards. Accessed September 2021. https://ecology.wa.gov/Water-Shorelines/Water-quality/Water-quality-standards

Washington State Department of Natural Resources. 2014. Washington Lidar Portal. Accessed August 2020. https://lidarportal.dnr.wa.gov/#45.97024:-122.36572:9

Welch, W. B., Johnson, K., Savoca, M., Lane, R. C., Fasser, E., Gendaszek, A., ... & Marshall, C. (2015). Hydrogeologic Framework, Groundwater Movement, and Water Budget in the Puyallup River Watershed and Vicinity, Pierce and King Counties, Washington. US Department of the Interior, US Geological Survey.

Winston, R.J., Hunt, W.F., DeBusk, K.M., Woodward, M.D., & Hartup, W.W. (2010). Certifying the landscape community in rain garden installation: The North Carolina experience. Low Impact Development 2010: Redefining Water in the City, Proceedings of the 2010 International Low Impact Development Conference, p. 568-578. https://doi.org/10.1061/41099(367)50

Woodward, M., Hunt, W.F., & Hartup, W. (2009). Lessons learned: The North Carolina backyard rain garden program. *Low Impact Development for Urban Ecosystem and Habitat Protection*. https://doi.org/10.1061/41009(333)104

Wu, J., Kauhanen, P. G., Hunt, J. A., Senn, D. B., Hale, T., & McKee, L. J. (2019). Optimal selection and placement of green infrastructure in urban watersheds for PCB control. *Journal of Sustainable Water in the Built Environment*, 5(2), 04018019.

5. SUMMARY AND CONCLUSIONS

The goal of my doctoral research was to understand the temporal trends and spatial distribution of non-point source pollution, with a specific focus on how factors such as landscape features, soil properties, and climatic changes affect non-point source pollution in agriculture and urban settings. In Chapter 2 and 3, I assessed the temporal trends of water erosion in past, present, and the future in the three agricultural watersheds of eastern Washington. In Chapter 4, I assessed the factors affecting stormwater runoff in an urbanizing watershed and identified suitable location for the placement of green stormwater infrastructure in areas prone to runoff generation.

Chapter 2

In Chapter 2, my main objective was to elucidate the past and present trends of water erosion in the inland Pacific Northwest and compared the trends with field sampled annual erosion data. I separated the climate record into the past (1940–1982) and the present (1983–2020) and delineated a watershed within each precipitation zone and carried out WEPP model simulations over the two periods for the three watersheds under different tillage practices and crop rotations. Major conclusions from this study:

1. WEPP-simulated average annual erosion rates decreased from the past to present by 32%, 57%, and 70% for the study watersheds in the low-, intermediate-, and high-precipitation zones, respectively. The decreases were due to the combined effects of changing climatic patterns and management practices.
2. The decrease in annual, particularly winter, precipitation, and the number of large precipitation events were the key climatic factors (or parameters) that led to a decrease

in erosion.

3. The shifts from two-year to three-year rotation, and from intense tillage to conservation tillage, were the key management changes that caused a decrease in erosion. Incorporating reduced- and no-till decreased WEPP-simulated average annual erosion by 31%, 35%, and 40% in WLCW-Low, UICW-Intermediate, and SFCW-High, respectively.
4. WEPP-simulated average annual erosion rate agreed with the Kaiser field data. WEPP reproduced year-by-year variations for certain periods, especially 1948–1979.
5. Erosion events were positively correlated with annual water input, runoff, and minimum temperature for all three watersheds. The number of annual freeze-thaw cycles was not correlated with annual erosion rates in the three watersheds. The number of annual rain-on-thawing-soil events was significantly correlated with annual erosion rates for the watersheds in the low- and high-precipitation zones.
6. The average annual erosion rate was significantly correlated with hillslope length and steepness for all three watersheds. Average annual erosion rate in SFCW-High was negatively correlated with soil depth, as deep soils have lower potential for runoff and erosion. However, the erosion rate was positively correlated with soil depth in WLCW-Low, because hillslopes with deeper soils in this watershed tend to be longer and steeper, with lower hydraulic conductivity and higher erodibility.

Chapter 3

In Chapter 3, I ventured further into predicting future erosion patterns for the three agricultural watersheds of Chapter 2. I conducted WEPP simulation for the three watersheds with three different tillage intensities and three crop rotations using the downscaled climates of 20

GCM models with historical scenario for the period of 1976–2005 and, RCP 4.5 and 8.5 scenario for the period of 2036–2060. I further assessed the problem areas in the watersheds that consistently produced high erosion and applied various management combinations to reduce erosion in the future. The findings from this study showed how changing climate factors can interact with one another and impact erosion, while sometime exacerbating or offsetting the effect of one another. The study showed that strategic land management practices could be used to decrease erosion in the future. Major conclusions of this study were:

1. There is a general increase in future ET in the three precipitation zones of Whitman County, caused by the projected increase in temperature and precipitation and in turn, biomass density. There is a general decrease in runoff due to an increase in ET, and projected increased infiltration capacity resulting from a decrease in frost depth in the area.
2. The annual water erosion decrease in the three precipitation zones of Whitman County. The majority of water erosion decrease in high- and low-precipitation zone occurred in winter months (2.2–3.5 Mg ha^{-1}), particularly due to a decrease in runoff and improved winter conditions due to an increase in temperature. The winter erosion slightly increased in the intermediate precipitation zone (0.2–1.2 Mg ha^{-1}) because of the competing effect of increased temperature and precipitation increase.
3. Even with the projected decrease in erosion, erosion amounts were often problematic, exceeding over 50 Mg ha^{-1} in steeper slopes and wheat years, especially in the high- and intermediate-precipitation zone.
4. The excessive erosion may be mitigated by targeted management practices. Retiring the areas with slope steepness >20% and reducing the tillage in rest of the watershed would

decrease the erosion by 57–77% across the three precipitation zones.

Chapter 4

In Chapter 4, I shifted my focus towards urban landscapes and assessed how landscape and soil features affected stormwater runoff in an urbanizing watershed. Using the Hydrological Sensitivity Index (HSI), I used locally available data to compute various indices and mapped areas susceptible to saturation and closely analyzed the relationship between HSI, hillslope characteristics, and soil properties. I designed a representative hillslope, varied soil and slope characteristics and conducted hydrological modeling to understand runoff generation and how it is related with Hydrological Sensitivity Index. Findings from this study demonstrate the adequacy and cost-effectiveness of the Hydrologic Sensitivity Index method and provides a strategy for local practitioners in optimizing the placement of rain gardens. Major conclusions from this study include:

1. For the Lower Puyallup River Watershed, λ_{HSI} ranged from −3.8 to 28.4. The high-λ_{HSI} areas that are more prone to runoff generation were clustered in the central-western flat portion of the watershed. The low-λ_{HSI} areas are in the southern part of the watershed with steeper slopes and deeper soils.
2. The WEPP-simulated runoff was significantly positively correlated with λ_{HSI}. WEPP-simulated runoff increased with contributing area and decreased with hillslope gradient as well as soil depth and hydraulic conductivity. Compared to the highest-λ_{HSI} scenario, the intermediate- and lowest-λ_{HSI} scenarios had a 44% and 99% decrease in simulated runoff.
3. Areas with moderate λ_{HSI} values are the most appropriate for siting rain gardens because

these areas do not generate excessive runoff that would overwhelm small-scale GSI practices such as rain garden, and yet contain adequate soil storage to receive and retain runoff.

4. Approximately 1% of the total study watershed was regarded most suitable for siting rain gardens. These areas are concentrated in the northeastern and north-central regions of the study area, in the low-lying areas near the Puyallup River.

Recommendations for Future Research

1. There is a pressing need to refine the adjustment of erodibility factors with change in climate and management within the WEPP model to achieve more accurate results, especially for winter months in the inland PNW.
2. Future erosion simulation efforts should allow for dynamic adaptation of crop rotation with time in sync with climatic changes.
3. Remotely sensed images should be used to gain insights into tillage characteristics of the study area. Integrating this with WEPP models can lead to more accurate simulation results.
4. Future study should account for characteristics of precipitation events (intensity and duration) while simulating temporal water erosion trends.
5. Conservation efforts should be more adaptive, adjusting on an annual basis rather than being static for long durations. For instance, wheat years producing extremely high erosion could be targeted for management efforts.
6. Benefit-cost analysis should be conducted for replacing the management in the steeper slopes with land retirement or no tillage, which decreased the erosion markedly in the area.

7. In the future studies, gully and channel erosion should be considered to have a more detailed picture of erosion in the area.
8. The indices computed from HSI methods should be tested against remotely sensed soil moisture data to understand it's relationship with soil moisture. Equifinality issue with HSI should be taken into consideration in the future studies and efforts should be made to overcome it.
9. Seasonal changes in soil saturation in various HSI classes across the watershed should be examined through field sampling to further corroborate the adequacy of the index method.
10. Future efforts may also include rain garden siting using both HSI method and urban rainfall-runoff models, and compare the cost intensiveness, accuracy, and efficiency of both methods.